Structural and functional studies of AMSH implicated in the endosomal sorting pathway and enveloped virus budding.

Julianna Solomons

Université Joseph Fourier - Grenoble I
Ecole Doctorale Chimie et Sciences du Vivant

Études Structurale et Fonctionelle d'AMSH impliquée dans la voie de tri endosomale et le bourgeonnement des virus enveloppés

Par **Julianna Solomons**

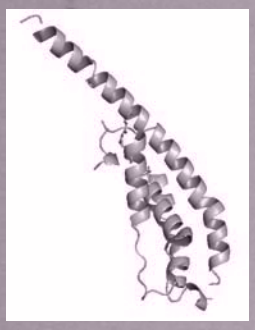

Pour obtenir le titre de:
DOCTEUR DE L'UNIVERSITÉ JOSEPH FOURIER - GRENOBLE I
en **BIOLOGIE STRUCTURALE ET NANOBIOLOGIE**

Soutenance le 26 Novembre 2009
devant le jury:

Président:	Prof.	Rémy Sadoul
Rapporteurs:	Dr.	Robin Buckland
	Dr.	John Briggs
Examinateurs:	Prof.	Wim Burmeister
	Prof.	Winfried Weissenhorn
	Dr.	Laurence Aubry

Directeur de Thèse Prof. Winfried Weissenhorn

Thèse préparée au sein de:
EMBL Grenoble
UVHCI (Unit of Virus Host Cell Interactions) UMI3265 UJF-EMBL-CNRS

Université Joseph Fourier - Grenoble I
Ecole Doctorale Chimie et Sciences du Vivant

Structural and Functional Studies of AMSH implicated in the Endosomal Sorting Pathway and Enveloped Virus Budding

By **Julianna Solomons**

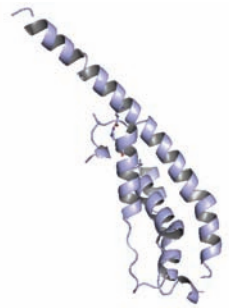

To obtain the title of:
DOCTOR OF UNIVERSITÉ JOSEPH FOURIER - GRENOBLE I
in **STRUCTURAL BIOLOGY AND NANOBIOLOGY**

To be defended 26th Novembre 2009
before a jury of:

President:	Prof.	Rémy Sadoul
Reporters:	Dr.	Robin Buckland
	Dr.	John Briggs
Examinators:	Prof.	Wim Burmeister
	Dr.	Laurence Aubry
	Prof.	Winfried Weissenhorn

PhD Supervisor Prof. Winfried Weissenhorn

Thesis work conducted at:
EMBL Grenoble
UVHCI (Unit of Virus Host Cell Interactions) UMI3265 UJF-EMBL-CNRS

Acknowledgements

I would like to recognise the scientific direction of my PhD supervisor Winfried Weissenhorn, and thank him for the opportunity to join his research group on such an interesting project.

I thank the members of my Thesis Advisory Committee, Stephen Cusack and Klaus Scheffzek for their helpful advice, and my jury members Rémy Sadoul, Laurence Aubry, John Briggs, Wim Burmeister and Robin Buckland for taking time out of their busy schedules to participate in my thesis defense.

I am grateful to the EMBL to have accepted me into their PhD Programme, to the UVHCI who welcomed me two years later, and to the DFG for funding my work at the UVHCI. I would like to thank the people of the EMBL Grenoble and UVHCI, past and present, for creating such a pleasant work environment, and the staff of both establishments who ensure the smooth running of the institutes.

I would like to thank Charles Sabin for the crystallography-related work, and for teaching me about data collection and structure determination, Jennifer McCarthy for her contribution to the proteolysis project, Guy Schoen for electron microscopy, Marc Jamin for MALLS, and Heinrich Göttlinger for the viral budding assays. My profound gratitude to Estela Pineda-Molina for her advice, patience and good humour, and Ricardo Pires for helpful discussions, his support and most of all for his understanding. Je remercie Alexandre Dias, pour l'élimination de l'accent anglais dans les parties traduits de mon manuscrit, et d'avoir partagé cette expérience de la thèse avec moi.

Most importantly, I would like to thank my parents Stephen and Christine Solomons, whose unfailing love, support, and wisdom provide the foundations for all my endeavours in life.

Julianna

Abstract

Receptors to be down-regulated via the lysosomal degradation pathway are targeted through a ubiquitin signal to the endosomal membrane, where incorporation into multi-vesicular bodies (MVBs) through invagination of the endosomal membrane commits them for degradation. The ESCRT (endosomal sorting complex required for transport) protein subcomplexes ESCRT-0, -I, -II and -III are responsible for identifying receptor cargo and MVB formation. AMSH (Associated Molecule of the SH3 domain of STAM), an auxiliary protein of the ESCRT machinery, contains a C-terminal JAMM metalloprotease domain that hydrolyses K-63 linked ubiquitin chains *in vitro*, leading to the hypothesis AMSH functions to remove ubiquitin from receptors before their incorporation into MVBs. AMSH also interacts with CHMP proteins of ESCRT-III through a predicted MIT domain-containing N-terminal domain, binding to a C-terminal auto-inhibitory domain implicating AMSH in the activation of CHMP proteins for polymerisation to effectuate membrane remodelling.

This work shows AMSH can bind to two distinct forms of CHMP3, one corresponding to an open, activated form, the second a closed, auto-inhibited form. The interaction of the AMSH N-terminal with both CHMP3 forms has been measured by isothermal titration calorimetry to be of nanomolar affinity, a value orders of magnitude higher than other MIT-CHMP interactions, with the last 40 amino acids of the CHMP3 C-terminal required for maximum affinity. The x-ray crystallographic structure of an AMSH N-terminal-CHMP3 complex has been determined to 1.7Å resolution, presenting a mode of CHMP3 binding distinct from previously characterised MIT-CHMP structures and a deviation from the classical MIT domain architecture, with an additional N-terminal helix implicated to function in dimerisation. We provide evidence that the N-terminal domain of AMSH interacts intramolecularly with the enzymatic JAMM domain, and that this interaction stimulates the deubiquitinating activity of the JAMM domain.

These results highlight a particularly high affinity binding between AMSH and CHMP3, where the dynamics of CHMP binding and the efficient deubiquitinating activity of AMSH can create a point of regulation in the endosomal sorting pathway.

Key words: AMSH, STAMBP, ESCRT, CHMP, endosomal sorting, multi-vesicular bodies, deubiquitination, JAMM.

Résumé

Les récepteurs marqués pour la voie de dégradation lysosomale sont dirigés vers l'endosome par addition d'ubiquitine. L'invagination de la membrane endosomale incorpore ces récepteurs dans les corps multivésiculaires (Multivesicular bodies, MVBs), et mène à leur dégradation. Les protéines ESCRT (Endosomal Sorting Complex Required for Transport), en subcomplexes ESCRT -0, -I, -II, –III, sont responsables de l'identification de ces récepteurs et de la formation des MVBs. AMSH (Associated Molecule of the SH3 domain of STAM), une protéine auxiliaire de la machine ESCRT, contient un domaine métalloprotéase JAMM au niveau de sa partie C-terminale. Celui-ci a montré, *in vitro,* la capacité d'hydrolyser les chaînes d'ubiquitine de liaison K-63, laissant supposer une fonction d'élimination des ubiquitines pour AMSH avant l'incorporation des récepteurs dans les MVBs. AMSH interagit aussi avec les protéines CHMP (Charged Multivesicular body Protein) d'ESCRT-III via un domaine N-terminal contenant un domaine MIT. De plus, la liaison d'AMSH avec un domaine C-terminal autoinhibitoire des protéines CHMP a impliqué AMSH dans l'activation de la polymérisation des protéines CHMP, occasionnant un remodelage membranaire suivi de la formation des vésicules.

Ce travail montre que AMSH se lie à deux formes de CHMP3, une correspondant à la forme ouverte et active, l'autre correspondant à la forme fermée et autoinhibée. L'interaction du domaine N-terminal d'AMSH avec ces deux formes de CHMP3 fut évaluée à l'échelle nanomolaire par isothermal titration calorimetry. La structure cristallographique du complexe AMSH domaine N-terminal CHMP3 fut résolue à 1.7Å. Celle-ci présente un mode de liaison CHMP différent des autres structures MIT-CHMP déjà déterminées et dévie de l'architecture classique du domaine MIT, avec une hélice de plus à l'extrémité N-terminale impliquée dans la dimérisation. On montre que les domaines N-terminal et JAMM d'AMSH interagissent entre eux, et que cette interaction stimule l'activité déubiquitinase du domaine JAMM

Mots Clés : AMSH, STAMBP, ESCRT, CHMP, tri endosomale, corps multivesiculaire, deubiquitination, JAMM.

.

Abbreviations

AAA	ATPase Associated with various cellular Activities
ALIX	ALG-2 Interacting protein X
AMSH	Associated Molecule of the SH3 domain of STAM
AMSH-LP	AMSH-Like Protein
CHC	Clathrin Heavy Chain
CHMP	CHarged Multivesicular body Protein/CHromatin Modifying Protein
DUB	Deubiquitinating Enzyme
EGF	Epidermal Growth Factor
Eps15	Epsin-15
ESCRT	Endosomal Sorting Complex Required for transport
ESP	Endosomal Sorting Pathway
FYVE	Fab1, YGLO23, Vps27, EEA1
GLUE	GRAM-Like Ubiquitin binding in EAP45
HD-PTP	His-Domain containing Protein Tyrosine Phosphatase
HIV	Human Immunodeficiency Virus
hIST1	Human IST1 homologue
Hrs	Hepatocyte growth factor-Regulated tyrosine kinase Substrate
ILV	IntraLumenal Vesicle
JAMM	JAB_MPN Motif
MIM	MIT Interacting Motif
MIT	Microtubule Interacting
MLV	Murine Leukemia Virus
MVBs	MultiVesicular Bodies
NLS	Nuclear Localisation Signal
NZF	Npl4 Zinc Finger
PI3P	PhosphatidylInositol 3-Phosphate
SBM	STAM Binding Motif
SIV	Simian Immunodeficiency Virus
SH3	Src-Homology domain-3
STAM	Signal Transducing Adaptor Molecule
TPR	Tetratricopeptide
TSG101	Tumor Suppressor Gene 101
Ub	Ubiquitin
UBPY	Ubiquitin-specific Processing Protease Y
UEV	Ubiquitin E2 Variant
UIM	Ubiquitin Interacting Motif
VHS	Vps27/Hrs/STAM
Vps	Vacuolar Protein Sorting

Introduction

0.1 The Endosomal Sorting Pathway in Receptor Downregulation

The Endosomal Sorting Pathway (ESP) is an important component of plasma membrane receptor regulation. Recognition of a sequence signal in the cytoplasmic tail of receptors to be downregulated leads to receptor endocytosis and incorporation into the early endosome. From here receptors can suffer one of two fates: recycling back to the cell membrane or trans-golgi network, or if ubiquitinated, retention at the endosomal membrane. Receptors that are not recycled from the endosome are included into intralumenal vesicles (ILVs) formed by vesiculation of the endosomal membrane (David J Katzmann et al. 2002), creating what is termed a multivesicular body (MVB). Once all receptors have been incorporated into ILVs the mature late endosome delivers receptors for degradation through fusion with the lysosomal membrane (Figure 1). Some integral membrane proteins such as iron and nutrient receptors undergo several cycles of internalization and recycling without ever passing by the lysosome, thus inclusion or exclusion of certain receptors from the endosomal membrane into MVBs must be a tightly regulated event. Recognition of the ubiquitinated cargo and membrane remodeling for MVB biogenesis is carried out by the Endosomal Sorting Complex Required for Transport (ESCRT) machinery, an intricate assembly of more than 60 proteins.

Receptor monoubiquitination, or multiple monoubiquitination, is the classic signature for endosomal sorting, as opposed to the Lys48-linked polyubiquitin chain signal that targets cytosolic and nuclear proteins to the proteosome (Haglund et al. 2003). It has since been shown that polyubiquitination, through Lys63 specific linkage of ubiquitin chains, can target the membrane receptor epidermal growth factor (EGF) receptor for internalization (F. Huang et al. 2006). Ubiquitination-deficient mutant EGF receptors are internalized at the same rate as wild-type receptors but their turnover rates are defective. Localisation experiments show the mutant receptors remain mostly at the early endosome, whilst only wt-receptors make it to the late endosome, suggesting ubiquitination mutation prevents MVB targeting of receptors, leaving receptors instead to recycle back to the plasma membrane (F. Huang et al. 2006). These studies show how ubiquitination is implicated in lysosomal targeting but not for initial internalization of receptors from the plasma membrane into endosomes.

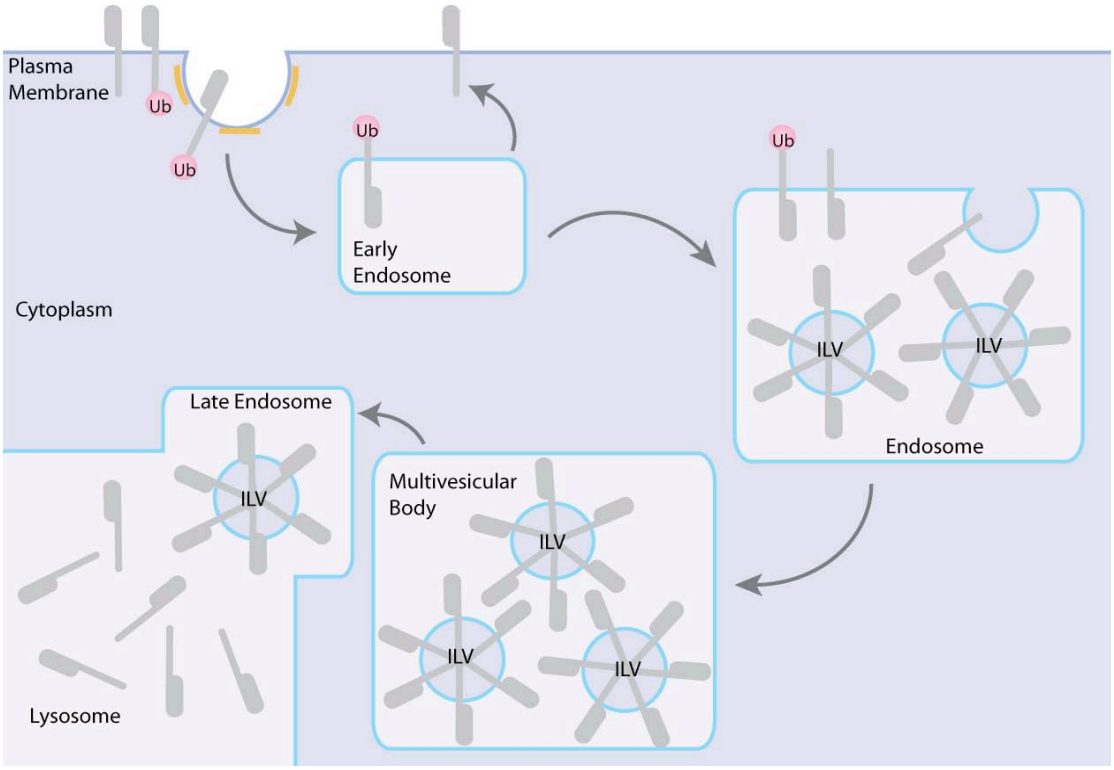

Figure 1. Receptor downregulation via the endosomal sorting pathway.

Receptors to be down-regulated at the plasma membrane are endocytosed and delivered to the early endosome. Receptors are then either recycled back to the plasma membrane or trans-golgi network, or retained at the endosomal membrane through an ubiquitination signal. Invagination of the endosomal membrane incorporates receptors into intralumenal vesicles, forming a compartment termed a multivesicular body. Once all receptors are been incorporated into ILVs, the now mature late endosome delivers receptors for degradation by fusing with the lysosome.

0.2 The ESCRT machinery

The components of the ESCRT machinery were first identified from vacuolar sorting mutants in yeast (the vacuole being the yeast functional equivalent to the mammalian lysosome), a method that has continued to be exploited to probe the individual function of ESCRT components (David J Katzmann et al. 2002).

There are four multi-subunit ESCRT complexes involved in MVB formation, termed ESCRT-0, -I, -II, -III. These are cytosolic proteins that are recruited to the endosomal membrane for receptor sorting. There are three main requirements of the ESCRT machinery; targeting to the endosomal membrane, recognition of ubiquitinated receptors to be sorted, and MVB biogenesis. ESCRT- 0,- I and -II serve to recognize and anchor the target receptor at the endosomal membrane, whilst ESCRT III is responsible for vesicle biogenesis, and for

interaction with the AAA ATPase Vps4 responsible for ESCRT disassembly. Together with an intricate network of auxiliary proteins, such as deubiquitinating enzymes, these ESCRT complexes bring about receptor incorporation into MVBs at the endosomal membrane (Figure 2). The constituent proteins of the ESCRT complexes are listed with equivalent yeast and human nomenclature in Table 1, along with some key domain features.

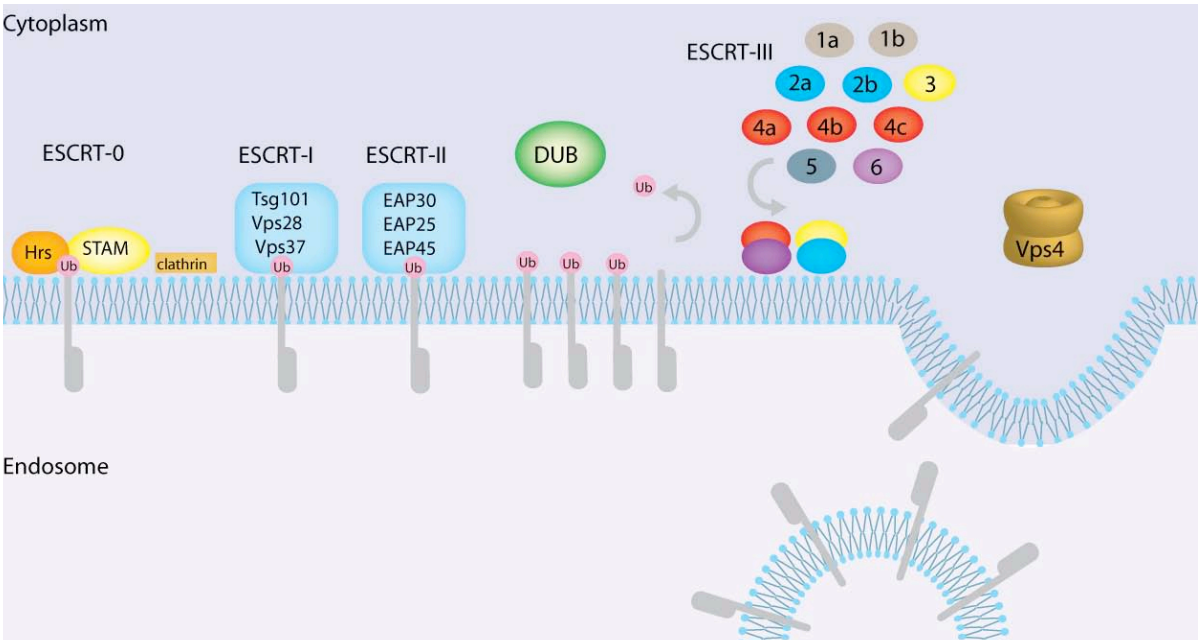

Figure 2. The cytosolic ESCRT complexes, ESCRT-0, -I, -II, -III are recruited to the endosomal membrane for receptor sorting.

The ESCRT machinery must be targeted to the endosomal membrane, recognise ubiquitinated receptors to be sorted, and instigate MVB biogenesis. ESCRT- 0, - I and -II recognize and anchor the target receptor at the membrane, ESCRT III packages the receptor into an inward budding vesicle for final ILV formation and interacts with accessory proteins like deubiquitinating enzymes and the AAA ATPase Vps4 responsible for ESCRT disassembly. Together with an intricate network of auxiliary proteins ESCRT complexes sort receptors for degradation.

0.3 ESCRT-0

ESCRT- 0 is composed of Hrs (hepatocyte growth factor-regulated tyrosine kinase substrate), STAM (signal-transducing adaptor molecule), and Eps15 (epsin-15). The Hrs/STAM/Eps15 complex is the initiator of MVB biogenesis, providing the first anchor point to the endosomal membrane through the endosome-specific PI(3)P (phosphatidylinositol3-phosphate) lipid binding motif FYVE (Fab1, YGL023, Vps27, and EEA1) of Hrs (Gaullier et al. 1998) (Bache et al. 2003).

	Human	Yeast	Domains /Features
ESCRT-0	Hrs	Vps27	FYVE, UIM
	STAM	Hse1	UIM, VHS,SH2
ESCRT-I	Tsg101	Vps23	UEV
	Vps28	Vps28	
	Vps37	Vps37	
	Mvb12		Ubiquitin-binding motif
ESCRT-II	EAP30	Vps22	
	EAP20	Vps25	
	EAP45	Vps36	GLUE
ESCRT-III	CHMP1A, 1B	Did2	MIM
	CHMP 2A, 2B, 2C	Vps2	MIM
	CHMP3	Vps24	MIM
	CHMP 4A, 4B	Snf7	MIM
	CHMP5	Vps60	
	CHMP6	Vps20	
	CHMP7		MIM
	hIST1		MIM1, MIM2
Associated proteins	Vps4A, Vps4B	Vps4	AAA ATPase
	ALIX, HD-PTP	Bro1	
	UBPY/USP8, AMSH/STAMBP, AMSH-LP	Doa4	Deubiquitinating enzyme

Table 1. Constituent proteins of each ESCRT complex are listed with the equivalent human and yeast nomenclatures, along with key domain features.

Monoubiquitinated receptors are recognized by the Ubiquitin Interacting Motif (UIM) of Hrs (Shih et al. 2002), and the UIM and VHS (Vps27/Hrs/Stam) domain of STAM (Bache et al. 2003)(Mizuno et al. 2003)(Hong et al. 2009). Hrs is a 540 kDa hexamer (Pullan et al. 2006), binding two ubiquitin molecules per monomer via a unique, double-sided UIM (Hirano et al. 2006), giving a total of 12 ubiquitin binding sites. The yeast homologue of Hrs, Vps27p, contains two UIMs, and the crystal structure of the second of these revealed that whilst Vps27p UIM2 is a monomeric helix in solution, the ubiquitin complex structure had formed a four-helix bundle (Fisher et al. 2003). Oligomerisation of ubiquitin binding proteins could explain how high affinity can be obtained through collective low ubiquitin affinity motifs (K_d

0.1 – 1mM) (Fisher et al. 2003). Similarly, each ubiquitin subunit of K63-linked diubiquitin can bind a UIM, so polyubiquitin chains binding several UIMs can increase affinity (Varadan et al. 2004).

Hrs also binds the clathrin coat of the endosomal membrane through a clathrin binding box at its C-terminal, thus stabilising the ubiquitinated receptor at the endosomal membrane and preventing its recycling back to the plasma membrane (Pullan et al. 2006). Finally, through the interaction of the UEV (ubiquitin E2 variant) domain of Vps27 (Hrs) with Vps23 (Tsg101), Hrs recruits the ESCRT-I complex (David J Katzmann et al. 2003).

0.4 ESCRT-I and ESCRT-II

The ESCRT-I complex was first established as a cytosolic heterotrimeric complex composed of Vps37, Vps28 and Tsg101 (Vps23 in yeast). Recognition of ubiquitinated cargo is through the ubiquitin E2 variant domain (UEV) of Vps23 (D J Katzmann et al. 2001). The highly basic N-terminal of Vps37 orients ESCRT-I on the membrane through endosomally enriched lipid phosphatidylinositol 3-phosphate (PI3P) interaction. Vps23 and Vps37 interact through a hydrophobic packing interaction, as do Vps23 and Vps28, with no direct contact made between Vps37 and Vps28 (Kostelansky et al. 2006)(Kostelansky et al. 2007). Later a fourth subunit, Mvb12, was identified (Oestreich et al. 2007)(Morita, Sandrin, Alam et al. 2007), interacting with Vps23 and Vps37, but not Vps28, and also containing a novel ubiquitin-binding motif (Shields et al. 2009). Both the ternary and quaternary complex has a 1:1:1:1 stoichiometry (Kostelansky et al. 2006)(Kostelansky et al. 2007).

ESCRT-II consists of one copy of EAP30 (Vps22) and EAP45 (Vps36), and two copies of EAP20 (Vps25), with two PPXY motifs of Vps25 contacting Vps22 and Vps36 (Teo et al. 2004)(Im & Hurley 2008). The NZF (npl4 zinc finger) ubiquitin binding domain of the Vps36 GLUE (GRAM-like ubiquitin binding in EAP45) domain binds to the C-terminal of Vps28 (Kostelansky et al. 2006), whilst ESCRT-II targeting to the endosomal membrane is carried out by the GLUE domain in concert with an N-terminal helix of Vps22 interacting with PI3P of the membrane (Im & Hurley 2008).

0.5 ESCRT-III

ESCRT-III in humans is composed of 11 Charged Multivesicular Body Proteins (CHMPs), CHMP1A and 1B, CHMP2A and 2B, CHMP3, CHMP4A, 4B and 4C, CHMP5, and CHMP6, all around 220 amino acids in length. CHMP7 was discovered later, being twice as many amino acids in length than the other CHMPs, and described to have greatest similarity with CHMP6, binding CHMP4B as CHMP6 does (Horii et al. 2006). Recently an eighth member, hIST, was identified as an ESCRT-III member isoform, binding to both ESCRT-I and CHMP1A and CHMP1B of ESCRT-III (Agromayor et al. 2009)(Bajorek, Schubert et al. 2009). Where appropriate, use of the yeast ESCRT-III homologues in described experiments is indicated in brackets.

CHMP6 is N-myristoylated, providing a membrane anchor for CHMP6 (Markus Babst et al. 2002). The N-terminal portion of CHMP6 binds to EAP20 (Vps25) of ESCRT-II and CHMP4B of ESCRT-III independent of N-myristoylation (Teo et al. 2004)(Yorikawa et al. 2005)(Im et al. 2009), providing a second independent point of recruitment to the endosomal membrane.

The CHMP proteins are characterized by a distinct charge polarization; a basic N-terminal portion of pI ~10 and an acidic C-terminal portion of pI ~4, the N-terminal region spanning a greater proportion of the overall molecule. In 2006 the first structure of an ESCRT-III protein was released, that of the basic N-terminal portion of CHMP3, revealing a four helix bundle composed of a long helical hairpin and two shorter helices, with a further C-terminal helix extending out perpendicular to the core (Figure 3A)(Muzioł et al. 2006). The recent structure of hIST1 residues 1-189 asks a reinterpretation of the data of Muziol et al (Bajorek, Schubert et al. 2009). Here, the fifth helix is assigned in a cis position, rather than in trans in Muziol et al.'s structure (Figure 3E and Figure 3F). The presence of two extra helices, termed αA and αB show the link between helix 4 and helix 5, thus leading to the repositioning of helix 5. However, although the structure of hIST1 allows us to position a small fragment of a C-terminal helix in relation to the rest of the basic N-terminal domain, helping to speculate about the location of the rest of the C-terminal domain in relation to the N-terminal domain, structural data of an intact CHMP protein is lacking.

Electrostatic potential maps identified a very basic charged exposed surface as a possible membrane interface within the CHMP3 structure (Figure 3B)(Muzioł et al. 2006). Mutation of key basic residues within this interface redistributed CHMP3 from predominantly plasma membrane and vesicular localization to the cytosol, implicating these residues in targeting of CHMP3 to endosomal membranes. The differential conservation of key basic residues

within this interface in the CHMP proteins suggests indirectly individual preferences for membrane composition between the human CHMP members. This orientation to the membrane would leave the other very acidic charged surface exposed on the opposite side. This is the surface where the final C-terminal of CHMP3 is speculated to be located, and would show how CHMP3 is orientated on the membrane to allow access of binding partners to its final C-terminal helix.

Two dimer interfaces were identified in the CHMP3 crystal structure, one from dimerisation of CHMP3 during crystallisation (Figure 3C), and the other formed by the crystal packing (Figure 3D). Mutation of the dimer interfaces relocated CHMP3 to a predominantly cytosolic location in cells, showing the dimer interfaces are important in CHMP3 targeting to endosomes. Conservation of dimerisation residues between CHMP3 and CHMP2 suggests heterodimers could form in the same manner as the homodimers seen in the crystal structure.

CHMP2 (Vps2), CHMP3 (Vps24), CHMP4 (Snf) and CHMP6 (Vps20) form large heterooligomeric complexes when membrane bound, including distinct subcomplexes of CHMP2/CHMP3 (Vps2/Vps24), and CHMP4/CHMP6 (Snf7/Vps20). The presence of the CHMP2/CHMP3 (Vps2/Vps24) subcomplex is required for the interaction with the CHMP4/CHMP6 (Snf7/Vps20 subcomplex. In solution CHMP2 (Vps2) and CHMP3 (Vps24) do not interact, but CHMP2 (Vps2) and CHMP3 (Vps24) co-dependantly localise to the endosomal membrane (Markus Babst et al. 2002). CHMP6 (Vps20) co-localisation to endosomal membrane bound CHMP4 (Snf7) is dependent on CHNP3 (Vps24), and CHMP2 (Vps2) and CHMP3 (Vps24) membrane localization is also dependant on the presence of CHMP4 (Snf7) and CHMP6 (Vps20) (Markus Babst et al. 2002). CHMP4 (Snf7) endosomal localisation is dependant on CHMP6 (Vps20), but the inverse is not true. Thus although there are individual interactions of the subunits with the endosomal membrane, this is much enhanced through cooperative binding of ESCRT-III proteins with the membrane. Overexpression of individual subunits does not increase their incorporation into the complex as compared with other subunits, suggesting an equimolar stoichiometry at the endosomal membrane.

The C-terminal domain of CHMP proteins interacts with their own N-terminal domain and this has been proposed as a mechanism of autoinhibition (Zamborlini et al. 2006). Removal of the C-terminal portion to mimic activated CHMP proteins produces polymers upon incubation with the respective CHMP binding partner; CHMP2 with CHMP3, and CHMP1 with hIST1. The CHMP membrane-binding surface is presented on the external face of the

tubule, indicating how CHMP polymerisation on the inside of a membrane deformation could induce vesicle formation (Lata, Schoehn et al. 2008)(Bajorek, Schubert et al. 2009). Out of CHMP3 and CHMP2 only C-terminally truncated CHMP2A polymerised alone, forming ring structures instead of tubes (Lata, Schoehn et al. 2008). Purifying Vps24, the yeast homologue of CHMP3, above concentrations of 10 mg/mL *in vitro* can induce polymer formation, but again the same phenomenon was not observed for the human CHMP3 protein (Ghazi-Tabatabai et al. 2008). CHMP4 (Snf7) spontaneously polymerises at the endosomal and plasma membranes when over-expressed, with membrane curvature away from the cytoplasm observed when CHMP4 is expressed without the C-terminal autoinhibitory domain (Hanson et al. 2008). A new proposal from the Emr group, based on their work with the yeast ESCRT-III homologues, pushes CHMP4 (Snf7) as the key building block for ESCRT-III polymers, where CHMP6 (Vps20) serves to anchor the CHMP4 (Snf7) polymer at the endosomal membrane, and Vps25 of ESCRT-II binding to CHMP6 (Vps20) on the membrane invokes a conformational change that could be interpreted as an activation event (Saksena et al. 2009). Both CHMP4 (Snf7) and CHMP6 (Vps20) demonstrated a conformational change in response to membrane binding, supporting evidence for membrane-stimulated activation of CHMP proteins.

CHMP4 (Snf7) and CHMP6 (Vps20) accumulate on the endosomal membrane in the absence of CHMP2 (Vps2) and CHMP3 (Vps24), implicating the CHMP2/CHMP3 (Vps2/Vps24) subcomplex in recruitment of Vps4 for ESCRT-III disassembly (M Babst et al. 1998)(Markus Babst et al. 2002). Vps4B was shown to disassemble *in vitro* polymer tubes of C-terminally truncated CHMP2A and full-length CHMP3 in the presence of ATP and Mg^{2+}, binding within the central cavity of the tube via the intact C-terminal domain of CHMP3 (Lata, Schoehn et al. 2008). In the yeast Vps24 (yeast homologue to CHMP3) filaments, Vps4 had no effect on polymer tube diassembly except when the C-terminal domain of Vps24 was replaced with the C-terminal domain of Vps2 (yeast homologue to CHMP2), further indicating a specific role for CHMP2 in the recruitment of Vps4 to the CHMP2/CHMP3 heterodimer, at least in the yeast system (Ghazi-Tabatabai et al. 2008). According to the Emr group's model, the CHMP2/CHMP3 (Vps2/Vps24) subcomplex is postulated to cap CHMP4 (Snf7) polymerisation before recruitment of Vps4 by CHMP2 (Vps2) disassembles CHMP polymers (Teis et al. 2008)(Saksena et al. 2009). The capacity of three ESCRT subunits, CHMP6 (Vps20), CHMP4 (Snf7) and CHMP3 (Vps24) to achieve membrane scission was finally demonstrated by the Hurley lab early this year, defining the role of CHMP2 (Vps2) to be after polymerisation to recruit Vps4 for CHMP polymer disassembly (Wollert et al. 2009).

There is a strong accumulation of evidence that CHMP proteins CHMP3, CHMP4 and CHMP6 are responsible for vesicle formation and scission, with CHMP tubule formation elucidating how CHMP proteins may form and close the pinching neck of a budding vesicle; polymer formation deforms the membrane into a vesicle, and subsequent recruitment by CHMP2 of Vps4 releases CHMP subunits and closes the neck. *In vivo* it is likely other adaptor proteins are involved to carefully regulate the morphology and timing of this process. ALIX (ALG-2 interacting protein X) forms crescent shaped dimers that bind to CHMP4 polymers and is speculated to serve as a scaffold for membrane remodelling (Pires et al. 2009).

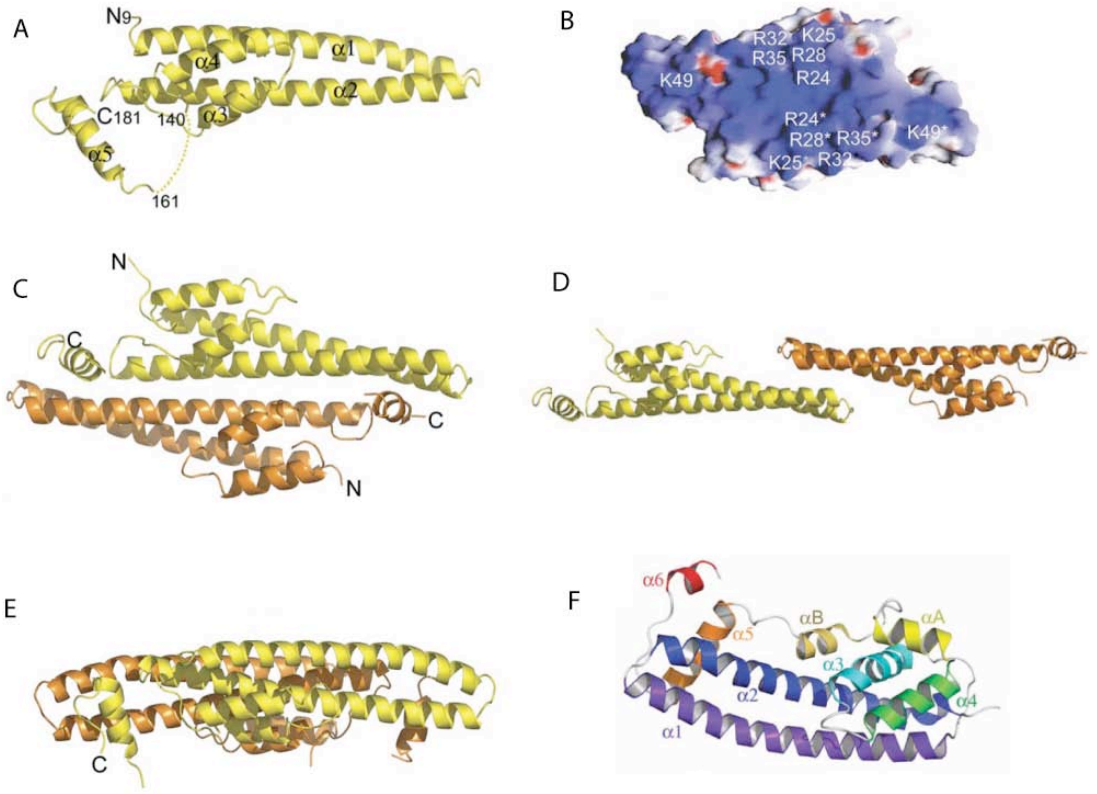

Figure 3. Crystal structure of dimeric CHMP3$^{9-183}$ and hIST1$^{1-189}$.

A. Crystal structure of CHMP$^{9-183}$. Ribbon representation of the four helices bundle constituting the CHMP$^{9-183}$ monomer. A fifth helix is portrayed packing perpendicularly to the helical bundle, the linking disordered loop represented by a dashed line.

B. Electrostatic potential map of CHMP$^{9-183}$ dimer 1. The basic surface exposed on one side of the dimer mediates CHMP3 targeting to the membrane and is required for efficient retroviral budding.

C. Ribbon representation of the CHMP3$^{9-183}$ dimer. The antiparallel dimerisation interface is mainly mediated by the long helical hairpin.

D. A second dimerisation interface via the tips of the helical hairpins arises from the crystal lattice.

E. Side view of the first dimer interface. The perpendicular packing of the fifth helix to the helical hairpin tips is highlighted.

F. Ribbon diagram and helix nomenclature for hIST1$^{1-189}$ structure.

Adapted from (Muziol et al. 2006)(Bajorek, Schubert et al. 2009).

0.6 Interaction of ESCRT-III with MIT domain-containing proteins – the MIT-MIM interaction

The AAA (ATPase Associated with various cellular Activities) ATPase Vps4, catalyses dissociation of ESCRT-III complexes. Human Vps4, composed of subunits Vps4A and Vps4B, associates into a bowl-shaped dodecamer of two stacking hexameric rings (Yu et al. 2008).

It was the structure of the MIT (Microtubule Interacting) domain of Vps4A that gave the first clues to how MIT domain - CHMP interactions are mediated. The Vps4A MIT domain consists of a three-helix bundle reminiscent of a classical TPR (tetratricopeptide) motif. Through alanine mutation studies Scott et al discovered a highly conserved leucine residue responsible for CHMP1B binding (Scott et al. 2005). In a classical TPR motif this leucine residue would be responsible for binding of the fourth helix, which led the authors to postulate that CHMP binding through the C-terminal helix may act to complete the TPR motif. In 2007 the structures of yeast Vps4 in complex with Vps2 (yeast homologue to CHMP2), Vps4A in complex with CHMP1B, and Vps4B in complex with CHMP2B, revealed that a CHMP C-terminal peptide, comprising the last 20 residues of the C-terminal, binds to the Vps4 MIT domain to complete the TPR motif, with the orientation of the CHMP C-terminal helix being in the opposite direction (Stuchell-Brereton et al. 2007)(Obita et al. 2007), with the consensus LXX+LAAL+ sequence required for Vps4 binding termed the MIT Interacting Motif (MIM).

The structure of CHMP1B in complex with spastin MIT identified another binding interface in the MIT domain (Yang et al. 2008), using helices 1 and 3 of the three-helix bundle, in contrast to helices 2 and 3 of the Vps4 MIT. Interestingly, spastin has unique specificity for CHMP1B, showing no binding even to its closest homologue CHMP1A (Yang et al. 2008), with several key residues non-conserved between the two proteins. The interaction is one of higher affinity than previous measurements binding CHMP1B to the MIT domain of Vps4, with K_d 12 μM compared to 33 μM for Vps4 (Stuchell-Brereton et al. 2007). Although both the Vps4 and spastin interaction with CHMP1B are predominantly hydrophobic in nature, an increase in affinity of spastin for CHMP1B can be explained by a larger buried surface area.

The affinity of binding of full-length CHMP6 is comparable with that of the CHMP1B Vps4 interaction, but optimal binding is achieved by deleting CHMP6 down to a 165−181 fragment (removing the MIM consensus sequence) resulting in a K_d 5.8 μM (Kieffer et al. 2008). The identification of key interaction residues further towards the N-terminal of the C-terminal domain of CHMP6 prompted the authors to term this motif the MIM2 sequence. The NMR

solution structure of a Vps4A MIT CHMP6$^{166-181}$ MIM2 complex shows binding between helices 1 and 3 of the MIT domain, the same binding arrangement seen for the CHMP1B spastin complex, but clearly demonstrating different sequence specificity determination. Intriguingly, a recent paper showed that hIST1 contains both MIM1 and MIM2 domains (Bajorek, Morita et al. 2009), thus the presence of two MIM domains in some CHMP proteins may create varying affinities for MIT domains.

0.7 Recruitment of Deubiquitinating enzymes (DUBs)

Ubiquitin recovery from ubiquitinated receptors before inclusion into MVBs is an important prerequisite for maintaining the cellular ubiquitin pool. In yeast the ubiquitin thioesterase Doa4 was identified responsible for removing the ubiquitin moieties through studies of *doa4* mutants. Cellular ubiquitin levels were found depleted in Doa4 mutants, an effect alleviated by mutations in endosomal sorting components (Amerik et al. 2000). It is not clear how Doa4 is recruited to the endosomal membrane, either directly through CHMP protein interaction, or via binding to Bro1 (Bowers et al. 2004).

ALIX, a Bro1 domain containing protein, was initially proposed as the human homologue of yeast Bro1, yet it was whilst investigating ALIX depletion effects on receptor sorting that another Bro1 domain-containing protein, His-domain containing protein tyrosine phosphatase (HD-PTP), was identified as functionally required for sorting (Doyotte et al. 2008). Like ALIX, HD-PTP binds CHMP4B of ESCRT-III and TSG101 of ESCRT-I (Ichioka et al. 2007). Later there was even found a third Bro1 domain-containing protein called Brox, also capable of interacting with CHMP4 (Ichioka et al. 2008). The structure of ALIX in complex with C-terminal fragments from CHMP4A, CHMP4B and CHMP4C shows how the arrangement of hydrophobic residues in the C-terminal domain of CHMP4 proteins, in particular the conserved Trp220, confers Bro-1 domain specificity in CHMP4s, in contrast to the MIT domain preference of CHMPs 1-3 (McCullough et al. 2008). This interaction showed an affinity comparable with that of Vps4 CHMP interactions of 44 ±6 μM for ALIX (Bro1 V domain) construct with CHMP4A$^{205-222}$. This adds another dimension to the ESCRT machinery; different CHMP proteins recruit different accessory effecter molecules.

So far three candidate DUBs have been identified as interacting with the ESP; AMSH (Associated Molecule of the SH3 domain of STAM), AMSH-LP (AMSH-like protein) and UBPY/USP8 (ubiquitin-specific processing protease Y). UBPY is a 1118 amino acid ubiquitin thioesterase, binding to the same SH3 domain motif of STAM as AMSH (M Kato et al. 2000),

and CHMP 1A, CHMP1B and CHMP7 of ESCRT-III (Row et al. 2007). In contrast to AMSH, UBPY shows no discrimination between K-48 linked and K-63 linked ubiquitin chains, and does not bind to CHMP3 (Row et al. 2006)(Row et al. 2007).

AMSH-LP, as the name suggests, contains similar features to that of AMSH; it is a 436 amino acid protein containing a C-terminal JAMM domain. One distinct difference is the replacement of an essential Lysine residue in the SBM of AMSH by a threonine in AMSH-LP (residue 250), meaning AMSH-LP no longer binds STAM (Kikuchi et al. 2003). AMSH-LP was confirmed to interact with clathrin, as does AMSH (Nakamura et al. 2006), but contrastingly does not bind CHMP1A, CHMP1B, CHMP2A or CHMP3 (Agromayor & Juan Martin-Serrano 2006). In 2008 the structure of the JAMM domain of AMSH-LP was published, both alone and in complex with Lys-63 linked di-ubiquitin, revealing the structural basis for selective hydrolysis of Lys-63 linked ubiquitin chains (Y. Sato et al. 2008).

0.8 AMSH domain architecture and binding partners

AMSH, also known as STAM Binding Protein (STAMBP), is a 424 amino acid protein expressed in all mammalian tissues, which as the name suggests was first identified as a binding partner of STAM of ESCRT-0 (N Tanaka et al. 1999). Since then it has been shown to bind the N-terminal domain of clathrin heavy chain (McCullough et al. 2006)(Nakamura et al. 2006) and a range of CHMPs of the ESCRT-III complex: CHMP1A, CHMP1B, CHMP2A, and CHMP3 (Agromayor & Juan Martin-Serrano 2006), CHMP4B (and weakly CHMP4A) (Tsang et al. 2006), and hIST (Agromayor et al. 2009). It is interesting to observe AMSH binding to both CHMPs 1-3 and CHMPs 4 in light of McCullough et al.'s suggestion of segregation between CHMP 1-3 binding to MIT domains and CHMPs 4 to Bro1 domains, and there are still conflicts in the literature over the solidity of AMSH's interaction with CHMP4A and CHMP4B, with pull-down assays showing the C-terminal of CHMP4B does not interact with AMSH (Zamborlini et al. 2006).

STAM binding is through a centrally located proline rich STAM-binding motif (SBM) PXXXRXXKP (Figure 4)(M Kato et al. 2000). A bipartite nuclear localization signal of KR[YTKEYTEYNEE]KKK is located in residues 112-127 of the N-terminal, and is required for nuclear localization of AMSH (Figure 4) (N Tanaka et al. 1999)(Kikuchi et al. 2003).

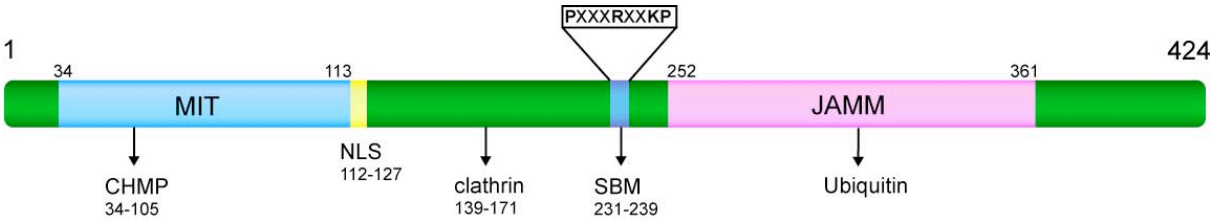

Figure 4. AMSH domain architecture.

A central proline rich motif, including a critical lysine residue, is required for STAM binding (SBM). At the N-terminal a MIT domain mediates CHMP interactions. Deubiquitinating activity is provided by a zinc-binding JAB-MPN motif at the C-terminal. A bipartite nuclear localisation signal targets AMSH to the nucleus, and a clathrin interaction domain has also been identified between residues 139 and 171.

Immunoprecipitation and subsequent pull-down assay identified clathrin heavy chain (CHC) interacting with AMSH (Nakamura et al. 2006)(McCullough et al. 2006). Deletion mutants highlight residues 139-171 of AMSH responsible for CHC binding (Figure 4) (Nakamura et al. 2006). Deletion of the clathrin binding site, as well as RNA interference depletion of CHC, prevents AMSH targeting to endosomes, but deletion of the SBM from AMSH failed to affect its localization to endosomes, highlighting a STAM-independent recruitment of AMSH to the endosomal membrane by clathrin anchoring (Nakamura et al. 2006). STAM also binds CHC, and along with Hrs' capacity to bind clathrin, a tripartite binding of clathrin by AMSH and ESCRT-0 is proposed as an initial anchor point for endosomal sorting (McCullough et al. 2006).

Database alignments identify in the AMSH C-terminal a JAB_MPN zinc-binding metalloprotease domain displaying the capacity to hydrolyse tetraubiquitin chains *in vitro* (Figure 4). A clear preference for K-63 linked chains over K-48 chains is observed, signalling an association of AMSH with non proteosome-linked ubiquitin regulated pathways (McCullough et al. 2006). A D348A mutation abolishes catalytic activity, probably by removing zinc binding as this aspartic acid lies within an EX_NHS/THX_7SXXD zinc binding motif (Tran et al. 2003)(Ambroggio et al. 2004). The *in vitro* deubiquitinating activity of AMSH is enhanced in the presence of STAM, but unaffected upon incubation with CHMP3 (McCullough et al. 2006). AMSH can simultaneously interact with STAM and CHMP3, providing a temporal connection between an efficient deubiquitinating activity of AMSH and CHMP binding (McCullough et al. 2006).

AMSH binds CHMP3 independantly of the JAB_MPN domain and SBM, requiring residues 1-191 of the N-terminal domain for this interaction (Agromayor & Juan Martin-Serrano 2006) (Tsang et al. 2006). Sequence homology analysis of the Vps4 MIT domain with AMSH identified an AMSH MIT domain spanning residues 34-113 (Tsang et al. 2006). Important sequence discrepancies between Vps4 and AMSH MIT domains, such as the lack of conservation of a key leucine residue (Leu64) required for optimal CHMP1B binding by Vps4 suggest a sequence based mechanism for diffferential CHMP binding by MIT containing proteins (Scott et al. 2005)(Tsang et al. 2006).

0.9 Suggested mechanisms for AMSH in Endosomal Sorting

The role of AMSH within the endosomal sorting pathway has yet to be determined, with conflicting evidence supporting several roles presented in the literature.

AMSH could act as a negative regulator, with the potential to 'rescue' ubiquitinated receptors (McCullough et al. 2004). This is supported by short-interfering RNA experiments, where knockout of AMSH results in increased EGF receptor degradation, and by the *in vitro* deubiquitination of ubiquitinated EGF receptors by AMSH (McCullough et al. 2004). In this model, AMSH would serve to oppose the action of the E3 ligases responsible for ubiquitination, where an increase in AMSH activity would shift the balance towards receptor recycling and a decrease in the degradation fate.

Initially UBPY was proposed as the negative regulator of the ESP. RNA interference depletion of UBPY accelerated degradation of EGF receptors, whilst over expression of UBPY reduced EGF receptor levels of ubiquitination and delayed EGF receptor degradation in EGF stimulated cells (Mizuno et al. 2005). Row et al. also found that ubiquitinated proteins accumulate on endosomes when catalytically inactive UBPY was over expressed, and siRNA treatment of UBPY increases total levels of ubiquitinated protein, but the observation that free cellular levels of ubiquitin remained unchanged led them to investigate whether UBPY may be acting as a regulator of the ubiquitination of endosomal components rather than endosomal cargo, for ubiquitination is also the mechanism for degradation of the ESP proteins. A subsequent depletion of STAM in UBPY knockdown cells, coupled with the recovery of ubiquitinated STAM in proteosome inhibited cells led them to conclude that UBPY may be regulating STAM polyubiquitination and targeting for proteosomal degradation, a theory concurring with UBPY processing of K-48 linked ubiquitin chains and a

later report by Mizuno et al. that Eps15, an ESCRT-0 associated protein, is a substrate for UBPY (Row et al. 2006)(Mizuno et al. 2006).

AMSH could be responsible for removing the ubiquitin signal from the cargo just before incorporation into vesicles in a role analogous to that of Doa4 in the yeast ESP. This theory is supported by the accumulation of ubiquitinated cargo and the block of EGF receptor degradation when catalytically inactive AMSH^{D348A} is expressed (Kyuuma et al. 2007)(Agromayor & Juan Martin-Serrano 2006), and also correlates with *in vitro* deubiquitination of ubiquitinated EGF receptors by AMSH (McCullough et al. 2004). Further evidence supporting this proposed role of AMSH is presented in the following section, which analyses data from studies of endosomal sorting components in retroviral budding studies.

0.10 The ESCRT machinery in HIV budding

Interest in the ESCRT protein machinery was heightened by the discovery that components of the ESP protein machinery are required for budding of enveloped retroviruses such as HIV. Enveloped viral particle budding can be considered topologically similar to that of MVB formation, both processes involving a deformation of membrane away from the cytosol (Figure 5). Much of the work done to characterize the functions of ESCRT proteins has exploited viral budding as a way of following functionality of the ESP.

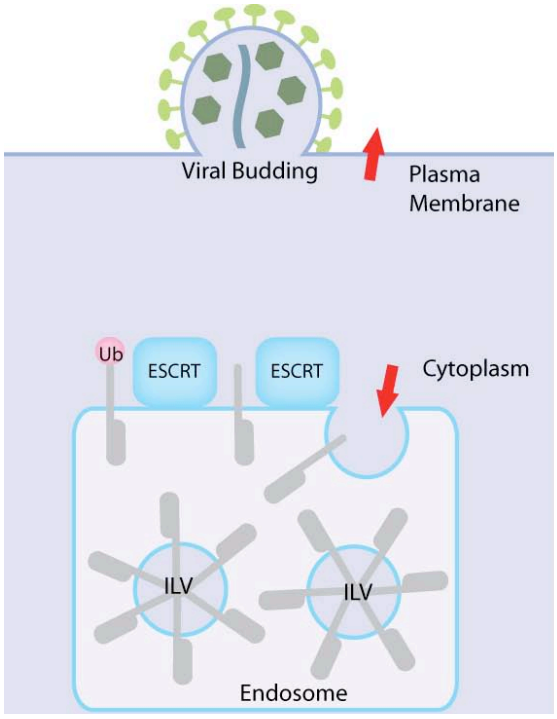

Figure 5. Enveloped viral budding is topologically similar to MVB biogenesis, both processes requiring a deformation of membrane away from the cytosol.

For retroviral virions to egress from the infected host cell, they require late assembly (L) domains located within gag, the *gag* gene product (H G Göttlinger et al. 1991). In HIV, the PTAP and LYPXL motifs of the p6 region of gag are responsible for recruiting TSG101 of ESCRT-I and ALIX respectively (Garrus et al. 2001)(J Martin-Serrano et al. 2001)(Bettina Strack et al. 2003), TSG101 in turn recruiting Vps28 to the site of viral budding (Juan Martin-Serrano et al. 2003). This is the same PTAP motif used by Vps27 (Hrs) of ESCRT-0 to contact Vps23 (TSG101) of ESCRT-I, showing clearly how the virus mimics the ESP to hijack components (Kostelansky et al. 2006).

Retroviruses also use ubiquitination to mimic the ESP, with ubiquitinated gag found in viral particles of HIV, SIV (Simian Immunodeficiency Virus) and MLV (Murine Leukemia Virus)(Ott et al. 1998). The p6 PTAP and PPXY motifs are critical for ubiquitination of gag, with PPXY recruiting HECT E3 ubiquitin ligases for conjugation of ubiquitin to HIV gag (B Strack et al. 2000). However, somewhat contradictorily, increased viral release correlates with decreased levels of ubiquitinated gag, suggesting deubiquitination by DUBs is required before gag incorporation and virion release, a hypothesis supported by the observation of little ubiquitinated gag found in released viral particles (Juan Martin-Serrano 2007).

CHMP3 membrane targeting is important in efficient retroviral budding (Muzioł et al. 2006). Deletions into the C-terminal domain, which would remove the autoinhibitory binding to CHMP3 N-terminal, convert CHMP3 into a dominant-negative inhibitor of HIV-1 budding. The same effect is seen with incubation of AMSH with full-length CHMP3, with stronger inhibition occurring upon incubation with a catalytically inactive $AMSH^{D348A}$ mutant, an effect abolished by point mutations in the CHMP3 binding site of AMSH (Zamborlini et al. 2006). AMSH was also observed to bind more strongly to CHMP proteins when catalytically inactive (Agromayor & Juan Martin-Serrano 2006). Expression of $AMSH^{D348A}$ inhibits retroviral budding in a dominant-negative manner and induces the accumulation of ubiquitinated HIV and MLV gag, yet AMSH is non-essential for viral budding as was shown by knockdown studies (Agromayor & Juan Martin-Serrano 2006). Inhibition of retroviral budding by $AMSH^{D348A}$ was unaffected by deletion of the STAM binding site, correlating with data that the function of STAM binding is to enhance AMSH catalytic activity and supporting an ESCRT-III related effect of the $AMSH^{D348A}$ mutant on retroviral budding (Agromayor & Juan Martin-Serrano 2006)(McCullough et al. 2006). Finally, CHMP3 binding is not required for AMSH's *in vitro* deubiquitinating activity, but *in vivo* expression of an AMSH mutant lacking CHMP3-binding ability ($AMSH^{83-424}$) resulted in accumulation of ubiquitinated cargo on aberrant endosomes (Kyuuma et al. 2007). These findings suggest AMSH activates CHMP3 through release of the autoinhibition mechanism, and show how the deubiquitinating

activity of AMSH affects endosomal receptor degradation and viral budding in a CHMP3 dependant manner, with both CHMP3 binding and enzymatic activity required for efficient endosomal sorting.

The requirement of CHMP3 binding for the endosomal deubiquitinating activity of AMSH combined with evidence AMSH activates CHMP3 by relieving its autoinhibitory state, suggests AMSH's deubiquitinating activity is localised towards the latter stages of the endosomal sorting pathway in concert with CHMP3 activation and involvement in vesicle formation, which would correspond to a role in removal of ubiquitin from receptors just prior to their incorporation into MVBs.

0.11 A New Role for ESCRT in Cytokinesis

In 2007 a new role for ESCRT proteins was demonstrated in cytokinesis (Carlton & Juan Martin-Serrano 2007). CHMP3 of the ESCRT-III complex was shown to localize at the midbody and be functionally required (Morita, Sandrin, Chung et al. 2007)(Dukes et al. 2008), whilst CHMP1B is required for spastin recruitment to the midbody for microtubule severation (Yang et al. 2008). CHMP1A is also required for cell abscission, as is its interaction with its heterodimeric partner hIST, suggesting CHMP polymerization is required (Agromayor et al. 2009) (Bajorek, Morita et al. 2009)(Bajorek, Schubert et al. 2009).

This is not the first time the CHMP proteins have been implicated in subnuclear processes. In 2001 Stauffer et al. reported localisation of CHMP1A to the nucleus as well as the cytoplasm through a bipartite nuclear localization signal (residues 20-35), and overexpresson of CHMP1 arrested cells in S-phase, indicating two parallel roles for CHMP1 in cytoplasmic endosomal sorting, and nuclear gene regulation. Interestingly, CHMP1A was also shown to recruit the polycomb repressor ring finger protein BMI1 (Stauffer et al. 2001).

Cellular distribution studies found AMSH predominantly in the cytoplasm, particularly localising to the proximity of the nuclear membrane (F. Itoh et al. 2001). Both DUBs AMSH and UBPY have since been shown to act during cytokinesis, with UBPY primarily at the midbody and AMSH shown to act at both the midbody and the midbody ring (Mukai et al. 2008). A relocalisation of ubiquitin during cytokinesis from the midbody to the midbody ring has been observed (Pohl & Jentsch 2008) and this could link in with the different location of these DUBs. Relocation of ubiquitin and thus localization of DUBs could sequentially mobilise associated proteins such as CHMPs to effectuate midbody ring constriction.

Aims and Objectives

The overall aim of the thesis work was to gain structural and functional data on AMSH. In particular, we wanted to elucidate the mechanism for interaction with CHMP3, investigating the proposition that AMSH activates CHMP3 for polymerisation. We also wanted to probe the function of the enzymatic domain and to interpret this activity in the context of the full-length protein. Here I present the objectives of the thesis work:

- To isolate soluble AMSH for crystallisation and structural studies.

- To verify CHMP3 binding to AMSH, to define the binding site on each molecule and assay the affinity of the AMSH CHMP3 interaction.

- To crystallise AMSH, or a defined CHMP3 binding domain, in complex with full-length CHMP3, in order to understand if AMSH could play a part in activation of CHMP3, and depending on the activation state crystallised, to gain information either on the arrangement of the CHMP3 C-terminal autoinhibitory domain to the N-terminal, or to determine how binding of AMSH could bring about CHMP3 activation.

- To define a soluble JAMM domain for structural studies in order to determine the structural basis of specificity for K-63 linked ubiquitin chains.

- To verify the deubiquitinating activity of AMSH, and to compare this with the activity of the JAMM domain alone.

Materials and Methods

Expression and Purification of MBP-tagged AMSH in E. coli.

The gene encoding for AMSH (BC007682) was PCR amplified and cloned by restriction digest with NheI / HindIII and T4 ligation into a pmalc2gTEV (EMBL) vector to create an N-terminal MBP fusion protein with TEV cleavage site. *E. coli* codonplus cells were transformed and used to initiate a pre-culture of 50 mL LB miller medium, 100 µg/mL Ampicillin and 34 µg/mL chloramphenicol. The pre-culture was added to 2 L Erlen flasks containing 1 L LB Miller medium, 100 µg/mL ampicillin and 34 µg/mL chloramphenicol and cultured at 37°C until an optical density at 600 nm of 0.8. The temperature was reduced to 16°C and 1ml of 1M IPTG added for overnight induction. Cells were collected by 15'centrifugation at 5000 rpm, and lysed by sonication in resuspension buffer 50 mM Tris pH 8.5, 100 mM NaCl, 5 mM betamercaptoethanol, one Roche complete EDTA-free protease inhibitor cocktail tablet. The supernatant was clarified by 30' centrifugation at 20 000 rpm and loaded onto an amylose column pre-equilibrated with 50 mM tris pH8.5, 100 mM NaCl, 5 mM betamercaptoethanol. The column was washed extensively with the same buffer and the MBP fusion protein eluted in 50 mM Tris pH8.5, 100 mM NaCl, 5 mM betamercaptoethanol, 10 mM maltose.

Expression and Purification of CHMP3$^{9-222}$ in E. coli.

N-terminal hexahis-tagged CHMP3$^{9-222}$ in a pProExHta plasmid was expressed in *E. coli* codonplus cells, inducing with 1ml of 1M IPTG, either for 3h at 37°C or o/n at 16°C. Cells were harvested and lysed by sonication in resuspension buffer (50 mM Tris pH 8.0, 100 mM NaCl, 5 mM betamercaptoethanol, one Roche complete EDTA-free protease inhibitor cocktail tablet). The supernatant was clarified by centrifugation and loaded onto a Chelating sepharose column (GE Healthcare) precharged with 100 mM $NiS0_4$. The column was washed with resuspension buffer, high salt buffers (1M NaCl / 1M KCl, 50 mM Tris pH 8.0, 5 mM betamercaptoethanol), resuspension buffer containing 20 mM imidazole and 50 mM imidazole, and then proteins were finally eluted with resuspension buffer plus 250 mM imidazole.

Expression and Purification of his-tagged AMSH in E. coli.

As for 'Expression and Purification of CHMP3$^{9-222}$ in E. coli', except his.AMSH elutes in the 20mM imidiazole wash, so only a 10mM imidazole wash was performed before elution in 250mM imidazole.

Expression and Purification of untagged AMSH in *E. coli*.

AMSH was PCR amplified and cloned into a pASK-IBA43plus vector using the restriction sites NheI and HindIII. Protein expression was in *E. coli* Rosetta cells, with 100 µg/ml ampicillin and 34 µg/mL chloramphenicol. Cells were grown at 37°C to an $O.D._{600\ nm}$ of 0.8, the temperature was reduced to 16°C and protein expression induced overnight with 400 µg anhydrous tetracycline. Cells were harvested and lysed by sonication in resuspension buffer 50 mM Tris pH 8.5, 25 mM NaCl, one Roche complete EDTA-free protease inhibitor cocktail tablet. After centrifugation at 20 000 rpm the clarified lysate was loaded onto a 30 mL self-packed Q-sepharose Biorad column. The column was washed extensively with resuspension buffer and then a salt gradient of 25 mM NaCl – 1M NaCl applied. By SDS-PAGE examination of the fractions, AMSH elutes early at >50 mM NaCl. The protein was concentrated by ultrafiltration (Amicon ultra 15) and loaded on to a Superdex™200 10/300 column (GE Healthcare), where it elutes ~12 mL.

Expression of AMSH in insect cells.

Protocols for general maintenance and manipulation of insect cells are taken from the Invitrogen manual 'Growth and Maintenance of Insect Cell Lines'. Sf21 and High Five™ cells were maintained in monolayer in Sf-900 II SFM supplemented with Foetal Bovine Serum (FBS) and Penicillin – Streptomycin 100 µg/ml, and passaged at confluency as required.

AMSH was introduced into insect cells using the Invitrogen Bac-to-Bac® Baculovirus Expression System. The gene for AMSH was PCR amplified and cloned by restriction digest with BsaI (NcoI) / HindIII and T4 ligation into the pFastBac™HT A vector to create an N-terminal hexahis-tagged protein with TEV cleavage site. The plasmid was then transformed into DH10Bac™ E-coli and plated on LB agar plates containing 50µg/mL kanamycin, 7µg/mL gentamycin, 10µg/mL tetracycline, 100µg/mL Bluo-gal (an alternative to X-gal) and 40µg/mL IPTG for blue/white selection. White colonies were then picked to inoculate a 5 mL liquid culture containing 50µg/mL kanamycin, 7µg/mL gentamycin, and 10µg/mL tetracycline and Bacmid DNA extracted by alkaline extraction according to the appendix of the Invitrogen Bac-to-Bac ® Baculovirus Expression System manual (page 51). Presence of the insert in the Bacmid DNA was verified by PCR using M13 forward and reverse primers as supplied by Invitrogen.

Transfection of insect cells was performed with two extracted bacmid DNA samples, according to the Transfection Procedure detailed in the Invitrogen Bac-to-Bac ® Baculovirus Expression System manual (page 28). Briefly, a confluent $75cm^2$ flask of SF21 cells in

monolayer was suspended in 20 mls of unsupplemented Sf-900 II SFM medium plus Penicillin – Streptomycin 100µg/mL and used to seed 2 ml per well of a 6 well plate (assuming the SF21 cell count of a confluent 75cm2 flask is 1.1 x 10^7, final SF21 cell number per well is 1.1 x 10^6). For each bacmid to be transfected, DNA:lipid complexes were prepared with three different ratios of bacmid:Cellfectin® Reagent; 5 µl:6 µl, 5 µl:10 µl, and 10 µl:6 µl. This gave a total of 6 transfections. Viral infection was followed by inspection under a light microscope and 6 P1 viral stocks were collected ~72 hours post-transfection.

For the P1 expression test, a confluent 75cm^2 flask of SF21 cells in monolayer was suspended in 20 mls of FBS-supplemented Sf-900 II SFM medium plus Penicillin – Streptomycin 100µg/mL and used to seed 2 ml per well of a 6 well plate (final SF21 cell number per well is 1.1 x 10^6). The P1 viral titres were assumed to be 1.6 x 10^6. For an initial expression test a multiplicity of infection (MOI) of 0.1 is recommended, MOI being the ratio between the number of virus particles and the number of cells to be infected. An inoculum volume of 110 µl per well was calculated based upon the following formula:

$$\text{Inoculum required (mL)} = \frac{\text{MOI (pfu / cell) x number of cells}}{\text{titer of viral stock (pfu / mL)}}$$

Cells were left for 30' to adhere to the well, the medium was removed and replaced with the 110 µl P1 virus inoculum and 690 µl medium; 800 µl of medium was added to the control well. After 1 hr the virus-containing medium was removed and replaced with fresh medium. After 72h, cells from each well were resuspended in the medium and pelleted in 2 mL eppendorf tubes by centrifugation at 500 g. The pellet was washed once with 1 mL PBS and resuspended in 100 µl of lysis buffer (50 mM NaCl, 20 mM Tris.HCl pH 8.5, 5 mM DTT, Roche complete EDTA-free protease inhibitor cocktail). Lysis was by three cycles of freeze / thaw between liquid nitrogen and a 37°C water bath and the soluble fraction was recovered by centrifugation at 12 000 g. The soluble and insoluble fractions were analysed by SDS-PAGE and Coomassie staining, and also by anti-His Western blotting.

P2 and P3 generations of virus were generated in SF21 cells, each time infecting with a MOI (multiplicity of infection) of 0.1 using an assumed viral titre of 1 x 10^6. A MOI value to be used with the P3 stock was determined empirically, assuming a viral titre of 1 x 10^7 pfu / mL. A confluent 75cm^2 flask of High Five™ cells in monolayer was suspended in 20 mls of FBS-supplemented Sf-900 II SFM medium plus Penicillin – Streptomycin 100µg/mL and used to seed 2 ml per well of a 6 well plate (assuming the High Five™ cell count of a confluent

75cm2 flask is 8 x 10^6, final High Five™ cell number per well is 8 x 10^5). Cells were infected at MOI values of 1, 2, 5, 10, and 20 and AMSH expression levels assayed after 48h by SDS-PAGE and anti-his Western blotting as described for the P1 expression test. For scale-up expressions, 150 cm^2 flasks of monolayer High Five™ cells were infected with P3 viral stock at a MOI of 2.

Purification of AMSH in insect cells

After 48h of infection, High Five™ cells were resuspended in medium and pelleted by centrifugation at 500 g. The pellet was washed with PBS before being resuspended in lysis buffer (150 mM NaCl, 50 mM Tris pH 8.5, 5 mM betamercaptoethanol) and lysed by sonication. Lysate was clarified by centrifugation at 20 000 rpm and hexahis-tagged AMSH extracted by metal affinity chromatography on a Ni-NTA column (Qiagen) (elutes in 10mM imidazole).

Expression and Purification of AMSH.CHMP3$^{9-222}$ complex in *E. coli*.

A pProExHta plasmid encoding N-terminal hexahis-tagged CHMP3$^{9-222}$ was provided by the host laboratory (W. Weissenhorn, UVHCI, Grenoble). 4 L of AMSH and 2 L of CHMP3$^{9-222,}$ were expressed in *E. coli* codonplus cells, inducing overnight at 16°C with 1mM IPTG. Cells were lysed by sonication in resuspension buffer (50 mM Tris pH 8.0, 100 mM NaCl, 5 mM betamercaptoethanol, one Roche complete EDTA-free protease inhibitor cocktail tablet), centrifuged, and the clarified supernatant loaded onto a Chelating sepharose column (GE Healthcare) precharged with 100 mM $NiS0_4$. The column was washed with resuspension buffer, high salt buffers (1M NaCl / 1M KCl, 50 mM Tris pH 8.0, 5 mM betamercaptoethanol), resuspension buffer containing 20 mM imidazole and 50 mM imidazole, and then proteins were finally eluted with resuspension buffer plus 300 mM imidazole. The eluted protein complex was loaded onto an amylose column, washed with resuspension buffer, and eluted with 10 mM maltose.

Expression and Purification of hisMBP-AMSH$^{1-206}$

AMSH was PCR amplified and cloned into a pBADM-41 vector to create an N-terminal hisMBP fused protein with TEV cleavage site. Expression and purification was as for MBP-tagged AMSH in *E. coli*, inducing protein over-expression with 0.02% L-Arabinose. The buffer NaCl concentration was diluted to 50 mM NaCl and loaded onto a 1 mL HiTrapQ (GE Healthcare) column. Extensive washing was followed by an applied salt gradient of 50 mM NaCl – 600 mM NaCl. Fractions containing soluble AMSH$^{1-206}$ were concentrated and run on a Superdex-200 column.

Expression and Purification of the AMSH$^{1-206}$ CHMP3$^{9-222}$ complex

MBP.AMSH$^{1-206}$ and CHMP3$^{9-222}$ were individually expressed and purified as above. To form the complex, CHMP3$^{9-222}$ was added in excess to MBP.AMSH$^{1-206}$, the complex TEV cleaved, and rerun on a Superdex-200 column to separate the complex from excess CHMP3$^{9-222}$ and uncleaved MBP.AMSH$^{1-206}$.

Expression and Purification of AMSH$^{235-424}$ construct

AMSH$^{235-424}$ was cloned into a pBADM-41 vector to create an N-terminal hexahis-MBP fused protein with TEV cleavage site. Purification was as 'Expression and Purification of AMSH in E. coli', inducing with 0.02% arabinose. The hexahis-MBP tag was cleaved off using 1:500 w/w Tobacco Etch Virus protease overnight at 4°C. The NaCl concentration was diluted to a final concentration of 50mM NaCl and loaded onto a MonoQ anionic exchange column, where the flowthrough containing the protein of interest was collected and the hexahis-MBP tag bound to the column. The flowthrough material was concentrated by ultrafiltration and loaded on to a Superdex 75 column, where fractions containing the pure protein of interest were pooled and concentrated by ultrafiltration.

Expression and Purification of AMSH$^{1-146}$ CHMP3$^{183-222}$ complex

AMSH$^{1-146}$ was cloned into a pProExHta vector to create an N-terminal hexahis-tagged protein with TEV cleavage site. CHMP3$^{183-222}$ was cloned in to pBADM-41 vector to create an N-terminal hexahis-MBP fusion protein with TEV cleavage site. AMSH$^{1-146}$ and CHMP3$^{183-222}$ were purified separately by Nickel-IMAC (CHMP3$^{183-222}$ elutes in the 50mM imidazole wash). Protein concentrations were determined by Bradford assay and CHMP3$^{183-222}$ added to AMSH$^{1-146}$ in a molar excess of at least 2-fold to avoid contamination of the AMSH$^{1-146}$ CH3CT complex with free AMSH$^{1-146}$, as the 3 kDa molecular weight difference of CH3CT was not expected to distinguish the two peaks by size exclusion chromatography. The protein complex was left for 48h at 4°C with TEV protease for cleavage of the tags, and then dialysed to remove imidazole before being passed (twice) over an amylose column and a second Nickel column to remove the hexa-his MBP tag and the hex-his tag and uncleaved protein. The sample was then concentrated by ultrafiltration and loaded onto a Superdex-75 column in buffer (10 mM HEPES pH 8.0, 100 mM NaCl). The complex eluted around 10.5 mL. Fractions containing the pure complex were pooled and again concentrated by ultrafiltration.

Limited Proteolysis

For time-course proteolysis, protease stocks of 1 mg/mL were added to the reaction mixture at a given ratio at time=0 and samples removed at 5', 15', 30' and 60', immediately boiled in SDS-loading buffer for 5' at 95°C, and kept on ice until all samples had been recovered. SDS-PAGE and Coomassie blue staining were used to visualise proteolytic fragments.

For protease to protein ratio assay, the given ratio of protease was added to the protein sample and incubated for 60'. Each sample was boiled in SDS - loading buffer for 5' at 95°C and proteolytic fragments visualised by SDS-PAGE and Coomassie blue staining. For scale-up proteolysis, protease stocks of 1mg/mL were added to the reaction mixture at a 1:500 ratio at time=0. After 5' 1mM PMSF was added and the mixture cooled on ice before loading onto a Superdex 75 size exclusion chromatography column.

Peptide mapping of proteolytic fragments was performed by the Proteomic Core Facility of the European Molecular Biology Laboratory (EMBL) in Heidelberg, with samples taken directly from the SDS-PAGE gel. N-terminal sequencing was performed by the Laboratoire de Spectrométrie de Masse des Protéines (LSMP) of the Institut de Biologie Structurale (IBS), Grenoble, for which the SDS-PAGE bands were electrotransferred to a PDVF membrane, stained with PDVF membrane stain (0.1% Coomassie Blue, 10% Acetic Acid, 50% methanol), and destained with 50% ethanol.

Chemical cross-linking

1mg of ethyleneglycol bis-succinimidylsuccinate (EGS) was weighed out on a precision balance and diluted in 40 µl dimethyl sulfoxide (DMSO) to give a 50 mM stock solution. Dilutions were made to have EGS solutions at 10 mM, 5 mM and 1 mM. Final working EGS concentrations were 5 mM, 1 mM, 0.5 mM and 0.1 mM. Stock solution of glutaraldehyde was made to a final concentration of 50mM and dilutions made as for EGS, with final working concentrations the same as for EGS. Samples were incubated with the respective EGS or glutaraldehyde concentrations for 20 mins followed by quenching with 1mM Tris for 1 min and 5 mins boiling at 95°C in SDS-PAGE loading buffer. Cross-linking of proteins was analysed by SDS-PAGE and Coomassie blue staining.

Ubiquitin hydrolysis assay

This assay was based on that previously described by (McCullough et al. 2006).

1 µg K63-linked tetraubiquitin chains (BostonBiochem) were incubated with 1 uM of the protein of interest for 15' at 37°C. Samples were resolved by SDS-PAGE and electrotransferred to a nitrocellulose membrane, followed by 30' in denaturing buffer (20 mM Tris pH 7.6, 6 M Guanidium hydrochloride) at 4°C and blocking in TBS + 0.1% TWEEN-20, 3% BSA at 4°C or overnight. Ubiquitin was probed for with mouse anti-ubiquitin antibody (Zymed®, Invitrogen), alkaline phosphatase-conjugated anti-mouse antibody (Promega) and development with Western Blue® Stabilized Substrate for Alkaline Phosphatase (Promega).

Isothermal Titration Calorimetry

Isothermal titration calorimetry was performed using a VP-ITC machine with a 1.4mL cell volume (MIcroCal). Titrations were performed at 25°C, each injection 10 µl with 300 s spacing. Data was analysed using Origin software. The interaction model was based on an independent single binding site, with parameters stoichiometry n, change in enthalpy ΔH and dissociation constant K_d iteratively fitted.

(supplementary methods for hisMBP-CH3CT ITC experiment).

Preparation of samples: after a first purification step of amylose, the CH3CT hisMBP fusion protein was run on anionic exchange in buffer (20mM HEPES pH 8.0, 100mM NaCl) to remove a large excess of free hisMBP, the final hisMBP being separated away from hisMBP-CH3CT by size exclusion chromatography.

Crystallisation of AMSH$^{235\text{-}424}$

AMSH$^{235\text{-}424}$ was concentrated to 8 mg/mL, 13 mg/mL and 24 mg/mL, as determined by A_{280} measurement and submitted to the EMBL crystallisation screening robot, where 576 conditions are screened by sitting drop vapour diffusion in 200 nL drops (100 nL protein sample, 100 nL precipitant). Hits were obtained under several conditions, including the formation of large, unique, rhombic crystals. Crystals from the robot drops were fished and flash-frozen in liquid nitrogen in cryo-conditions of 10 – 30 % glycerol, and for PEG crystallisation conditions 20 – 30 % PEG was also tested unsuccessfully. Measurements were made on ID14-4 at the European Synchotron Radiation Facility and a native data set of 3.2 Å resolution was collected from a crystal grown in 0.1M Tris.HCl pH 8.5, 4 % (w/v) PEG 8000, protein concentration 24 mg/mL, cryo 20 % glycerol. Manual hanging drops of 2 µl (1 µl protein, 1 µl precipitate) equilibrated against 800 µl reservoir were set up, giving crystals

of the same geometry as the robot crystals. No better diffraction was obtained, with a best resolution of 3.5 Å obtained from crystals grown in 0.1M Tris.HCl pH 8.0, 4% PEG 8K with a protein concentration of 16 mg/mLs.

Crystallisation of AMSH$^{1-146}$ and CHMP3$^{183-222}$ in complex

The AMSH$^{1-146}$ CHMP3$^{183-222}$ complex was concentrated to 3.3 mg/mL and sent to the EMBL crystallisation screening robot. One hit was obtained in 1.9 M Sodium malonate. Manual hanging drops of 2 µl (1 µl protein, 1 µl precipitate) were set up to screen around the condition, using protein concentrations of 3.6 mg/mL and 7.2 mg/mL, which for the 7.2 mg/mL drops gave micro-crystalline/precipitate in precipitant concentrations ~2.2 M sodium malonate. This was used to streak-seed fresh drops containing 7.2 mg/mL protein, resulting in large, well defined crystals in precipitant concentrations between 1.8 M and 2.2 M sodium malonate. Crystals from a 1.8 M sodium malonate drop were flash-frozen in liquid nitrogen with cryo-protectant of 1.8 M sodium malonate, 30% glycerol. A full data set was collected at 1.7 Å resolution at ID-14-4 of the ESRF.

Manual hanging drops of 2 µl (1 µl protein, 1 µl precipitate) were set up for selenomethionine-substituted protein, using protein concentrations of 3.6 mg/mL and 7.2 mg/mL. This gave microcrystalline precipitate, which was used in a streak-seeding experiment. After repeated seeding experiments single crystals were obtained. Crystals were flash-frozen using 3M sodium malonate as a cryoprotectant, and diffracted to 2.7 Å at the ID14-4 beamline of the ESRF, allowing a SAD dataset to be collected.

Preparation of Selenomethionine-Substituted Protein

The protocol is adapted from (Doublié 1997), where certain amino acids are excluded from the starting medium to inhibit *de novo* synthesis of methionine in *E. coli*.

5 mL minimal medium (MM) plus appropriate antibiotics were inoculated with a single colony from an LB-agar plate and grown for 48h at 37°C. 2 mL were then diluted into 50 mL MM and grown overnight. 8 mL of this preculture were used to inoculate 6 x 1 litre of MM supplemented with 200mg/L thiamine, which were grown at 37°C until an O.D. of 0.6 was reached. The temperature was dropped to 16°C and amino acids and selenomethionine were added. 30' later cells were induced with 1mm IPTG and left overnight for protein expression, after which harvesting and purification was as described above.

Data processing and Solving of the AMSH$^{1-146}$CH3CT Structure

The datasets were processed with MOSFLM (Leslie, A.G.W. 1992) and Scala (Evans 2006). The crystals belong to space group $P4_1$ with unit cell dimensions of a, b = 45.97 Å , c= 206.91 Å and two complexes per asymmetric unit.

Data were analyzed using the Auto-Rickshaw platform at EMBL Hamburg (Panjikar et al. 2005). Selenium sites were localized at 2.8 Å resolution with the program SHELXD (Schneider & Sheldrick 2002). The correct hand for the substructure was determined using the programs ABS (Hao 2004) and SHELXE (Sheldrick 2002). Initial phases were calculated after density modification using the program SHELXE (Sheldrick 2002). An initial model was built using the program ARP/wARP (Perrakis et al. 1999) and used as a search model for molecular replacement with MOLREP (Vagin, A.A. & Teplyakov, A. 1997)(CCP4 1994) using the native data to 1.75 Å resolution. Automatic model building was completed with ARP/wARP (Perrakis et al. 1999), manual model building using COOT (Emsley & Cowtan 2004) and refinement with the program Refmac (Murshudov et al. 1997). The structure contains AMSH residues 1 to 146 and CHMP3 residues 200 to 222 and was refined to an R factor of 19% and an R_{free} of 23.0 %. 100% of the residues are within the most favored regions of a Ramachandran plot (CCP4 1994). All molecular graphics figures were generated with pymol (Delano, W. 2009).

Results 1 – Determining soluble AMSH constructs

1.1. Expression of full-length AMSH in *E. coli.*

The first question to be addressed was whether full-length AMSH could be expressed in a bacterial system. In consideration that the most important prerequisite to a structural project is soluble material to work with, an MBP tag was employed to maximise solubilisation of AMSH. The resulting MBP-AMSH fusion protein was well over-expressed in *E. coli*, but amylose affinity purification yielded small amounts of protein. Cleavage of the tag was also poor, suggesting an insolubility of the fusion protein. Centrifugation of the cleavage material found the fusion protein in the pellet and was thus deemed insoluble. Further attempts to purify the soluble, cleaved AMSH by anionic exchange were complicated by large amounts of MBP and only a small amount of AMSH present.

1.2 AMSH binds CHMP3.

It was hypothesised addition of CHMP3 as a binding partner could stabilise AMSH and efforts were moved towards co-purification of the complex. CHMP3 binding to MBP-AMSH was confirmed, by co-purification techniques and co-elution of the complex on a superdex-200 SEC column, where free CHMP3 would normally elute at 15 mL (Figure 6). It was interesting to see two peaks corresponding to the MBP_AMSH CHMP3 complex eluting outside of the void volume; one eluting around 12.8 mL, and another around 10 mL. which could either correspond to a large conformational change, or a higher oligomeric state. TEV cleavage of the MBP fusion protein from AMSH was still poorly efficient in the presence of CHMP3 thus the overall yield of the complex was low, probably due to the initial low levels of soluble AMSH. A further trial was performed using the CHMP3 construct $CHMP3^{9-222}$, which misses the first 9 N-terminal amino acids, a modification known to improve solubility of CHMP3 (Weissenhorn, W., personal communication), with no improvement in yields of AMSH. It is not surprising that once aggregated, the protein cannot be resolubilised by a binding partner.

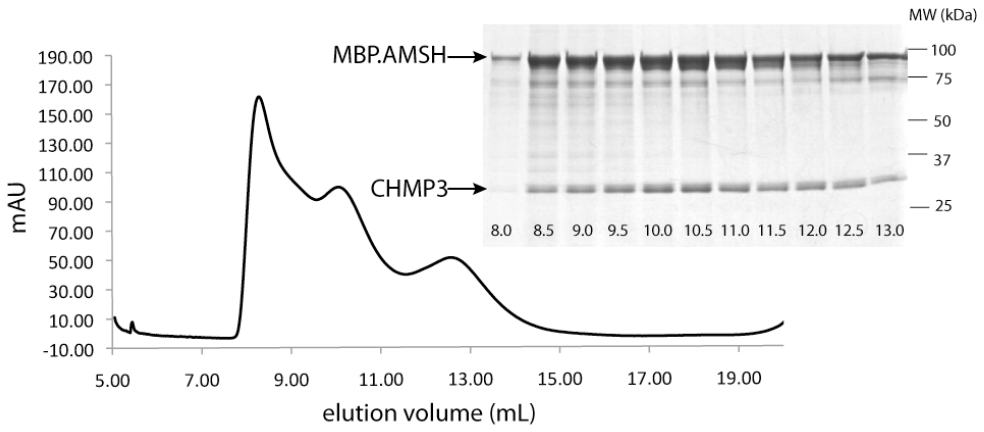

Figure 6. AMSH binds CHMP3.

A. MBP-AMSH and CHMP3 co-elute on a superdex-200 column.

1.3 Limited proteolysis of the AMSH CHMP3 complex yields defined N-terminal AMSH fragments.

Time-course limited proteolysis of the AMSH CHMP3 complex gave smaller, well-defined bands (Figure 7A). Western blotting with an anti-his antibody was employed to eliminate from the analysis of the AMSH proteolytic pattern the CHMP3 C-terminal truncation product CHMP3$^{1\text{-}183}$ (CHMP3ΔC) produced upon proteolysis of CHMP3 alone (Muzioł et al. 2006) (Figure 7B). It was noted that although full-length CHMP3 is extremely susceptible to proteolysis, particularly at the position of Lys183, the presence of AMSH gives some protection of this site from proteolysis, with full-length CHMP3 still present after 5 minutes of proteolysis. It was speculated that addition of the AMSH CHMP3 binding domain to CHMP3 would prevent the degradation of the CHMP3 C-terminal domain and permit crystallisation and structural determination of the full-length CHMP3 molecule.

Large scale limited proteolysis followed by gel filtration was performed to see if any of the proteolytic fragments were soluble and thus suitable cloning targets. Several fragments eluted in soluble fractions from a superdex-75 size exclusion column and blotted samples were analysed by N-terminal sequencing to clarify where to clone (Figure 7C). Sequence information was only obtained for one 16 kDa band. The N-terminal sequence given was XASMSDHG, in accordance with the first residues of AMSH preceded by vectorial residues, indicating that the N-terminal of AMSH is soluble. Based on this data and sequence homology analysis with other MIT domains (Tsang et al. 2006) a minimal AMSH MIT domain was cloned as an MBP-tagged protein, spanning residues 1-117. At a MW of 17 kDa it eluted in the void volume of a Superdex75 and was deemed insoluble.

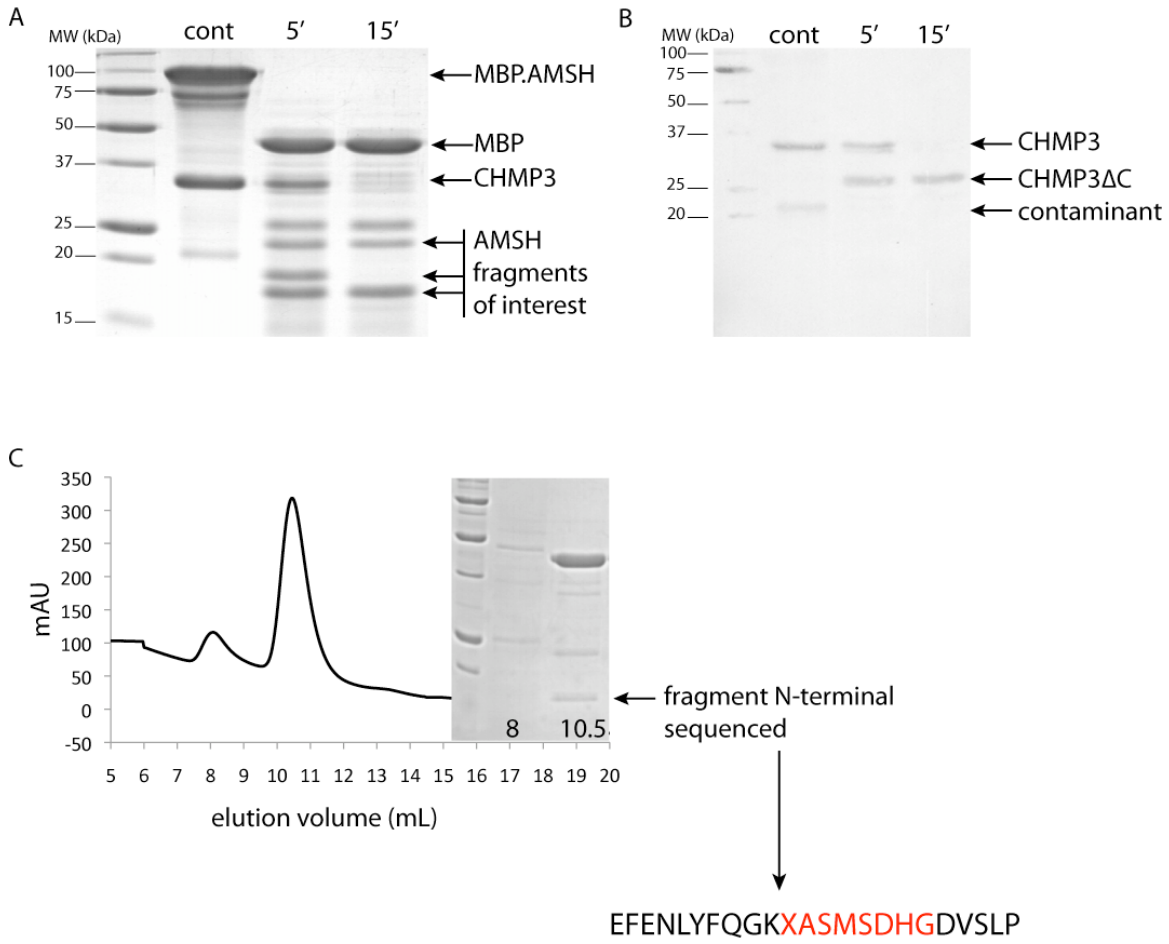

Figure 7. Limited proteolysis of the AMSH CHMP3 complex.

A. The AMSH CHMP3 complex was subjected to a time-course limited proteolysis, and fragments analysed by SDS-PAGE.

B. Western blotting with an anti-his antibody eliminates CHMP3 C-terminal proteolysis products from the analysis of the AMSH proteolytic pattern.

C. Large-scale proteolysis followed by SEC yields soluble AMSH proteolytic fragments. Soluble fragments were identified by N-terminal sequencing.

1.4 AMSH N-terminal constructs are soluble as hisMBP fusion proteins.

In combination with secondary structure prediction (Figure 8), and the previous finding that the N-terminal of AMSH is soluble, several N-terminal constructs were designed to contain the N-terminal predicted coiled-coil section of AMSH (Appendix 1).

The first constructs were designed to remain as close to the secondary structure prediction as possible, incorporating residues 1-184 and 1-189. AMSH$^{1\text{-}184}$ and AMSH$^{1\text{-}189}$ were cloned as GST-fusions, because the solubilising properties of GST were considered necessary, yet

the smaller size of GST compared to MBP (26 kDa instead of 42 kDa) was considered less likely to cause steric structure disruption. Whilst AMSH$^{1-184}$ was completely insoluble and expressed in inclusion bodies, AMSH$^{1-189}$ could be purified in small amounts on a glutathione column. However, once cleaved from the GST tag AMSH$^{1-189}$ was completely insoluble. In hindsight, the use of GST tags for the initial AMSH N-terminal constructs may have contributed to their insolubility, as GST dimerises in solution, and this interaction would have facilitated aggregation of the AMSH N-terminal domain.

As the AMSH N-terminal domain was predicted to be responsible for CHMP3 binding, co-purification with CHMP3$^{9-222}$ was tried to help solubilise the AMSH$^{1-184}$ and AMSH$^{1-189}$ constructs, and to confirm these residues as sufficient for CHMP3 binding. However, this strategy did not work as no CHMP3$^{9-222}$ was fished out during co-purification on a glutathione column, probably due more to the aggregated nature of the bound AMSH$^{1-189}$ than a disproof of these N-terminal residues' involvement in CHMP3 binding.

Longer constructs of hisMBP tagged AMSH$^{1-194}$, AMSH$^{1-199}$ and AMSH$^{1-206}$ proved more encouraging, and although TEV cleavage of the hisMBP tag left the AMSH N-terminal constructs insoluble, Superdex-200 SEC revealed the fusion proteins to be soluble (**Figure 9**A). The discovery of hisMBP-AMSH$^{1-206}$ in both the soluble fractions and the void volume of the size exclusion column suggested the amylose-purified material was in a partly aggregated, partly soluble form. To try and improve soluble yields anionic exchange was employed to separate the two forms, as it is often characteristic of proteins with an aggregation tendency that over time the aggregation provides the nucleus for drawing further soluble protein into the aggregate. HiTrapQ anionic exchange yielded three peaks. SDS-PAGE shows the first peak is a contamination of free hisMBP, but both the second and third peaks contain hisMBP-AMSH$^{1-206}$ (**Figure 9**B).

Fractions from the third peak were chosen for the first solubility assay as they contained almost pure fusion protein without free MBP contamination. However, Superdex-200 size exclusion chromatography (SEC) of these fractions yielded only a small quantity of soluble fusion protein, with most eluting in the void volume of the column. In contrast, those fractions from peaks one and two, containing the free MBP and contaminants, yielded only soluble fusion protein, with no void volume content, and a clear separation by size of the fusion protein from the free MBP contaminants was obtained by SEC (**Figure 9**C).

Lowering the induction temperature to 18°C overnight removed the apparition of contaminants and subsequently the first peak on the anionic exchange profile. It was imperative to perform anionic exchange purification of the material on the same day as protein rupture to obtain decent soluble yields, again to remove the aggregation nucleus that would draw in soluble material over time.

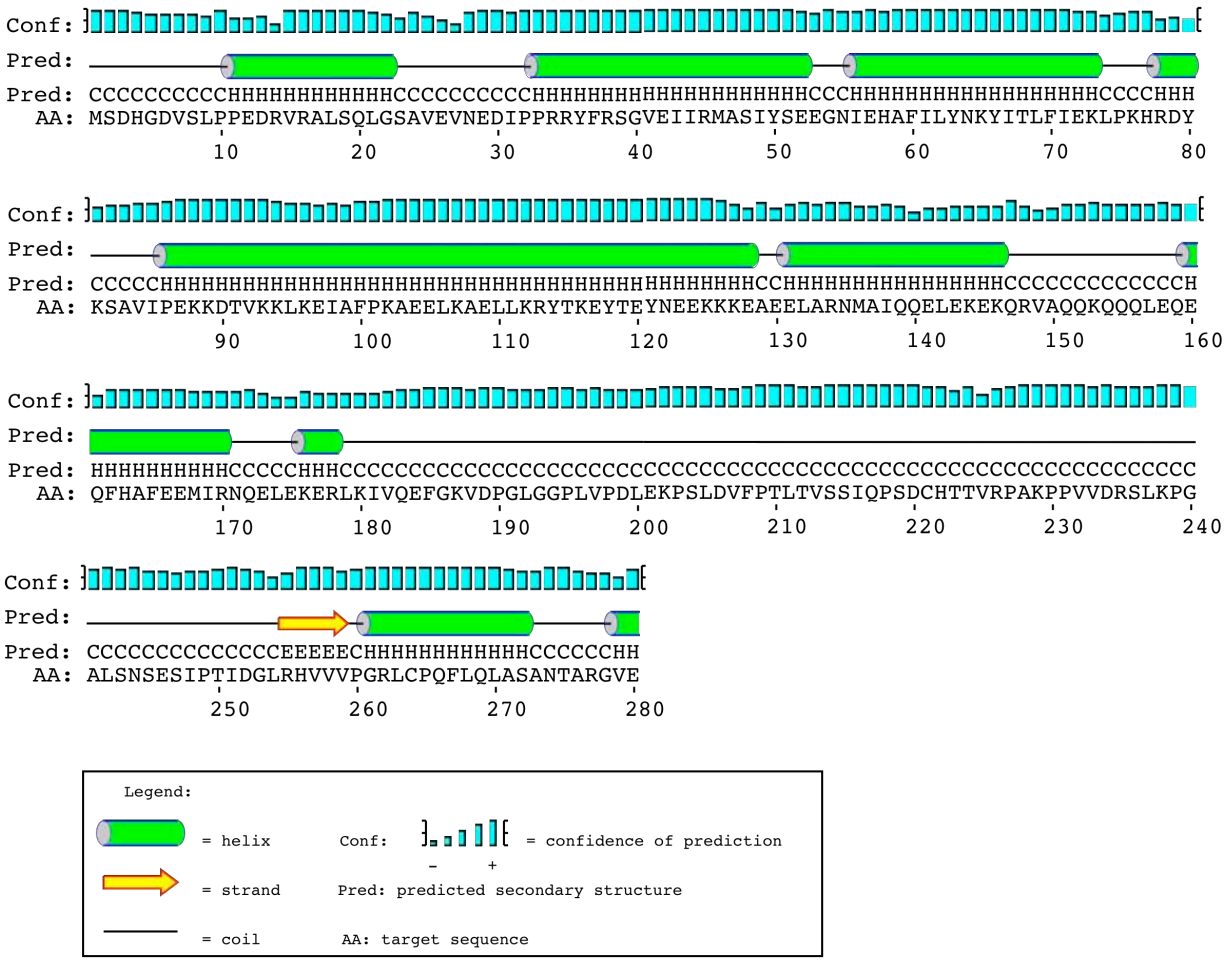

Figure 8. Protein secondary structure prediction from the PSI-PRED server.

A very strong prediction for a coiled secondary structure is made from residue 11 to 178 of the AMSH primary sequence. PSIPRED (McGuffin et al. 2000)(Jones 1999).

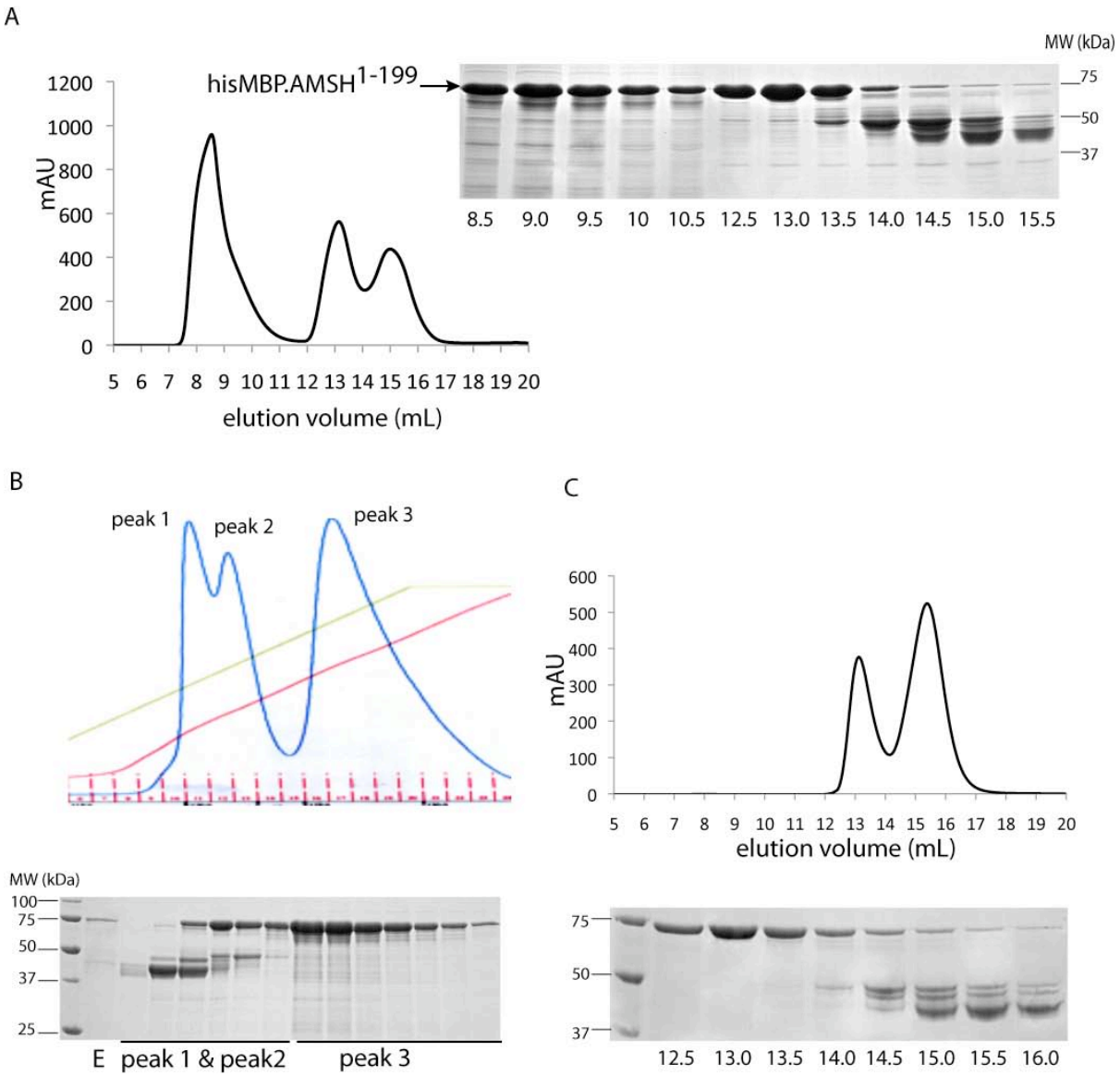

Figure 9. AMSH$^{1-199}$ and AMSH$^{1-206}$ are soluble as hisMBP-fusion proteins.

A. AMSH$^{1-199}$ hisMBP-fusion protein is purified in soluble and aggregated forms, as shown by superdex-200 SEC.

B. Anionic exchange of the amylose elution mixture produces three peaks, peak 1 containing MBP contaminants and peaks 2 and 3 containing hisMBP tagged AMSH$^{1-206}$.

C. The second peak from the anionic exchange contains the soluble hisMBP.AMSH1-206, which Superdex-200 SEC cleanly separates from the hisMBP contaminants.

Results 2 – Interaction of the AMSH N-terminal domain with CHMP3

2.1 The N-terminal of AMSH constitutes the CHMP3 binding site.

The AMSH N-terminal constructs designed in Chapter I contained the proposed CHMP3 binding site. We set out to verify the interaction between the AMSH N-terminal and CHMP3, with the extended aim of stabilising full-length CHMP3 with AMSH, by protecting the C-terminal from degradation, and of solubilising the AMSH N-terminal constructs once cleaved of their hisMBP tags by binding the very soluble CHMP3. The final target would be crystallisation studies of the complex, gaining information about the individual components and of their interaction mechanism.

Co-purification of hisMBP-tagged AMSH$^{1-206}$ fusion protein and his-tagged CHMP3 on an amylose column did not fish out any CHMP3. As the majority of AMSH$^{1-206}$ purified from the amylose column is in an aggregated form it is unsurprising that CHMP3 is unable to bind. When isolated as soluble hisMBP-tagged fusion proteins using the anionic exchange technique described in Chapter I, AMSH$^{1-194}$ and AMSH$^{1-206}$ bind CHMP3$^{9-222}$; addition of CHMP3$^{9-222}$ to AMSH$^{1-206}$ causes a peak shift in Superdex-200 size exclusion chromatography, and both proteins are found together in the newly formed peak (Figure 10A). A second small peak can be seen for the excess CHMP3$^{9-222}$. SDS-PAGE analysis of the size exclusion fractions shows how the CHMP3ΔCT proteolytic fragment is specifically excluded from the AMSH$^{1-206}$ CHMP3 complex, affirming the requirement of the CHMP3 C-terminal domain for AMSH binding (Figure 10A).

Chemical cross-linking demonstrates formation of a hisMBP-AMSH$^{1-206}$ CHMP3$^{9-222}$ complex (Figure 10B). Control cross-linking of hisMBP-AMSH206 and CHMP3$^{9-222}$ separately show no new bands formed, thus each one can be assumed to be monomeric. HisMBP-AMSH$^{1-206}$ alone runs around 75kDa, CHMP3$^{9-222}$, despite a molecular mass of 25kDa, migrates in a reducing SDS-PAGE around 30kDa. The resulting cross-linked band of AMSH mixed with CHMP3 runs at 150kDa, which would correspond to two CHMP3$^{9-222}$ monomers binding to hisMBP-AMSH$^{1-206}$. However, the resolution of the gel is not high enough to draw a conclusion about stoichiometry; the complex may have a 1:1 stoichiometry but as both monomeric AMSH and CHMP3 migrate at higher than expected masses when cross-linked individually, the resulting 1:1 complex may also migrate at a higher than expected molecular mass.

Complex formation was also confirmed by native gel electrophoresis. When compared to migration of hisMBP-AMSH$^{1-206}$ and CHMP3$^{9-222}$ alone a new higher band is seen upon mixing, corresponding to the hisMBP-AMSH$^{1-206}$ CHMP3$^{9-222}$ complex (Figure 10C).

The hisMBP tag was efficiently cleaved from AMSH$^{1-206}$ in the presence of CHMP3$^{9-222}$. By adding an excess of CHMP3$^{9-222}$, contamination of the AMSH$^{1-206}$ CHMP3$^{9-222}$ complex by free uncleaved hisMBP-AMSH$^{1-206}$ on size exclusion was avoided, and a pure sample of the complex was obtained. Concentrated samples of 5 mg/mL and 10 mg/mL were sent for crystallisation trials at the EMBL crystallisation robot facility, but no hits were obtained.

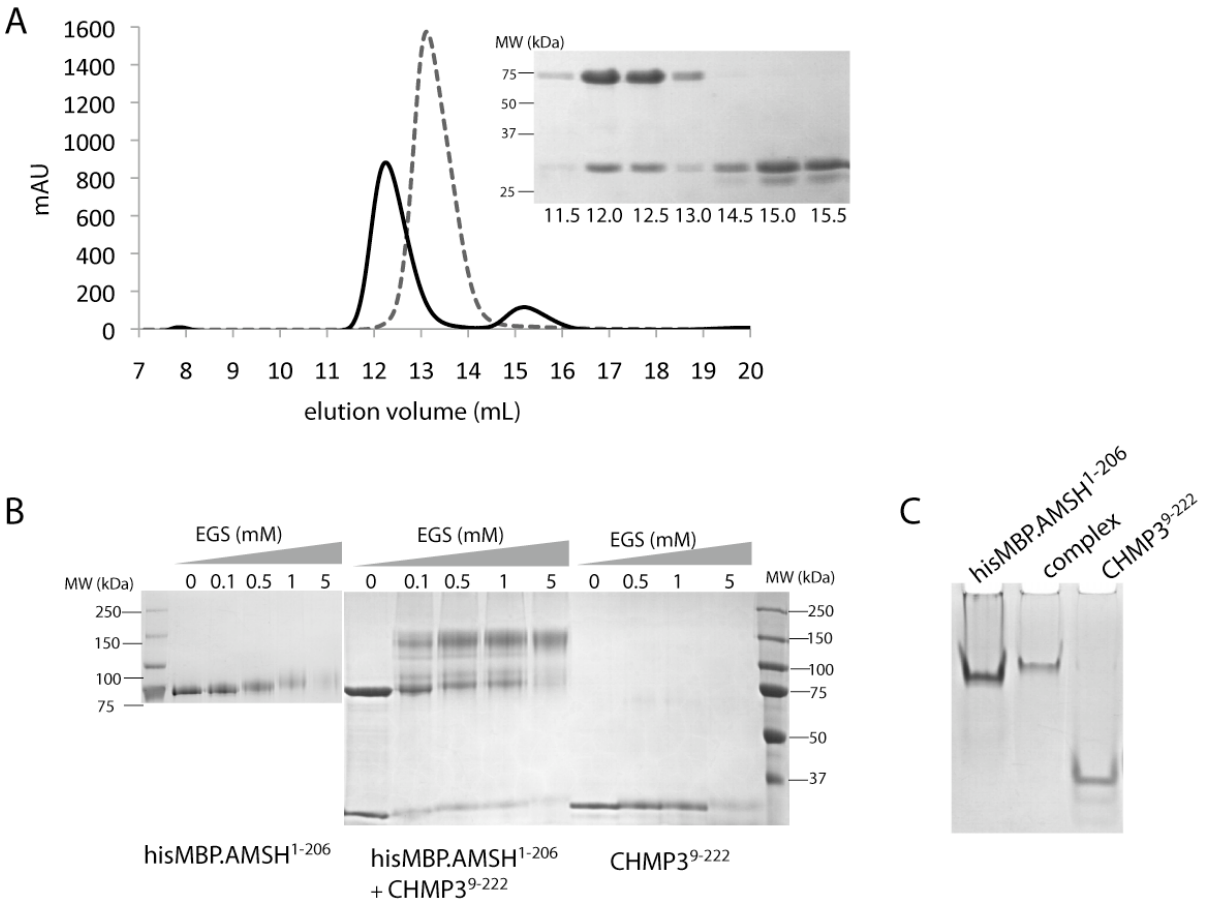

Figure 10. The AMSH N-terminal construct AMSH$^{1-206}$ binds to CHMP3.

A. Addition of CHMP3 to hisMBP-tagged AMSH$^{1-206}$ causes a peak shift of the AMSH$^{1-206}$ peak, with hisMBP-tagged AMSH$^{1-206}$ and CHMP3 co-eluting at 12.3 mL. Dotted line: hisMBP-AMSH$^{1-206}$. Solid line: hisMBP-AMSH$^{1-206}$ and CHMP3$^{9-222}$ together. A second smaller peak corresponds to excess CHMP3$^{9-222}$ for hisMBP-AMSH$^{1-206}$ and CHMP3$^{9-222}$ mixed together. The SDS-PAGE gel reveals exclusion of the CHMP3 degradation product from the AMSH$^{1-206}$ CHMP3 complex.

B. Neither hisMBP-AMSH$^{1-206}$ nor CHMP3$^{9-222}$ form higher molecular weight species when cross-linked alone. When AMSH$^{1-206}$ and CHMP3$^{9-222}$ are mixed, a new band is formed, running in an SDS-PAGE at 150 kDa.

C. A band shift is seen upon incubation of hisMBP-tagged AMSH$^{1-206}$ with CHMP3$^{9-222}$.

2.2 Probing the affinity of the AMSH N-terminal for CHMP3.

$CHMP3^{9-222}$ can be induced to adopt two conformations using low and high salt content buffers, eluting from a superdex-75 size exclusion chromatography column at 9.1 mL and 10.8 mL for 0 mM NaCl and 500 mM NaCl respectively (Figure 1, (Lata, Roessle et al. 2008). Model determination using Small Angle X-ray Scattering (SAXS) shows two distinct species are formed under the differing ionic strengths, with 0 mM NaCl showing a closed conformation and 500 mM NaCl creating an open conformation (Figure 3, (Lata, Roessle et al. 2008). Fittings of the crystal structure of $CHMP3^{1-183}$ into the SAXS envelopes demonstrate how the closed and open CHMP3 forms could correspond to the auto-inhibited and activated forms, with opening of the structure corresponding to a displacement of the C-terminal from its interaction with the N-terminal (Figure 3, (Lata, Roessle et al. 2008).

Isothermal titration calorimetry (ITC) was used to assay the affinity of the AMSH N-terminal for CHMP3. $CHMP3^{9-222}$ was titrated into $AMSH^{1-206}$ at the physiological salt concentration of 150 mM, and the binding affinity was calculated to be K_D 31.9 nM (Figure 4 (Lata, Roessle et al. 2008). This value is orders of magnitude higher than those previously published for MIT-CHMP interactions, which are of micro-molar affinity (Stuchell-Brereton et al. 2007)(Yang et al. 2008). ITC studies were repeated using no salt (0 mM NaCl) and high salt (500 mM NaCl) buffers to induce single species of either closed or open CHMP3 and the resulting affinities of K_D 5.6 nM and K_D 392 nM respectively show AMSH binds strongly to both, with a high affinity maintained for open CHMP3 even in high buffer salt conditions.

A C-terminal peptide of CHMP3 was designed based on sequence alignment of CHMP3 with the MIT binding sequences of the C-termini of other CHMP proteins, which always involved the last 20 amino acids of the CHMP C-terminal, thus it was speculated that the same 20 residues of the C-terminal of CHMP3 would be required for AMSH binding (Stuchell-Brereton et al. 2007)(Obita et al. 2007). To be cautious about the MIT binding site in CHMP3 a slightly longer peptide comprising the last 28 amino acids of the CHMP3 C-terminal was ordered ($CHMP3^{CT28}$). Surprisingly, the affinity of $CHMP3^{CT28}$ was significantly lower than that of full-length AMSH at K_D 24 µM, indicating a possibly larger binding site involved in the interaction with AMSH. A control titration using CHMP3ΔC (the CHMP3 construct of the crystal structure, residues 9-183) showed no measurable interaction, highlighting the requirement of CHMP3 C-terminal residues 183-222 for AMSH binding.

doi:10.1016/j.jmb.2008.03.030 J. Mol. Biol. (2008) 378, 818–827

Available online at www.sciencedirect.com
ScienceDirect

Structural Basis for Autoinhibition of ESCRT-III CHMP3

Suman Lata[1], Manfred Roessle[2], Julianna Solomons[1], Marc Jamin[1], Heinrich G. Göttlinger[3], Dmitri I. Svergun[2] and Winfried Weissenhorn[1]*

[1]*Unit for Virus Host Cell Interaction, UMR 5233 UJF-EMBL-CNRS, 6 rue Jules Horowitz, 38042 Grenoble Cedex 9, France*

[2]*European Molecular Biology Laboratory, Notkestrasse 85, 22603 Hamburg, Germany*

[3]*Program in Gene Function and Expression, Program in Molecular Medicine, University of Massachusetts Medical School, Worcester, MA 01605, USA*

Received 19 December 2007; received in revised form 6 March 2008; accepted 11 March 2008
Available online 20 March 2008

Edited by J. E. Ladbury

Endosomal sorting complexes required for transport (ESCRT-0, ESCRT-I, ESCRT-II, and ESCRT-III) are selectively recruited to cellular membranes to exert their function in diverse processes, such as multivesicular body biogenesis, enveloped virus budding, and cytokinesis. ESCRT-III is composed of members of the charged multivesicular body protein (CHMP) family—cytosolic proteins that are targeted to membranes *via* yet unknown signals. Membrane targeting is thought to result in a membrane-associated protein network that presumably acts at a late budding step. Here we provide structural evidence based on small-angle X-ray scattering data that ESCRT-III CHMP3 can adopt two conformations in solution: a closed globular form that most likely represents the cytosolic conformation and an open extended conformation that might represent the activated form of CHMP3. Both the closed and open conformations of CHMP3 interact with AMSH with high affinity. Although the C-terminal region of CHMP3 is required for AMSH interaction, a peptide thereof reveals only weak binding to AMSH, suggesting that other regions of CHMP3 contribute to the high-affinity interaction. Thus, AMSH, including its MIT (microtubule interacting and transport) domain, interacts with ESCRT-III CHMP3 differently from reported Vps4 MIT domain–CHMP protein interactions.

Keywords: CHMP3; ESCRT-III; AMSH; budding; autoinhibition

Introduction

Multivesicular body biogenesis, cell division cytokinesis, and enveloped virus budding are seemingly unrelated processes that involve a topologically identical membrane-remodeling event, namely, budding away from the cytosol. These normal cellular and pathological membrane-remodeling processes are orchestrated by either the entire or a subset of the class E vacuolar protein sorting (Vps) machinery that was first implicated in receptor downregulation *via* multivesicular body (MVB) formation.[1–5] Receptor downregulation and MVB biogenesis are largely catalyzed by ESCRT-0, ESCRT-I, ESCRT-II, and ESCRT-III (endosomal sorting complexes required for transport) complexes, which are sequentially recruited to the endosomal membrane and exert their action in protein sorting and vesicle budding[5,6] with the assistance of a variety of cytosolic accessory proteins and protein complexes. ESCRT complexes 0, I, and II contain ubiquitin binding domains that recognize ubiquitinated cargo and have been thus implicated in receptor sorting into vesicles that bud off into the endosomal lumen.[3] Although ESCRT-III is uncoupled from direct ubiquitin recognition, ESCRT-III family members recruit deubiquitinating enzymes associated molecule of SH3 domain of STAM (AMSH)[7–11] and Ub-specific protease Y (UBPY).[12] The deubiquitin isopeptidase activities of UBPY (Doa4) and AMSH precede cargo incorporation into vesicles, thereby ensuring a constant pool of free ubiquitin and early disengagement of cargo from the MVB pathway.[13] Although AMSH depletion does not impair epidermal growth factor receptor degradation,[14,15] inhibition of its recruitment to endosomes by ESCRT-III charged

**Corresponding author.* E-mail address: weissenhorn@embl.fr.

Abbreviations used: ESCRT, endosomal complex required for transport; MVB, multivesicular body; CHMP, charged multivesicular body protein; MIT, microtubule interacting and transport; ITC, isothermal titration calorimetry; SEC, size-exclusion chromatography; MALLS, multiangle laser light scattering; SAXS, small-angle X-ray scattering; Vps, vacuolar protein sorting; AMSH, associated molecule of SH3 domain of STAM; UBPY, Ub-specific protease Y.

0022-2836/$ - see front matter

MVB protein (CHMP) 3 impairs epidermal growth factor receptor degradation.[11] Furthermore, overexpression of a catalytically inactive form of AMSH exerts a dominant-negative effect on HIV-1 budding.[9]

ESCRT-III is composed of 6 and 11 members in yeast[16] and mammals, respectively, which have been named CHMP proteins.[17,18] CHMP proteins form binary subcomplexes[16–18] and have been suggested to polymerize into a protein lattice on membranes, which acts at a late budding step.[17,19–21] CHMP proteins are targets for the AAA-type ATPase Vps4 whose MIT (microtubule interacting and transport) domain interacts with a C-terminal peptide region of CHMP1 and CHMP2 as well as yeast Vps2 (CHMP2) and Vps24 (CHMP3).[22,23] Recruitment of Vps4 in turn is required for efficient disassembly and recycling of ESCRT complexes from membranes[16,24,25]; catalytic inactive Vps4 thus acts as a dominant-negative inhibitor of retroviral budding.[17,19] CHMP family members recruit accessory ESCRT factors such as Alix *via* CHMP4,[17,19,26] AMSH *via* CHMP3,[9,10] and UBPY *via* CHMP7.[12] Furthermore, they communicate with ESCRT-I *via* a Vps28–CHMP6/Vps20 interaction and with ESCRT-II *via* a Vps25–Vps20/CHMP6 interaction.[27–29]

A hallmark of the ESCRT-III family members is biased distribution of charged amino acids, with two-thirds of the N-terminus carrying a basic charge and the remaining C-terminal region being acidic. The crystal structure of CHMP3 revealed a flat helical arrangement with two distinct and mutually exclusive CHMP–CHMP interaction surfaces and a large basic surface required for membrane targeting; both membrane targeting and CHMP–CHMP interactions were shown to be required for HIV-1 budding.[21] The crystal structure lacks part of the C-terminal acidic region (residues 184–222), including the Vps4 and AMSH MIT domain interaction sites[9,23]. The structure was suggested to represent the activated conformation of CHMP3, because removal of the acidic C-terminus leads to membrane targeting *in vivo*, whereas full-length CHMP3 is found predominantly in the cytosol when expressed in the absence of any additional signals.[21] The C-terminal region has been suggested to exert a control function keeping CHMP proteins in a cytosolic state, which is consistent with the activation hypothesis.[9,30] A potential release of the autoinhibition in CHMP3 was indirectly attributed to its interaction with AMSH, because it turned full-length CHMP3 into a potent HIV-1 budding inhibitor.[9]

Here we present structural evidence for closed and open conformations of full-length CHMP3, which confirms the activated state represented by the CHMP3 crystal structure. Both conformations do not reveal any changes in their secondary structure content or in their overall thermal stability, indicating that a first step in activation entails detachment of the C-terminal module from the N-terminal core. Both conformations reveal high-affinity binding to AMSH *in vitro* as measured by isothermal titration calorimetry (ITC). This suggests that the AMSH MIT domain interaction with CHMP3 differs substantially from the low-affinity Vps4 MIT domain interaction.[22,23]

Results

Characterization of CHMP3 conformations

While we were performing size-exclusion chromatography (SEC) on a Superdex™ 75 column with ^{200}HBS as the running buffer, purified CHMP3 showed two distinct peaks at elution volumes 9.1 and 10.8 ml (Fig. 1a). It had been previously hypothesized that the C-terminal acidic tail of CHMP proteins may interact with the N-terminal basic region *via* electrostatic interactions. We therefore examined the effect of ionic strength on the polydispersity of CHMP3 by SEC. CHMP3 eluted as single symmetric peaks in ^{0}HBS and ^{500}HBS at 9.1 and 10.8 ml, respectively (Fig. 1a), revealing a distinct effect of the ionic strength on the elution profile. This salt-dependent change in elution profile was confirmed on a Superdex™ 200 column with three NaCl concentrations, namely, 0, 100, and 500 mM. CHMP3 eluted as a broad peak in ^{100}HBS, whereas with ^{0}HBS and ^{500}HBS as the running buffers, single symmetric peaks at 13.1 and 15.7 ml, respectively, were observed (Fig. 1b). Furthermore, separation of the high-salt form in ^{0}HBS produced a single peak at 13.1 ml and separation of the low-salt form in ^{500}HBS revealed a peak at 15.7 ml (data not shown). Collectively, these findings suggested that the two forms of CHMP3 were in a dynamic equilibrium with one another; depending on the ionic strength of the medium, one form could be exclusively converted into the other in a reversible fashion, thus providing preparative means for isolating a pure CHMP3 form at a time.

Analytical SEC in combination with multiangle laser light scattering (MALLS) was performed (Fig. 1c) in order to determine the oligomeric state of these two CHMP3 forms. As expected, depending on the ionic strength of the running buffer, CHMP3 eluted as a single symmetric peak at two elution volumes. With ^{500}HBS as the running buffer, CHMP3 eluted at 10.8 ml with an observed average molecular weight (M_w) of 24.1±0.2 kDa, which is in excellent agreement with the calculated molecular weight of 24.5 kDa for monomeric CHMP3. In ^{0}HBS, CHMP3 eluted at 8.9 ml, with an M_w of 23.3±2 kDa, implying that the change in elution volume/hydrodynamic radius did not result from CHMP3 oligomerization but did from a conformational change.

Circular dichroism (CD) analysis on both CHMP3 conformers showed no substantial difference in the secondary structure content as the observed spectra in ^{0}HBS and ^{500}HBS (Fig. 2a) were very similar, with only a small difference at around 208 nm that most likely resulted from a difference in NaCl concentration. Two minima observed at 208 and 222 nm are consistent with the α-helical fold of CHMP3.[21] Thermal unfolding showed transitions at ~65°C for both ^{0}HBS and ^{500}HBS buffer conditions (Fig. 2b), indicating that high salt had no effect on the stability of the helical structure content.

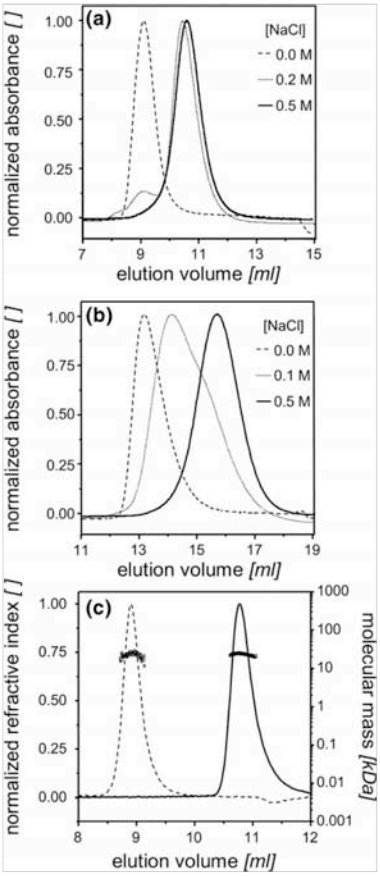

Fig. 1. Enrichment of CHMP3 conformers: Analytical SEC recorded by measuring absorbance at 280 nm (a) on a Superdex™ 75 10/300 GL column with the running buffers ^{0}HBS (broken line), ^{200}HBS (dotted line), and ^{500}HBS (continuous line) as well as (b) on a Superdex™ 200 10/300 GL column with the running buffers ^{0}HBS (broken line), ^{100}HBS (dotted line), and ^{500}HBS (continuous line). A small change in NaCl concentration from ^{100}HBS to ^{200}HBS produces a large change in the elution profiles. (c) SEC in combination with refractive index measurement and MALLS performed on a Shodex Protein KW-804 column reveals that CHMP3 in ^{0}HBS(broken line) and CHMP3 in ^{500}HBS (continuous line) elute with the observed M_w values of 23.3±2 kDa (open circle) and 24.1±0.2 kDa (open square), respectively, which are in agreement with the calculated molecular mass of 24.5 kDa for monomeric CHMP3.

Structural models of CHMP3 conformations based on small-angle X-ray scattering analyses

Both CHMP3 conformers were analyzed by small-angle X-ray scattering (SAXS), which produced interpretable scattering intensity patterns (Fig. 3a). Maximal protein dimensions (D_{max}) of approximately 8.5 and 11 Å were found in ^{0}HBS and ^{500}HBS, respectively, by the distance distribution function $p(r)$ computed by Fourier transformation of the scattering intensity. The shapes of the CHMP3 conformers were determined *ab initio* from the scattering data using the program DAMMIN.[31] Ten independent models of CHMP3 in ^{0}HBS and ^{500}HBS fitted the corresponding experimental data with discrepancy χ values of 1.66–1.98 and 1.58–1.62, respectively (Fig. 3a). The *ab initio* modeling of CHMP3 in ^{0}HBS showed a compact ~75-Å-long elongated structure (Fig. 3b). The overall shape is consistent with the crystal structure of a C-terminally truncated form of CHMP3 and accommodates the 70-Å-long helical hairpin of the four-helical-bundle core structure,[21] as can be seen from the manual fit of the structure into the molecular envelope of the SAXS model (Fig. 3b). The volume of the model (~35%) not accounted for by the crystal structure (136 of 222 residues) appears to wrap around the central body of the structure (Fig. 3b). In contrast, in the model of high-salt CHMP3, this part extends from the main body and generates an elongated ~106-Å-long structure (Fig. 3c). The core CHMP3 structure composed of the four-helical bundle can be fitted manually into

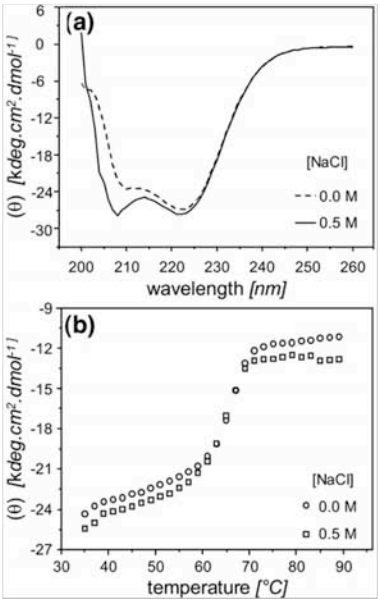

Fig. 2. CD shows that both the "low-salt" and "high-salt" conformations of CHMP3 have (a) a similar α-helical content as shown by the CD spectra in ^{0}HBS (broken line) and ^{500}HBS (continuous line) as well as (b) the same thermal unfolding transition at ~65° as was measured by recording ellipticity at 222 nm in ^{0}HBS (open circle) and ^{500}HBS (open square) as a function of temperature.

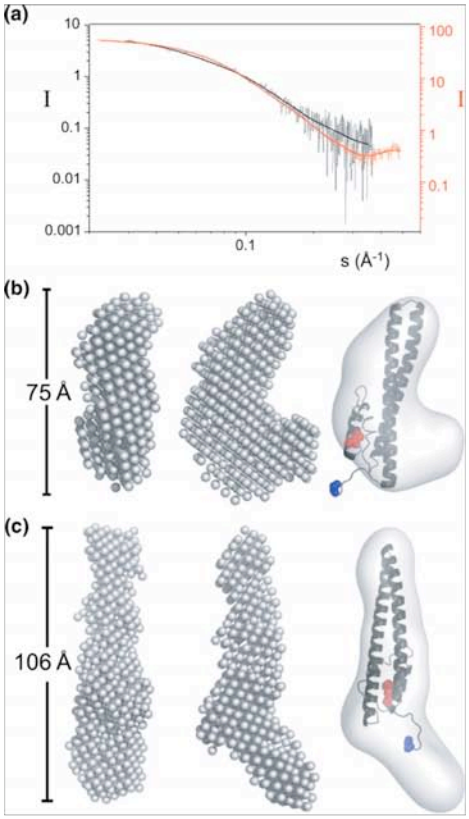

Fig. 3. SAXS analysis of CHMP3. (a) SAXS profiles of CHMP3 in ^{0}HBS (dotted black line) and ^{500}HBS (dotted red line). Scattered intensity I is shown *versus* s [$s = 4\pi\sin(\theta)/\lambda$, 2θ = scattering angle, and λ = wavelength]; $\log_{10}$ scale for I and s are chosen for better visualization of the differences between the scattering curves at high and low s values. SAXS profiles calculated from the *ab initio* models are shown as continuous black and red lines. (b) The *ab initio* calculated model of CHMP3 in ^{0}HBS buffer conditions reveals an elongated L-shaped molecule. Two orientations rotated by 90° are shown (left two panels). The core of the CHMP3 crystal structure (gray ribbon) composed of an elongated four-helical bundle was fitted manually into the molecular envelope calculated from the SAXS model (right panel). (c) The calculated model of CHMP3 in ^{0}HBS buffer conditions reveals an elongated 106-Å-long molecule. Two orientations rotated by 90° are shown (left two panels). The core of the CHMP3 crystal structure (gray ribbon) was fitted into the elongated structure (right panel). The N-terminal residue is indicated in blue, whereas the C-terminal residue is shown in red.

the elongated molecular envelope (Fig. 3c). Thus, the data indicate that the CHMP3 model obtained under no-salt conditions represents the "closed" conformation of CHMP3 where the C-terminal acidic tail interacts with the larger N-terminal basic core and that the model obtained under high-salt conditions represents the "open" conformation where the C-terminal acidic tail is displaced and extends from the N-terminal basic core.

CHMP3–AMSH interaction

Having established that the two forms of CHMP3 were structurally different from each other, we analyzed their interaction with the deubiquitin isopeptidase AMSH, which requires the C-terminal region of CHMP3 for interaction.[9,10] Consistent with the proposed interaction, we detected binding of AMSH (residues 1–206) [AMSH(1–206)] to CHMP3 (residues 9–222) [CHMP3(9–222)] by gel-filtration chromatography (data not shown) and native gel electrophoresis; both CHMP3(9–222) and AMSH(1–206) migrate as distinct bands on native gel (Fig. 4a, lanes 1 and 2, respectively); a complex formed by the two proteins results in a new band migrating slower than AMSH(1–206) alone (Fig. 4a, lane 3). In order to better understand the interaction and the functional properties of the salt-induced conformational change in CHMP3, we assessed AMSH binding affinity to both the closed and open conformations of CHMP3 by using ITC. Table 1 summarizes the enthalpy $\Delta H°$, interaction stoichiometry n, and equilibrium dissociation constant K_d, as obtained by fitting to the binding isotherm a 1:n interaction model, which assumes a single type of binding sites. We measured a K_d of 5.6 nM for the "closed" conformer in ^{0}HBS (Fig. 4b), that of 31.9 nM at physiological ^{150}HBS buffer conditions (Fig. 4c), and that of 392 nM for the open form in ^{500}HBS (Fig. 4d), thus a ~70-fold difference in affinity. No substantial difference in enthalpy was observed as we determined $\Delta H°$ values of −16.9 and −17.5 kcal/mol in ^{500}HBS and ^{0}HBS, respectively. Because it has been proposed that the C-terminal tail of CHMP3 is necessary for the interaction with AMSH, we titrated the C-terminal CHMP3 peptide (residues 196–222) with AMSH in ^{0}HBS and ^{500}HBS; although no interpretable isotherm was produced with 500 mM NaCl, a K_d of 24 μM (Fig. 4e) was determined in 0 mM NaCl, which is ~4500 times larger as compared with the CHMP3(9–222) interaction. Consistent with previous data,[9] CHMP3(9–183) lacking the C-terminal peptide region did not interact with AMSH(1–206) in the ^{50}HBS, ^{150}HBS, and ^{500}HBS buffer conditions using ITC. These results suggest that the C-terminal region is important for establishing the interaction with AMSH, which then induces additional contacts with CHMP3 resulting in a high-affinity interaction. Because the C-terminal region carries a substantial negative charge, the NaCl concentration-dependent difference in K_d suggests that the electrostatic interactions may play a role in CHMP3–AMSH interaction. Very similar $\Delta H°$ values of −17.5, −18.0, and −16.9 kcal/mol were observed in ^{0}HBS, ^{150}HBS, and ^{500}HBS, respectively, thus demonstrating that the interaction enthalpy was independent of the ionic strength. Trials to determine whether CHMP3 binds only to the AMSH MIT domain could not be per-

formed because we were unable to obtain a soluble monodisperse form of the AMSH MIT domain.

Discussion

ESCRT-III proteins are predominantly cytosolic proteins that are targeted to cellular membranes by yet unknown signals. Removal of C-terminal residues 151–222 of CHMP3 induced efficient membrane targeting *in vivo*, indicating that the presence of the C-terminus prevents membrane interaction.[21] Furthermore, CHMP3 residues 151–222 were used to pull down the core structure of CHMP3 composed of residues 1–150, demonstrating an interaction between the N-terminal core and the C-terminal region.[9] The models of CHMP3 in its closed and open conformations based on the SAXS analysis reveal an extension of the C-terminal region in the open form that wraps around the N-terminal core in the closed form. Both structures are in good agreement with the four-helical-bundle core of CHMP3. The SAXS models confirm further the previous suggestion that the crystal structure represents the "activated" form of CHMP3, because the C-terminal region containing residues 140–183 is detached from the core four-helical-bundle structure and involved in intermolecular interactions that are important for CHMP protein polymer formation *in vivo*.[21] The fact that ionic strength can change the conformation of CHMP3 indicates that monomeric CHMP3 is in a metastable conformation. The removal and reattachment of the C-terminal region toward the core are reversible and have no apparent influence on the secondary structure content and overall thermostability of CHMP3. CHMP3 contains a low activation barrier because it exists already as a mixture of both closed and open forms at physiological salt conditions *in vitro*. Including the complete N-terminus of wild-type CHMP3 (conserved residues 1–8) did not change the presence of two peaks observed by SEC under ^{0}HBS and ^{500}HBS buffer conditions and produced similar peaks as those obtained for CHMP3(9–222) SEC analysis; thus, the conserved N-terminus of CHMP proteins does not seem to contribute to the stability of the closed conformation of CHMP3 *in vitro*.

The open CHMP3 conformation under high ionic strength conditions does not polymerize *in vitro*; this is most likely due to the presence of high salt, because polar interactions have been previously implicated in CHMP polymer formation.[21] It is yet unclear which signals will actually target CHMP proteins to cellular membranes. One possibility is that their interaction partners confer membrane recruitment or *vice versa*: CHMP4 *via* the interaction with Alix or Bro1,[17,19,26] CHMP3 *via* AMSH,[9,10] CHMP7 *via* UBPY,[12] and Vps20/CHMP6 *via* ESCRT-I Vps28[27,28] and/or ESCRT-II.[27,29] Any of these interactions may lead to activation of individual CHMP proteins. Furthermore, heteromeric CHMP–CHMP protein interactions contribute to efficient membrane targeting because CHMP3 mutations that abrogate dimerization *in vitro* abolish membrane targeting of CHMP3 *in vivo*.[21]

The structure of the human Vps4B MIT domain in complex with a peptide derived from CHMP1B revealed three conserved leucine residues (Leu187, Leu190, and Leu194; corresponding to CHMP3 Met213, Leu217, and Leu220, respectively) binding to a hydrophobic pocket on the MIT domain; the interaction is further stabilized by salt bridges (Glu184, Arg190, and Arg195; corresponding to CHMP3 Arg216, and Arg221, respectively).[23] The binding motif is the same as that described for the yeast Vps4p–MIT–Vps2p complex, namely, (Asp/Glu) xxLeuxxArgLeuxxLeu(Lys/Arg),[22] which is not completely conserved within the C-terminus of CHMP3 (210-***Leu***xx***Met***xxArgLeuxxLeuArg-221). Mutational analysis of the CHMP3–AMSH interaction implicated CHMP3 residues Arg216 and Leu217 in binding[9]; both residues are part of the proposed Vps4–MIT–CHMP interaction motif. This implies that AMSH recognizes the same CHMP3 region as Vps4B MIT. Binding studies of 17-amino-acid-long peptides corresponding to the extreme C-terminus of CHMP1A, CHMP1B, CHMP2A, and CHMP2B revealed variable K_d values between ~4 and 200 μM; a similar binding affinity (~28 μM) was determined for the yeast Vps2p C-terminal peptide (residues 183–232) binding to Vps4p MIT.[22] Although the C-terminal CHMP3 peptide shows a similar affinity for AMSH interaction, full-length CHMP3 interacts much tighter with AMSH revealing nanomolar dissociation constants (K_d=5.6 nM), thus indicating that other regions of CHMP3 contribute substantially to the AMSH interaction. Although the C-terminal binding motif may be crucial for recruitment of CHMP3 to AMSH,[9] other regions of CHMP3 seem to confer tight association with AMSH. Because we could not express a soluble form of the AMSH MIT domain alone, we do not know whether CHMP3 interacts only with the MIT domain or also with other regions of AMSH. Interestingly, the structure of Vps4p MIT in complex with Vps2p (residues 183–232) reveals a second MIT interaction site formed by two short additional helical segments; however, the binding affinity of this longer Vps2p peptide is similar to that determined for short mammalian CHMP peptides, namely, 28 μM.[22] Nevertheless, the structure may indicate how the C-termini of full-length CHMP proteins might interact with MIT domains *via* a larger surface, leading to substantially higher binding affinity.

We show that AMSH binds to CHMP3 in ^{0}HBS (closed conformation) and ^{500}HBS (open conformation) with dissociation constants of 5.6 and 392 nM,

Fig. 4. AMSH(1–206) interaction with CHMP3. (a) Native gel electrophoresis of CHMP3(9–222) (lane 1), AMSH(1–206) (lane 2), and AMSH(1–206) in complex with CHMP3(9–222) (lane 3). ITC binding curves for the AMSH(1–206)–CHMP3(9–222) interaction in (b) ^{0}HBS, (c) ^{150}HBS, (d) ^{500}HBS, and (e) AMSH(1–206) titration curve with the CHMP3 peptide (residues 196–222) in ^{0}HBS.

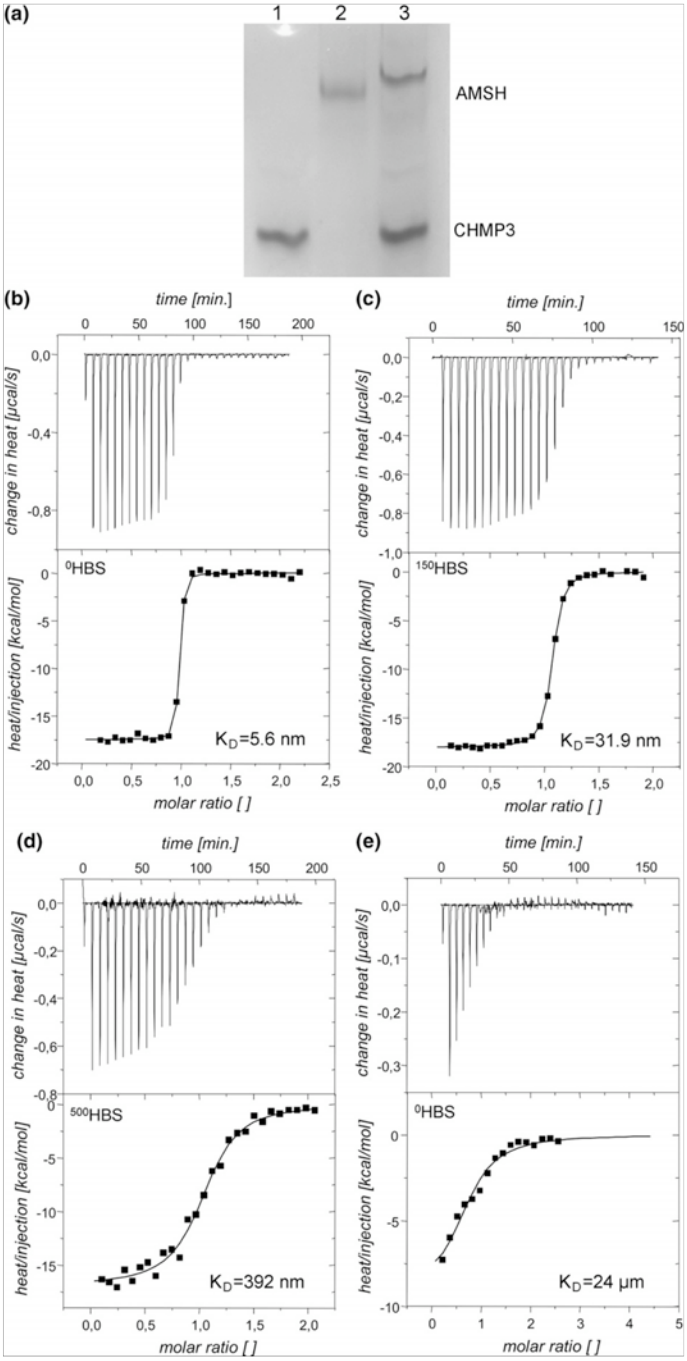

Fig. 4 (*legend on previous page*)

Table 1. ITC of the CHMP3–AMSH interaction

	CHMP3(9–222)		CHMP3(196–222)	
	^{0}HBS	^{150}HBS	^{500}HBS	^{0}HBS
n	0.950±0.002	1.04±0.002	1.04±0.01	0.706±0.083
K_d (nM)	5.6±1	31.9±3	392±40	23,690±5000
ΔH^0 (kcal/mol)	−17.5±0.08	−18.0±0.05	−16.9±0.29	−12.5±1.9
[AMSH] (cell) (μM)	15	16	15	7
[CHMP3] (syringe) (μM)	160	150	150	150

respectively, implying that the closed conformer binds tighter to AMSH as opposed to the open conformer. However, there are two reasons why the CHMP3–AMSH interaction may induce CHMP3 opening as suggested.[9] First, the low activation barrier of CHMP3 favors stabilization of an open conformation by AMSH. Second, the high-affinity interaction requires more than the C-terminal CHMP3 peptide region; this implies indirectly that the high-affinity interaction is mediated *via* one distinct CHMP3 conformation. Thus, the interaction occurs most likely *via* the open conformation, which suggests that AMSH may indeed open a closed CHMP3 conformation; the observed difference in affinity may simply result from a difference in NaCl concentration as charged residues have been implicated in the interaction.[9] On the other hand, mutagenesis analyses showed that CHMP3 residues implicated in AMSH binding (Arg216, Leu217) do not affect the interaction of the CHMP3 C-terminus with its N-terminal core,[9] indicating that AMSH interaction does not compete with the C-terminus binding to the CHMP3 core. The high-affinity CHMP3–AMSH interaction may explain why AMSH overexpression renders full-length CHMP3 dominant negative with respect to HIV-1 budding,[9] because it may sequester CHMP3 in a state that inhibits its function during budding. Because CHMP3 within a functional ESCRT-III complex seems to act late in budding, the presence of a high-affinity CHMP3–AMSH interaction would ensure efficient deubiquitination before budding is completed. In principle, CHMP3 could interact with Vps4 *via* a similar region; this, however, raises the question as to how a high-affinity CHMP3–AMSH interaction switches to a low-affinity CHMP3–Vps4 interaction, because Vps4 will not be able to compete off AMSH when bound to CHMP3. Alternatively, CHMP3 may not be a target for Vps4. The high-affinity interaction may provide stable complex formation coupled to continuous deubiquitination guaranteeing a free pool of ubiquitin, consistent with the proposal that deubiquitination precedes cargo incorporation into vesicles.[13]

Materials and Methods

Protein expression and purification

CHMP3 cDNA encoding amino acids 9–222 was expressed and purified as described previously.[21] Briefly, N-terminally His-tagged CHMP3 was expressed in *Escherichia coli* BL21 codon+ cells (Invitrogen) and purified by immobilized metal ion affinity chromatography. The His tag was cleaved off by using tobacco etch virus protease, and CHMP3 was separated from uncleaved CHMP3 and tobacco etch virus protease by another round of immobilized metal ion affinity chromatography. A final purification step included SEC in a buffer containing 20 mM Hepes, pH 7.6, and 150 mM NaCl (^{150}HBS). Further exchanges in buffers containing 20 mM Hepes, pH 7.6, and variable ionic strength levels of 0, 100, 150, 200, and 500 (^{0}HBS, ^{100}HBS, ^{150}HBS, ^{200}HBS, and ^{500}HBS, respectively) were done by SEC as indicated. The cDNA corresponding to AMSH (accession code 095630) residues 1–206 was cloned into a pBADM-41 vector (N-terminal maltose binding protein fusion) and expressed in BL21(DE3) codon+ cells (Invitrogen). Cells were lysed in Hepes buffer (50 mM Hepes, pH 8.0, and 100 mM NaCl), and AMSH(1–206) was purified on an amylose column in the same buffer. For further purification, the protein was bound on a HiTrapQ column (GE Healthcare) in Hepes buffer (50 mM Hepes, pH 8.0, and 50 mM NaCl) and eluted with a linear gradient of NaCl. Finally, a buffer exchange in ^{0}HBS, ^{100}HBS, ^{150}HBS, and ^{500}HBS was done by SEC on a Superdex™ 200 10/300 GL (GE Healthcare).

SEC and MALLS

SEC was performed with a Shodex Protein KW-804 HPLC column (300 mm × 8.0 mm). The column was equilibrated in ^{0}HBS and ^{500}HBS; the runs were performed at 20 °C with a flow rate of 0.8 ml/min. Online detection was performed by MALLS using a DAWN-EOS detector (Wyatt Technology Corp., Santa Barbara, CA) equipped with a laser emitting at 690 nm and by refractive index measurement using an RI2000 detector (Schambeck SFD). Light-scattering intensities were measured at different angles relative to the incident beam, and analysis of the data was performed with the ASTRA software (Wyatt Technology Corp.). The excess light-scattering intensity at angle θ (R_θ) is related to the molecular mass of the solute particle according to Zimm's formalism of the Rayleigh–Debye–Gans model for a diluted polymer solution.[32] For small (gyration radius, <100 nm) noninteracting particles, R_θ is given by

$$\frac{R_\theta}{K^*C} = M \tag{1}$$

where R_θ is the measured excess Rayleigh ratio, C is the protein concentration (grams per milliliter) as measured by an online refractive index detector, M is the molar mass (grams per mole), and K^* is an optical constant given by the following equation:

$$K^* = \frac{1}{N_A}\left(\frac{2\pi n_0}{\lambda^2}\right)^2\left(\frac{dn}{dc}\right)^2 \tag{2}$$

where N_A is Avogadro's number, n_0 is the refractive index of the solvent at the incident radiation wavelength (1.33 for a diluted aqueous buffer), dn/dc (milliliters per gram) is the specific refractive index increment of the solute (0.185 ml/g), and λ is the wavelength of the incident light in void (690 nm). Within the elution peak, the chromatogram is divided in slices, and for each slice, MALLS and refractive index measurements are used to calculate the molecular weight. Weight-averaged (M_w) molecular weights are obtained from the molecular weight distribution across the elution peak.

CD

CD measurements were carried out on a Jasco J-810 spectropolarimeter (Jasco Ltd., Tokyo, Japan) equipped with temperature control. Thermal unfolding of CHMP3 (3 μM) in buffers ^{0}HBS and ^{500}HBS was monitored by recording the ellipticity at 220 nm as a function of temperature.

SAXS data collection and analysis

The synchrotron radiation X-ray scattering data were collected following standard procedures on the X33 SAXS beamline (Deutsches Elektronen Synchrotron DESY and EMBL Hamburg).[33,34] A MAR345 image plate with online readout (MarResearch, Germany) was used at a sample–detector distance of 2.7 m, covering the range of momentum transfer $0.012<s<0.45$ Å^{-1} [$s=4\pi \sin(\theta)/\lambda$, where θ is the scattering angle and $\lambda=0.15$ nm is the X-ray wavelength]. The s-axis was calibrated by the scattering pattern of silver-behenate salt (d-spacing = 5.84 nm). Scattering data from CHMP3 protein solutions with concentrations of 7.2 and 2.8 mg/ml in ^{0}HBS and those of 4.2, 2.3, and 0.9 mg/ml in ^{500}HBS were measured to check for particle–particle interactions. Repetitive measurements of 180 s at 15 °C of the same protein solution were performed in order to check for radiation damage. Stable intensities especially at low angles indicated that no protein aggregation took place during the exposure times. The data were normalized to the intensity of the incident beam; the scattering of the buffer was subtracted, and the difference curves were scaled for concentration. All the data-processing steps were performed using the program package PRIMUS.[35] The forward scattering $I(0)$ and the radius of gyration R_g were evaluated using the Guinier approximation,[36] assuming that at very small angles ($s<1.3/R_g$), the intensity is represented by $I(s)=I(0)\exp(-(sR_g)^2/3)$. These parameters were also computed from the entire scattering patterns using the indirect transform package GNOM[37], which also provides the distance distribution function $p(r)$ of the particle as defined:

$$p(r) = 2\pi \int I(s) sr \sin(sr) ds \qquad (3)$$

The molecular mass of both CHMP3 conformers was calculated by comparison with the forward scattering from the reference solution of bovine serum albumin. From this procedure, a relative calibration factor for the molecular mass can be calculated using the known molecular mass of bovine serum albumin (66 kDa) and the concentration of the reference solution.

Ab initio shape modeling of CHMP3

Low-resolution models of both CHMP3 conformers were built by the program DAMMIN,[31] which represents the protein as an assembly of dummy atoms inside a search volume defined by a sphere of the diameter D_{max}. Starting from a random model, DAMMIN employs simulated annealing to build a scattering equivalent model fitting the experimental data $I_{exp}(s)$ to minimize discrepancy:

$$\chi^2 = \frac{1}{N-1}\sum_j \left[\frac{I_{exp}(s_j) - cI_{calc}(s_j)}{\sigma(s_j)}\right]^2 \qquad (4)$$

where N is the number of experimental points, c is a scaling factor, and $I_{calc}(s_j)$ and $\sigma(s_j)$ are the calculated intensity and the experimental error at the momentum transfer s_j, respectively. Ten independent DAMMIN bead models were calculated for both CHMP3 conformers, and final models were obtained by superposition of the independent shape reconstructions using the program packages DAMAVER[38] and SUBCOMP.[39]

ITC

Calorimetric measurements were carried out using a VP-ITC instrument with a cell volume of 1.4569 ml (MicroCal, LLC). CHMP3 and AMSH were exchanged in the same batch of a given buffer (^{0}HBS, ^{150}HBS, ^{500}HBS) by SEC. The same batch of the buffer was used for further dilutions and for dissolving the CHMP3 peptide (containing residues 196–222). Interaction constants characterizing the AMSH and CHMP3 protein–peptide interaction were determined by direct titration in ^{0}HBS, ^{150}HBS, and ^{500}HBS at 25 °C. The concentrations used are summarized in Table 1. The solution in the cell was stirred at 286 rpm to ensure rapid mixing. The interaction isotherms were analyzed using the Origin software package supplied by MicroCal. An interaction model assuming n independent and equivalent binding sites was applied, and the stoichiometry n, change in enthalpy ΔH^0, and binding constant K_d were iteratively fitted.

Acknowledgements

This work was supported by Deutsche Forschungsgemeinschaft SPP-1175 (W.W.), the Agence Nationale de Recherche sur le SIDA (W.W.), the University Joseph Fourier (W.W.), and the National Institutes of Health (AI29873 to H.G.). S.L. was supported by European Molecular Biology Organization and Human Frontier Science Program postdoctoral fellowships.

References

1. Morita, E. & Sundquist, W. I. (2004). Retrovirus budding. *Annu. Rev. Cell Dev. Biol.* **20**, 395–425.
2. Hurley, J. H. & Emr, S. D. (2006). The ESCRT complexes: structure and mechanism of a membrane-

trafficking network. *Annu. Rev. Biophys. Biomol. Struct.* **35**, 277–298.
3. Williams, R. L. & Urbe, S. (2007). The emerging shape of the ESCRT machinery. *Nat. Rev. Mol. Cell Biol.* **8**, 355–368.
4. Carlton, J. G. & Martin-Serrano, J. (2007). Parallels between cytokinesis and retroviral budding: a role for the ESCRT machinery. *Science*, **316**, 1908–1912.
5. Saksena, S., Sun, J., Chu, T. & Emr, S. D. (2007). ESCRTing proteins in the endocytic pathway. *Trends Biochem. Sci.* **32**, 561–573.
6. Katzmann, D. J., Odorizzi, G. & Emr, S. D. (2002). Receptor downregulation and multivesicular-body sorting. *Nat. Rev. Mol. Cell Biol.* **3**, 893–905.
7. Tsang, H. T., Connell, J. W., Brown, S. E., Thompson, A., Reid, E. & Sanderson, C. M. (2006). A systematic analysis of human CHMP protein interactions: additional MIT domain-containing proteins bind to multiple components of the human ESCRT III complex. *Genomics*, **88**(3), 333–346.
8. McCullough, J., Row, P. E., Lorenzo, O., Doherty, M., Beynon, R., Clague, M. J. & Urbe, S. (2006). Activation of the endosome-associated ubiquitin isopeptidase AMSH by STAM, a component of the multivesicular body-sorting machinery. *Curr. Biol.* **16**, 160–165.
9. Zamborlini, A., Usami, Y., Radoshitzky, S. R., Popova, E., Palu, G. & Gottlinger, H. (2006). Release of autoinhibition converts ESCRT-III components into potent inhibitors of HIV-1 budding. *Proc. Natl Acad. Sci. USA*, **103**, 19140–19145.
10. Agromayor, M. & Martin-Serrano, J. (2006). Interaction of AMSH with ESCRT-III and deubiquitination of endosomal cargo. *J. Biol. Chem.* **281**(32), 23083–23091.
11. Ma, Y. M., Boucrot, E., Villen, J., Affar, E. B., Gygi, S. P., Gottlinger, H. G. & Kirchhausen, T. (2007). Targeting of AMSH to endosomes is required for EGF receptor degradation. *J. Biol. Chem.* **282**(13), 9805–9812.
12. Row, P. E., Liu, H., Hayes, S., Welchman, R., Charalabous, P., Hofmann, K. *et al.* (2007). The MIT domain of UBPY constitutes a CHMP binding and endosomal localisation signal required for efficient EGF receptor degradation. *J. Biol. Chem.* **282**(42), 30929–30937.
13. Clague, M. J. & Urbe, S. (2006). Endocytosis: the DUB version. *Trends Cell Biol.* **16**, 551–559.
14. Bowers, K., Piper, S. C., Edeling, M. A., Gray, S. R., Owen, D. J., Lehner, P. J. & Luzio, J. P. (2006). Degradation of endocytosed epidermal growth factor and virally ubiquitinated major histocompatibility complex class I is independent of mammalian ESCRTII. *J. Biol. Chem.* **281**, 5094–5105.
15. McCullough, J., Clague, M. J. & Urbe, S. (2004). AMSH is an endosome-associated ubiquitin isopeptidase. *J. Cell Biol.* **166**, 487–492.
16. Babst, M., Katzmann, D. J., Estepa-Sabal, E. J., Meerloo, T. & Emr, S. D. (2002). ESCRT-III: an endosome-associated heterooligomeric protein complex required for MVB sorting. *Dev. Cell*, **3**, 271–282.
17. von Schwedler, U. K., Stuchell, M., Muller, B., Ward, D. M., Chung, H. Y., Morita, E. *et al.* (2003). The protein network of HIV budding. *Cell*, **114**, 701–713.
18. Horii, M., Shibata, H., Kobayashi, R., Katoh, K., Yorikawa, C., Yasuda, J. & Maki, M. (2006). CHMP7, a novel ESCRT-III-related protein, associates with CHMP4b and functions in the endosomal sorting pathway. *Biochem. J.* **400**, 23–32.
19. Strack, B., Calistri, A., Popova, E. & Gottlinger, H. (2003). AIP1/ALIX is a binding partner for HIV-1 p6 and EIAV p9 functioning in virus budding. *Cell*, **114**, 689–699.
20. Martin-Serrano, J., Yarovoy, A., Perez-Caballero, D. & Bieniasz, P. D. (2003). Divergent retroviral late-budding domains recruit vacuolar protein sorting factors by using alternative adaptor proteins. *Proc. Natl Acad. Sci. USA*, **100**, 12414–12419.
21. Muziol, T., Pineda-Molina, E., Ravelli, R. B., Zamborlini, A., Usami, Y., Gottlinger, H. & Weissenhorn, W. (2006). Structural basis for budding by the ESCRT-III factor CHMP3. *Dev. Cell*, **10**, 821–830.
22. Obita, T., Saksena, S., Ghazi-Tabatabai, S., Gill, D. J., Perisic, O., Emr, S. D. & Williams, R. L. (2007). Structural basis for selective recognition of ESCRT-III by the AAA ATPase Vps4. *Nature*, **449**, 735–739.
23. Stuchell-Brereton, M. D., Skalicky, J. J., Kieffer, C., Karren, M. A., Ghaffarian, S. & Sundquist, W. I. (2007). ESCRT-III recognition by VPS4 ATPases. *Nature*, **449**, 740–744.
24. Babst, M., Wendland, B., Estepa, E. J. & Emr, S. D. (1998). The Vps4p AAA ATPase regulates membrane association of a Vps protein complex required for normal endosome function. *EMBO J.* **17**, 2982–2993.
25. Yoshimori, T., Yamagata, F., Yamamoto, A., Mizushima, N., Kabeya, Y., Nara, A. *et al.* (2000). The mouse SKD1, a homologue of yeast Vps4p, is required for normal endosomal trafficking and morphology in mammalian cells. *Mol. Biol. Cell*, **11**, 747–763.
26. Katoh, K., Shibata, H., Suzuki, H., Nara, A., Ishidoh, K., Kominami, E. *et al.* (2003). The ALG-2-interacting protein Alix associates with CHMP4b, a human homologue of yeast Snf7 that is involved in multivesicular body sorting. *J. Biol. Chem.* **278**, 39104–39113.
27. Bowers, K., Lottridge, J., Helliwell, S. B., Goldthwaite, L. M., Luzio, J. P. & Stevens, T. H. (2004). Protein–protein interactions of ESCRT complexes in the yeast *Saccharomyces cerevisiae*. *Traffic*, **5**, 194–210.
28. Pineda-Molina, E., Belrhali, H., Piefer, A. J., Akula, I., Bates, P. & Weissenhorn, W. (2006). The crystal structure of the C-terminal domain of Vps28 reveals a conserved surface required for Vps20 recruitment. *Traffic*, **7**, 1007–1016.
29. Teo, H., Perisic, O., Gonzalez, B. & Williams, R. L. (2004). ESCRT-II, an endosome-associated complex required for protein sorting: crystal structure and interactions with ESCRT-III and membranes. *Dev. Cell*, **7**, 559–569.
30. Shim, S., Kimpler, L. A. & Hanson, P. I. (2007). Structure/function analysis of four core ESCRT-III proteins reveals common regulatory role for extreme C-terminal domain. *Traffic*, **8**, 1068–1079.
31. Svergun, D. I. (1999). Restoring low resolution structure of biological macromolecules from solution scattering using simulated annealing. *Biophys. J.* **76**, 2879–2886.
32. Wyatt, P. J. (1998). Submicrometer particle sizing by multiangle light scattering following fractionation. *J. Colloid Interface Sci.* **197**, 9–20.
33. Koch, M. H. J. & Bordas, J. (1983). X-ray diffraction and scattering on disordered systems using synchrotron radiation. *Nucl. Instrum. Methods*, **208**, 461–469.
34. Roessle, M. W., Klaering, R., Ristau, U., Robrahn, B., Jahn, D., Gehrmann, T. *et al.* (2007). Upgrade of the small angle X-ray scattering beamline X33 at the EMBL Hamburg. *J. Appl. Crystallogr.* **40**, S190–S194.
35. Konarev, P. V., Volkov, V. V., Sokolova, A. V., Koch, M. H. J. & Svergun, D. I. (2003). PRIMUS: a Windows PC-based system for small-angle scattering data analysis. *J. Appl. Crystallogr.* **36**, 1277–1282.

36. Guinier, A. (1939). La diffraction des rayons X aux tres petits angles; application a l'etude de phenomenes ultramicroscopiques. *Ann. Phys. (Paris)*, **12**, 161–237.
37. Svergun, D. I. (1992). Determination of the regularization parameter in indirect transform methods using perceptual criteria. *J. Appl. Crystallogr.* **25**, 495–503.
38. Volkov, V. V. & Svergun, D. I. (2003). Uniqueness of *ab initio* shape determination in small-angle scattering. *J. Appl. Crystallogr.* **36**, 860–864.
39. Kozin, M. B. & Svergun, D. I. (2001). Automated matching of high- and low-resolution structural models. *J. Appl. Crystallogr.* **34**, 33–41.

Results 3 – Structure of the AMSH N-terminal domain CHMP3 Complex

3.1 Determination of the minimal CHMP3 binding region of AMSH.

As crystallisation attempts for AMSH$^{1-206}$ CHMP3$^{9-222}$ failed, limited proteolysis of the complex was employed to identify a minimal AMSH fragment to complex with CHMP3, with the rationale being that proteolysing away any flexible loops and regions would aid the crystallisation process. Test time-course limited proteolysis of the AMSH$^{1-206}$ CHMP3$^{9-222}$ complex yielded several well-defined bands, and it is interesting to note that intact CHMP3$^{9-222}$ is present even after 60 minutes of proteolysis, despite previous proteolysis experiments involving CHMP3 alone show it is quickly proteolysed away under the same experimental conditions, thus AMSH protects CHMP3 from proteolysis (Figure 11A). Protection of the natural proteolysis site at residue 183 would be important for stabilising the C-terminal domain of CHMP3 with the N-terminal region of the previously determined CHMP3 structure to allow full-length CHMP3 to be structurally determined. A subsequent scale-up proteolysis run on a superdex75 size exclusion column demonstrated one of the defined fragments is soluble, and co-elution with intact CHMP3$^{9-222}$ confirmed that this fragment binds to CHMP3 (Figure 11B). Peptide mapping revealed this fragment to be residues 17-146 of AMSH. Due to the previous proteolysis result in Chapter I that identified the extreme N-terminal residues of AMSH in the AMSH CHMP3 complex, and the solubilising properties of MBP for constructs AMSH$^{1-199}$ and AMSH$^{1-206}$, residues 1-146 were cloned into an MBP-tag vector.

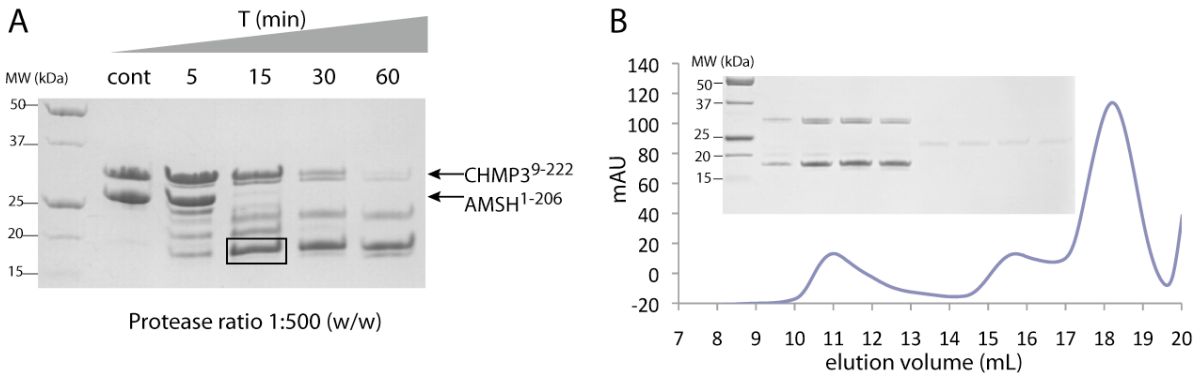

Figure 11. Limited proteolysis of the AMSH$^{1-206}$ CHMP3$^{9-222}$ complex identifies smaller soluble AMSH fragments.

A. Time-course limited proteolysis of the AMSH$^{1-206}$ CHMP3$^{9-222}$ complex produces smaller well-defined fragments. A black box outlines the fragment that was subsequently mapped.

B. Scale-up limited proteolysis and subsequent Superdex-75 size exclusion chromatography reveals a well-defined proteolytic fragment co-eluting with intact CHMP3$^{9-222}$.

3.2 AMSH$^{1-146}$ binds CHMP3$^{9-222}$.

MBP-AMSH$^{1-146}$ pulls out his-tagged CHMP3$^{9-222}$ when purified by amylose column, confirming binding. Application of the amylose elution material to a nickel column binds his-tagged CHMP3$^{9-222}$ with a now stoichiometric quantity of MBP-AMSH$^{1-146}$, with excess MBP-AMSH$^{1-146}$ from the first amylose purification step eluting in the flow-through fraction. TEV cleavage of the MBP tag from MBP-AMSH$^{1-146}$ is poor when alone, but enhanced to almost 100% efficiency in the presence of CHMP3$^{9-222}$, showing an encouraging solubilising effect of CHMP3$^{9-222}$ on MBP-AMSH$^{1-146}$ (Figure 12A). Co-elution of AMSH$^{1-146}$ with CHMP3$^{9-222}$, and a shift in elution profile from 15 mL to 13.8 mL for CHMP3$^{9-222}$, confirms complex formation (Figure 12B, 11D left gel). The complex was concentrated and sent for crystallisation trials at the EMBL robot crystallisation facility (Figure 12C), but no hits were obtained. Native gel analysis confirms no excess CHMP3 present in the complex sample sent from the 13.5 mL eluting fraction, yet reveals several species of the complex are present, which is probably why crystallisation failed (Figure 12D right gel).

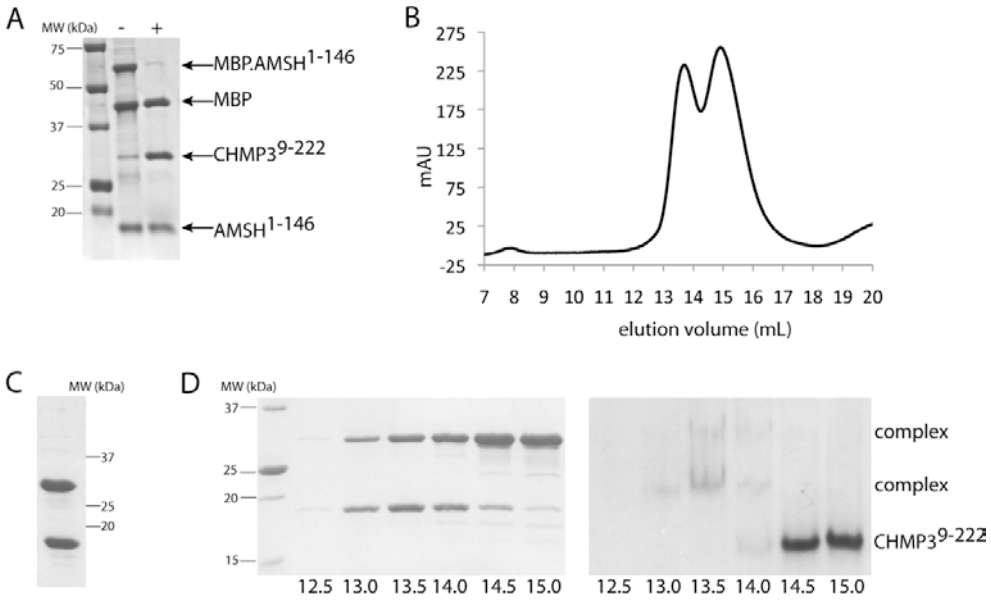

Figure 12. AMSH$^{1-146}$ and CHMP3$^{9-222}$ form a heterogenous complex.

A. TEV cleavage of the MBP tag from MBP-AMSH$^{1-146}$ is greatly enhanced in the presence of CHMP3$^{9-222}$ (- no CHMP3$^{9-222}$, + CHMP3$^{9-222}$ added).

B. The AMSH$^{1-146}$ CHMP3$^{9-222}$ complex elutes separately from free CHMP3$^{9-222}$ on superdex-200 SEC. The first peak corresponds to the complex, the second peak to free CHMP3$^{9-222}$.

C. A pure 1:1 AMSH$^{1-146}$ CHMP3$^{9-222}$ complex was concentrated and sent for crystallisation trials.

D. Left: SDS-PAGE analysis of the size exclusion profile shows free CHMP3$^{9-222}$ elutes apart from the AMSH$^{1-146}$ CHMP3$^{9-222}$ complex. Right: Native gel analysis reveals the size exclusion fractions corresponding to the AMSH$^{1-146}$ CHMP3$^{9-222}$ complex do not contain excess CHMP3$^{9-222}$ but contains multiple forms of the complex.

3.3 AMSH$^{1-146}$ is stabilised with a minimal 40 amino acid CHMP C-terminal construct.

Crystallisation attempts of full-length CHMP3 with AMSH$^{1-146}$ were tried both with the MBP-tagged version shown here, and also with a his-tagged AMSH$^{1-146}$ construct that was later determined to be partially soluble (see chapter V for details). As no crystal hits were ever obtained, it was felt a new approach was needed. Failure to crystallise seemed to be a question of heterogeneity within the complex sample, and it can be speculated that the multiple species present were various states of open and closed conformations of CHMP3, as AMSH has been implicated in the activation of CHMP3. To eliminate this it was decided to clone just the minimal AMSH binding portion of the CHMP3 C-terminal.

The discrepancy between binding of the N-terminal portion of CHMP3 (CH3ΔCT) and the C-terminal 28 amino acid peptide in the ITC data presented in *Results II* indicate the missing residues 183-193 not present in CH3ΔCT or the peptide could contribute to the binding affinity of CHMP3 to AMSH, posing the question whether AMSH binds a much longer region of CHMP3 than the binding sites previously seen in MIT CHMP interactions. The entire C-terminal portion of CHMP3 spanning residues 183-222 was cloned as a hisMBP fusion protein, termed CH3CT, and used for ITC experiments with the longer AMSH$^{1-206}$ construct used in the previous ITC studies. The resulting K_D 63 nm is orders of magnitude higher than the affinity of the 28 amino acid peptide, demonstrating the importance of residues 183-196 in CHMP3 binding (Figure 13). The nanomolar affinity is also comparable with the K_D 31.9 nm found for the interaction between AMSH$^{1-206}$ and full-length CHMP3 in physiological salt conditions. The 2-fold higher affinity of the full-length CHMP3 molecule is within the concentration error range. The strong binding affinity encouraged the use of the CH3CT construct for crystallisation trials with AMSH$^{1-146}$.

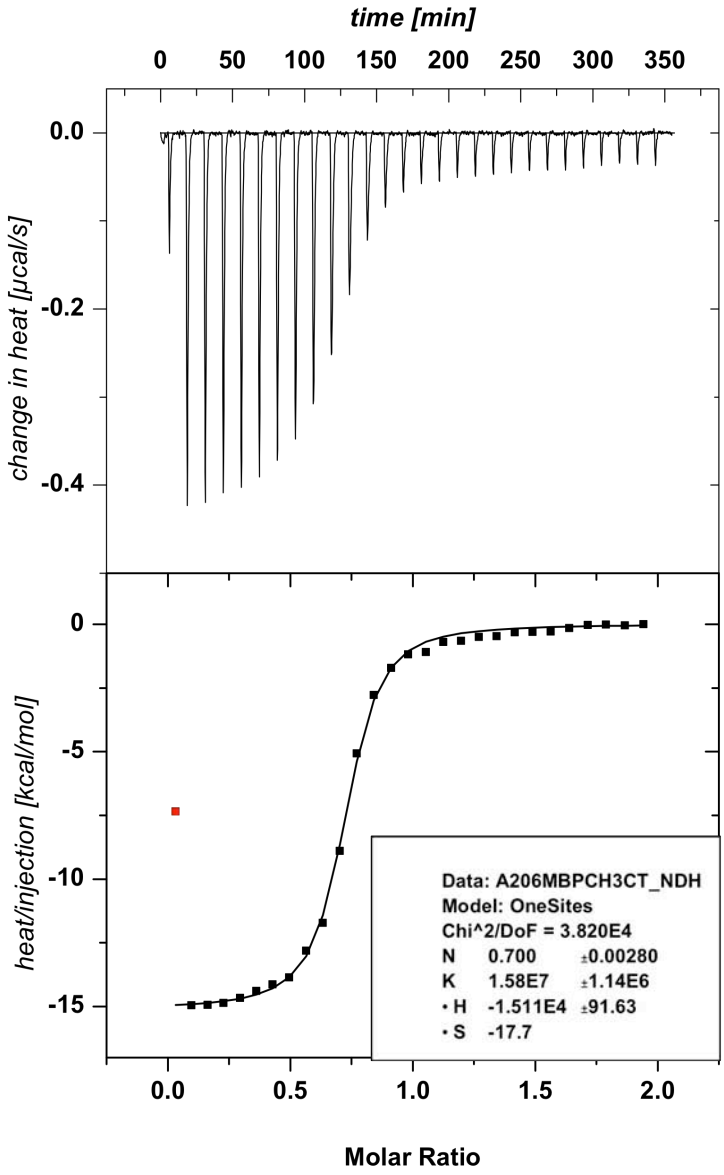

Figure 13. CH3_CT binds to hisMBP-AMSH$^{1-206}$ with nanomolar affinity.

Above: The raw calorimetric titration data for CH3_CT titrated into hisMBP-AMSH$^{1-206}$. Below: The one binding site fitting curve.

The same his-tagged AMSH$^{1-146}$ construct that was later determined to be partially soluble (see chapter V for details) and used as described above in crystallisation trials with full-length CHMP3, was used to form a complex with CH3CT (**Figure 14**A). A peak shift can be seen on the superdex75 profile from free AMSH$^{1-146}$ to AMSH$^{1-146}$ bound to CH3CT (**Figure 14**B). Free AMSH$^{1-146}$ characteristically binds high levels of RNA, due to its positive charge in pH 8.0; although the overall pI of this construct is only 7.3, removing just a few amino acids from the N-terminal increases the calculated pI to 9, revealing the potential for a highly positively charged surface in the middle of the N-terminal domain which would complement

the basic nature of the C-terminal domain of CHMP3 to form a strong electrostatic interaction.

Visualisation of CH3CT was difficult on account of its small size and poor staining in a Coomassie SDS-PAGE, but its presence in complex with AMSH$^{1-146}$ was sensed by the improvement in behaviour of AMSH$^{1-146}$, who alone always showed a concentration dependant aggregation; upon addition of CH3CT to the AMSH$^{1-146}$ construct yields of soluble protein were increased and concentrated samples were monodisperse, as assayed by dynamic light scattering. Mass spectrometry of the AMSH$^{1-146}$ CH3CT complex confirmed the presence of CH3CT, the calculated masses for AMSH$^{1-146}$ and CH3CT being 17332 g and 4645 g respectively (Figure 15).

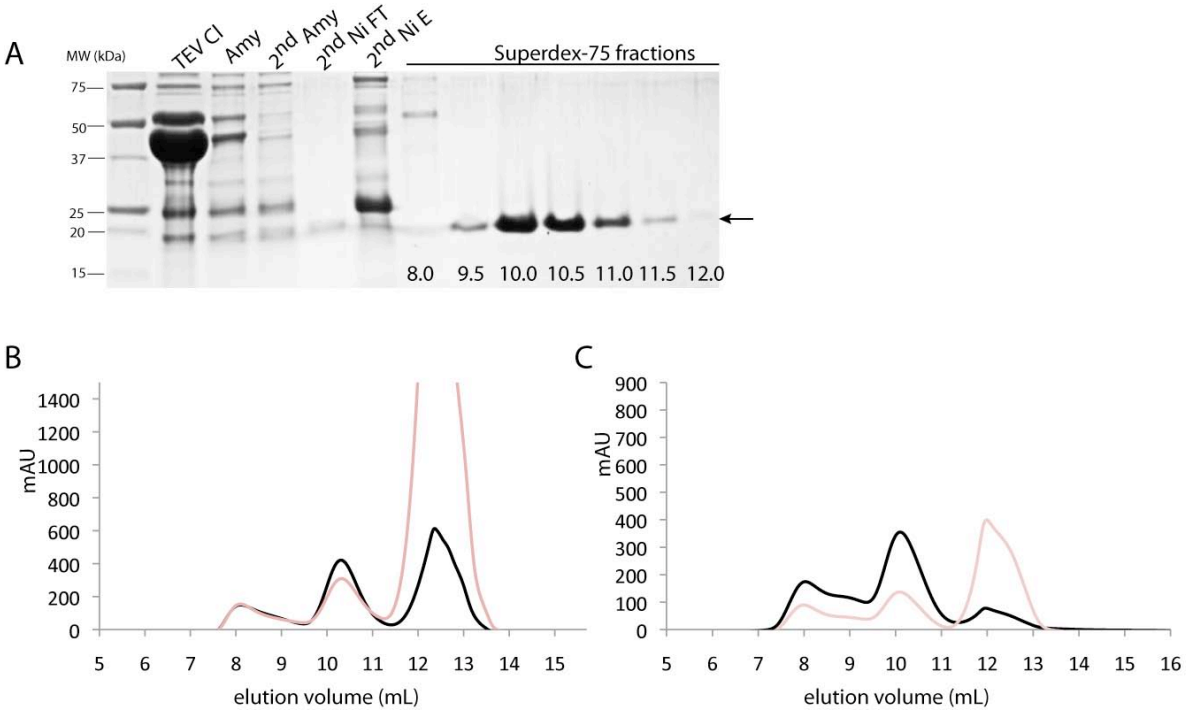

Figure 14. Purification of the AMSH$^{1-146}$ CH3CT complex.

A. After separate nickel IMAC purification of his-tagged AMSH$^{1-146}$ and hisMBP-tagged CH3CT, the AMSH$^{1-146}$ CH3CT complex is constituted and TEV cleaved to remove the tags. Amylose and second nickel IMAC purification removes the tags and uncleaved material. The flow-through from the second nickel IMAC (2nd Ni FT) was loaded onto a superdex-75 size exclusion column, yielding the pure AMSH$^{1-146}$ CH3CT complex.
B. Superdex-75 size exclusion profile of the AMSH$^{1-146}$ CH3CT complex eluting at 10.1 mL. Free AMSH$^{1-146}$ elutes later, heavily contaminated with RNA (RNA shown in red). A void volume peak is also seen for aggregated free AMSH$^{1-146}$.
C. Superdex-75 size exclusion profile of the selenomethionine substituted AMSH$^{1-146}$.CH3CT complex.

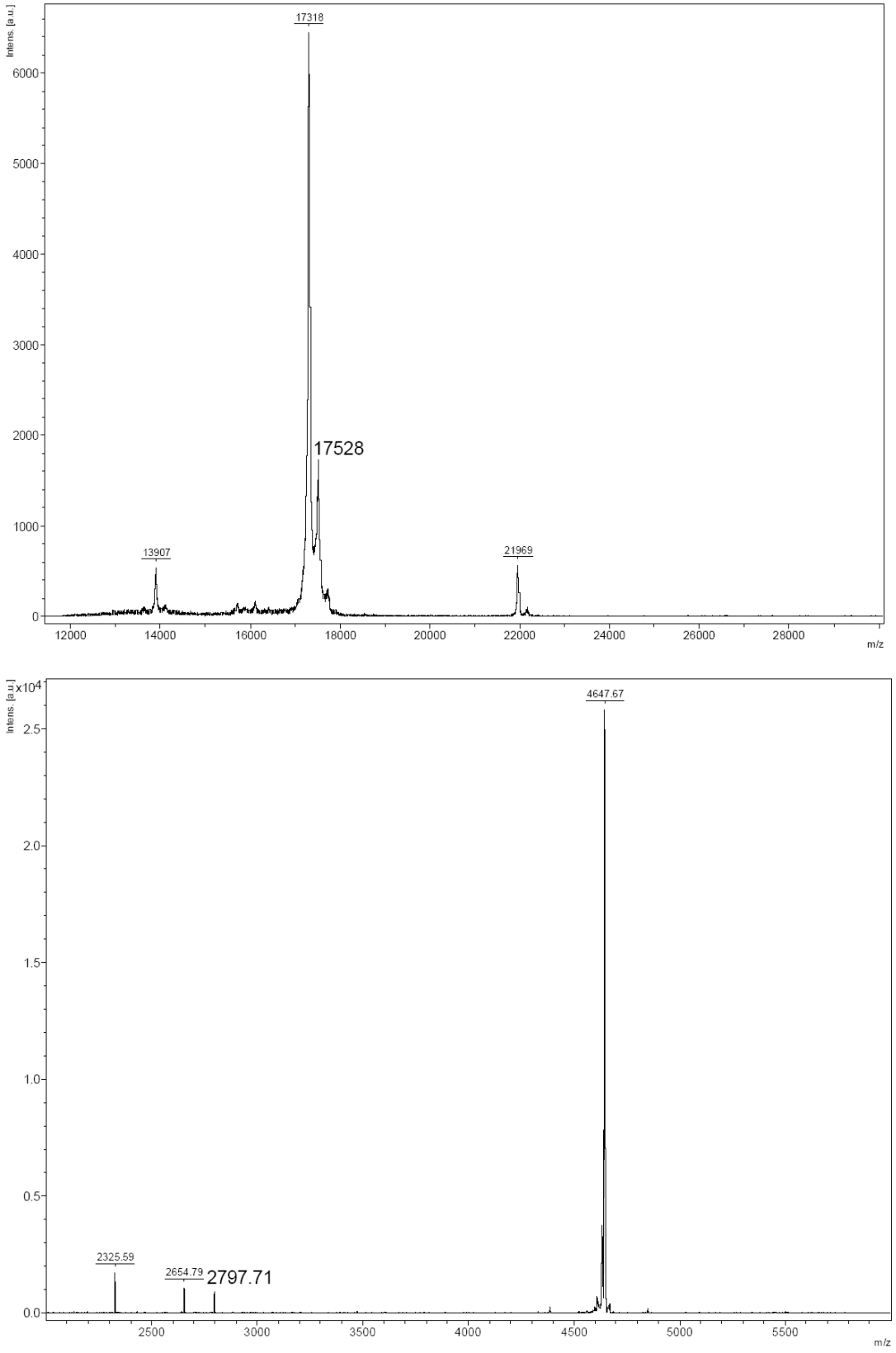

Figure 15. Mass spectrometry of the AMSH$^{1-146}$ CH3CT complex confirms presence of CH3CT.

Top panel: The mass 17318g corresponds to AMSH$^{1-146}$. Bottom panel: The mass 4647g corresponds to CH3CT.

3.4 The AMSH$^{1-146}$ CH3CT complex crystallises.

A sample of the AMSH$^{1-146}$ CH3CT complex was concentrated to 3.3 mg/mL, and submitted to the EMBL crystallisation robot facility where irregular formed, 3-dimensional crystals were obtained in one condition: 1.9M Sodium Malonate (Figure 16A, zoom Figure 16B). Although initial screening by hand gave no crystals, nice crystalline precipitate was produced (Figure 16C), which was employed in a streak-seeding experiment, giving large facetted pyramidal shaped crystals, growing in three days (Figure 16D). Streak-seeding also gave other crystal forms, which were more plate-like in nature and often overlaid on each other (Figure 16E, Figure 16F). Crystal growth was also observed within the drops used as source precipitate for the streak seeding experiments, after the streaking had taken place, demonstrating the subtle and unpredictable dynamics of crystallisation. The single facetted pyramidal crystals were frozen in 1.8 M sodium malonate, 30% glycerol and taken to ID-14-4 of the ESRF synchrotron radiation facility, where they diffracted to a resolution limit of 1.7Å (Figure 18A).

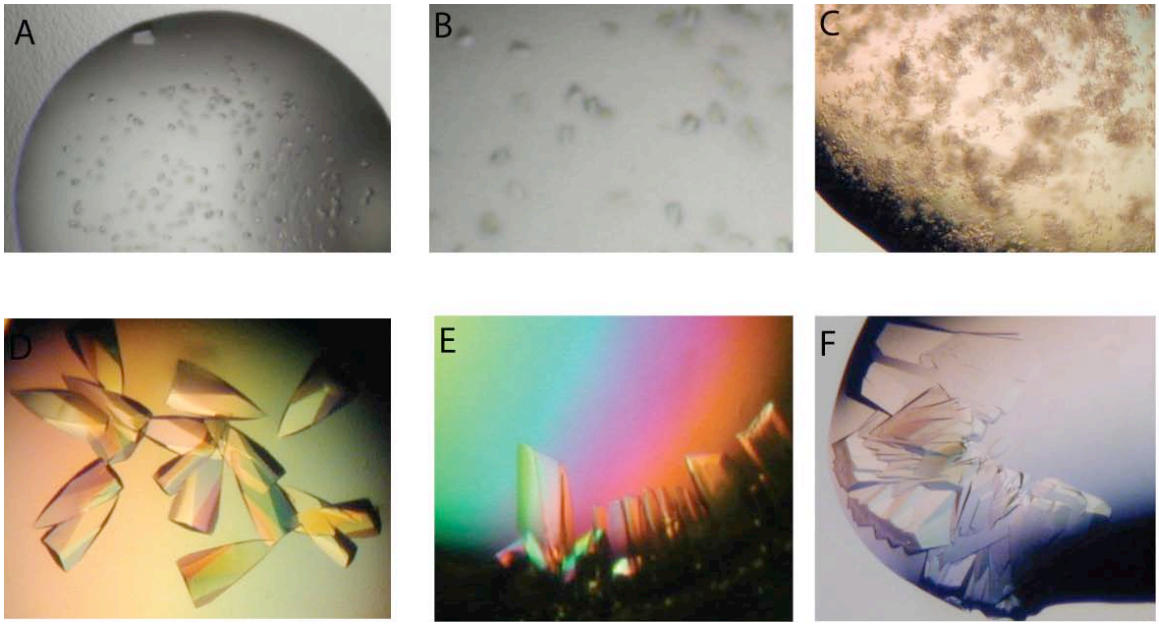

Figure 16. Crystals of the AMSH$^{1-146}$ CH3CT complex.

A. A single hit was obtained from the EMBL crystallisation robot in 1.9 M Sodium Malonate pH 6.0.

B. Zooming in on the robot crystals reveal them to be 3-dimensional, if irregular in shape.

C. Hand-set drops gave crystalline precipitate at first. Here shown in 2.2 M Sodium Malonate pH 6.0.

D. Large speed boat-shaped crystals appeared in a drop containing 1.8 M Sodium Malonate pH 6.0, after streak-seeding with crystalline precipitate from the drop of 2.2 M Sodium Malonate pH 6.0.

E. Other more plate-like crystal forms grew in drops of 1.7 M to 2 M Sodium Malonate.

F. Plate-like crystal forms were also obtained, but discarded as they were often overlaid.

Selenomethionine substituted AMSH$^{1-146}$ protein was prepared for SAD phasing, with two methionines Met46, Met136 available for seleno-labelling (**Figure 14**C). Although selenium incorporation in proteins can cause solubility and crystal reproducibility problems none of these problems were encountered for the AMSH$^{1-146}$ CH3CT complex. As with the native protein, hand set crystallisation drops gave crystalline precipitate rather than crystals (**Figure 17**A). After the success of streak-seeding with the native protein, this technique was employed for the selenomethionine crystalline precipitate, which at first only gave micro-crystals (**Figure 17**B). Interestingly, after 2 weeks small crystals began to form in the original drops used for the seeding source, in precipitant concentrations of 2.3 M sodium malonate (**Figure 17**D) and 2.4 M sodium malonate pH 6.0 (**Figure 17**C). The better crystals from the 2.3 M sodium malonate drop were frozen as for the native crystals, and diffracted to ~4Å on ID-14-2 of the ESRF.

A streak-seeding experiment was performed using the triangular plate crystals grown in the seed source drop of 2.4 M sodium malonate, where over a further two week time period tiny but beautifully defined micro-pyramidal crystals had grown behind the triangular plates orignally observed. Finally more solid 3-dimensional crystals were obtained, perfectly pyramidal in form, and although often twinned as base-to-base double pyramids, single crystals could be isolated (Figure 17E). One month later a new crystal form appeared, octagonal in shape, at first easily mistaken as bubbles/phase separation, yet developing into 3-dimensional crystal over time. The octagonal crystals did not diffract x-rays. The pyramidal crystals diffracted to 2.7 Å at the ID14-4 beamline of the ESRF, allowing a SAD data set to be collected at wavelength 0.9795 Å.

The datasets were processed with MOSFLM (Leslie, A.G.W. 1992) and Scala (Evans 2006). The crystals belong to space group $P4_1$ with unit cell dimensions of a, b = 45.97 Å , c= 206.91 Å and two complexes per asymmetric unit. Data were analyzed using the Auto-Rickshaw platform at EMBL Hamburg (Panjikar et al. 2005). Selenium sites were localized at 2.8 Å resolution with the program SHELXD (Schneider & Sheldrick 2002). The correct hand for the substructure was determined using the programs ABS (Hao 2004) and SHELXE (Sheldrick 2002). Initial phases were calculated after density modification using the program SHELXE (Sheldrick 2002). An initial model was built using the program ARP/wARP (Perrakis et al. 1999) and used as a search model for molecular replacement with MOLREP (Vagin, A.A. & Teplyakov, A. 1997)(CCP4 1994) using the native data to 1.75 Å resolution. Automatic model building was completed with ARP/wARP (Perrakis et al. 1999), manual model building using COOT (Emsley & Cowtan 2004) and refinement with the program Refmac (Murshudov et al.

1997). The structure contains AMSH residues 1 to 146 and CHMP3 residues 200 to 222 and was refined to an R factor of 19% and an R_{free} of 23.0 % (Figure 18B).

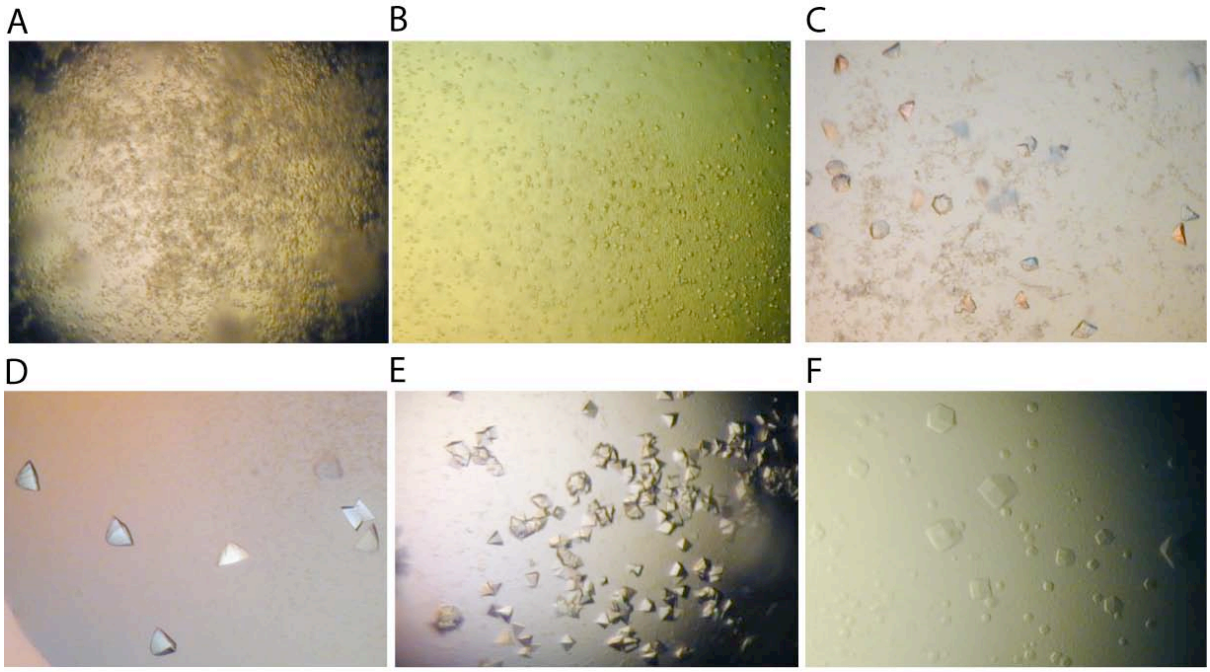

Figure 17. Selenomethionine substituted AMSH$^{1-146}$ CH3CT complex crystallises.

A. Hand-set drops initially gave crystalline precipitate. Here shown in 1.9 M Sodium Malonate pH 6.0.

B. Streak-seeding with crystalline precipitate gave microcrystals. Here shown in 2.5 M Sodium Malonate pH 6.0.

C. After twelve days thin triangular crystals appeared in the source drops for the first streak-seeding experiment. Here shown in 2.4 M Sodium Malonate pH 6.0.

D. Thin triangular crystals that appeared after the first streak-seeding experiment. These crystal were taken to ID-14-2 of the ESRF where they diffracted to ~4Å. Here shown in 2.3 M Sodium Malonate pH 6.0.

E. Beautiful pyramidal crystals grew after 3 days from streak-seeding the thin triangular crystals from the first streak-seeding experiment in 2.4 M Sodium Malonate pH 6.0 into fresh drops of 1.8 M Sodium Malonate pH 6.0.

F. An additional octagonal crystal form grew after 1 month.

A

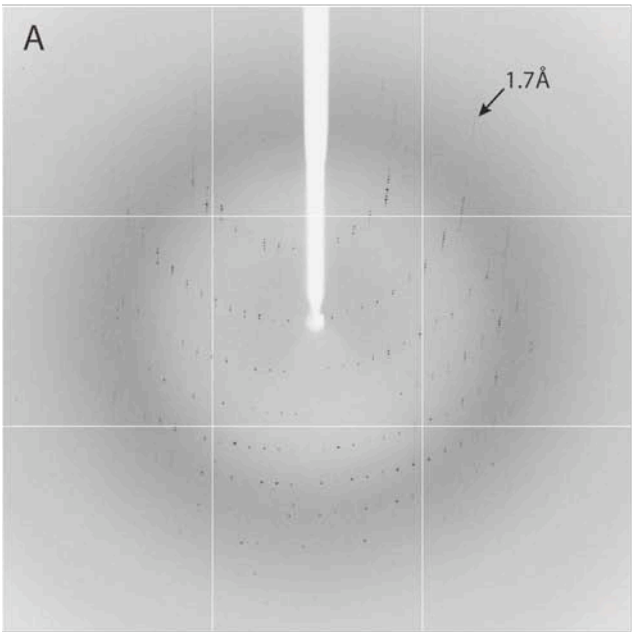

B

	Native	SeMet
Data collection		
Space group	$P4_1$	
Cell dimensions		
a = *b*, *c* (Å)	45.97, 206.91	
		Peak
Wavelength (Å)	0.9760	0.9795
Resolution (Å)	44.86 -1.75 (1.84 - 1.75)	69.84 - 2.90 (3.06-2.90)
R_{merge}	0.08 (0.64)	0.14 (0.52)
$I / \sigma I$	5.1 (1.2)	5.1 (1.4)
Completeness (%)	99.8 (100.0)	99.9 (100.0)
Redundancy	3.3 (3.3)	4.1 (4.2)
Refinement		
Resolution (Å)	1.75	
No. reflections	141,404 (20,743)	
R_{work} / R_{free}	0.19 / 0.23	
No. atoms		
Protein	2698	
Water	386	
B-factors		
Protein	32.56	
Water	45.55	
R.m.s deviations		
Bond lengths (Å)	0.02	
Bond angles (°)	1.29	

*Values in parentheses are for highest-resolution shell.

Figure 18. Diffraction data for AMSH$^{1-146}$ CH3CT native crystals, diffracting to 1.75Å resolution.

A: X-ray diffraction pattern, to a 1.75 Å resolution limit.

B: Table of diffraction statistics.

The monomeric structure of AMSH$^{1-146}$ in complex with CH3CT presented in this work shows how the N-terminal of AMSH folds into a four-helix bundle, where three of the helices are reminiscent of previously determined TPR-like MIT domains. One notable difference is the third helix of the AMSH MIT domain that spans 70 Å in length, extending beyond the helix bundle of the MIT domain. The fourth additional helix located at the extreme N-terminal (helix-0) is hinged to the second and third helices of the MIT domain via a His4-Glu57 and Arg14-Glu117 salt bridge (Figure 20A, B). The similarity of our structure with that of the N-terminal domain of UBPY suggests we have crystallised the closed form of this domain, where in the UBPY structure unhinging of the autoinhibitory helix from the third MIT helix permits dimerisation through helix exchange. Avvakumov et al. propose that dimerisation through the N-terminal domain leads to dimerisation of the full-length molecule of proteins such as UBPY and AMSH (Figure 20C)(Avvakumov et al. 2006).

CH3CT binds in a parallel fashion to AMSH$^{1-146}$ between helices 2 and 3 of the AMSH MIT domain (Figure 19A). CHMP3 contacts AMSH via a series of polar interactions; salt bridges of Glu203 to Lys88, Arg216 to Glu104, Arg221 to Glu72 as well as a hydrogen bond of Glu207 to Tyr80. AMSH Lys107 coordinates three hydrogen bonds to the CHMP3 peptide carbonyls of Thr219, Leu220 and Ser222 (Figure 19B). Hydrophobic contacts play a minor role and include packing of Leu210 into a pocket made up by Ile71, Val92 and the aliphatic portion of Lys88, Met213 is within a pocket made up by Ile71, Leu95, Phe100 and the aliphatic portion of Lys96, Leu220 is surrounded by Ile67, Phe60 and 100, and the aliphatic portions of Asn64 and Glu104. In terms of helix arrangement, in comparison with other MIT-CHMP interactions, the AMSH MIT CHMP3 structure demonstrates a helix 2/3 mode of binding. The hydrogen bond and salt bridge contacts between CHMP3 and AMSH MIT in this structure are in contrast to previously characterized MIT-MIM structures that rely predominantly on hydrophobic contacts (Figure 21). CHMP3 residues 183-194 are not seen in the electron density, despite ITC studies demonstrating the significant contribution of these residues to the binding affinity of CHMP3 for the AMSH MIT domain (see Chapter II for ITC data).

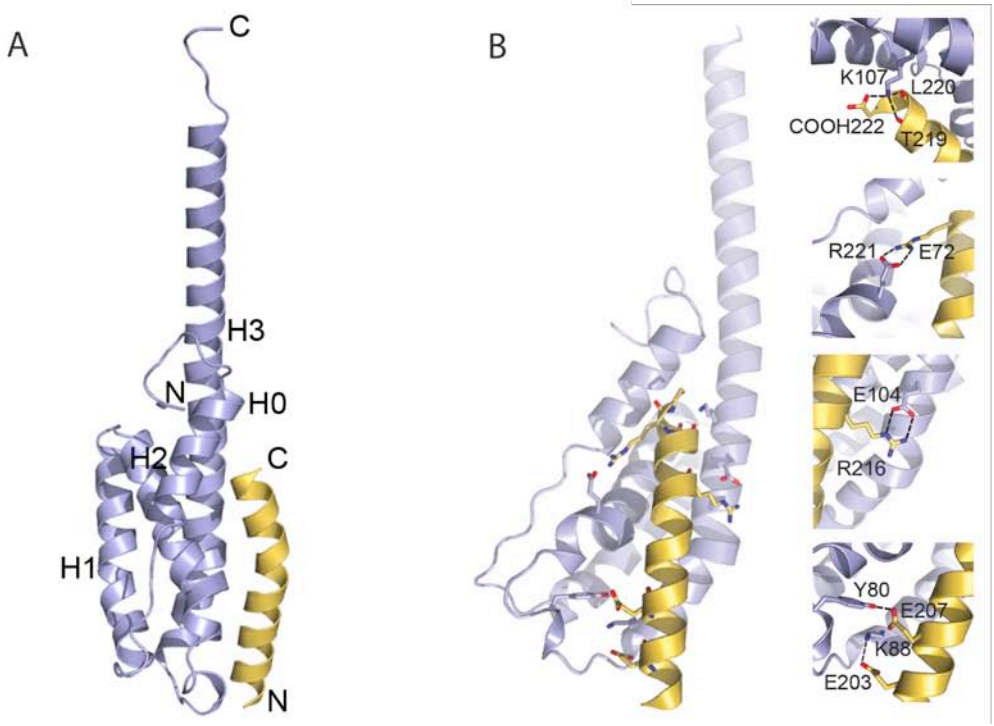

Figure 19.. CHMP3 residues 200-222 binds between helices 2 and 3 of the AMSH MIT domain.

A. Overall topology of the AMSH$^{1-146}$ CHMP3$^{200-222}$ structure, with CHMP3 binding in a parallel fashion along a groove formed by helices 2 and 3 of the AMSH MIT domain.

B. CHMP3 contacts AMSH through a series of hydrogen bonds and salt bridges. Images prepared using PyMol (http://www.pymol.org/).

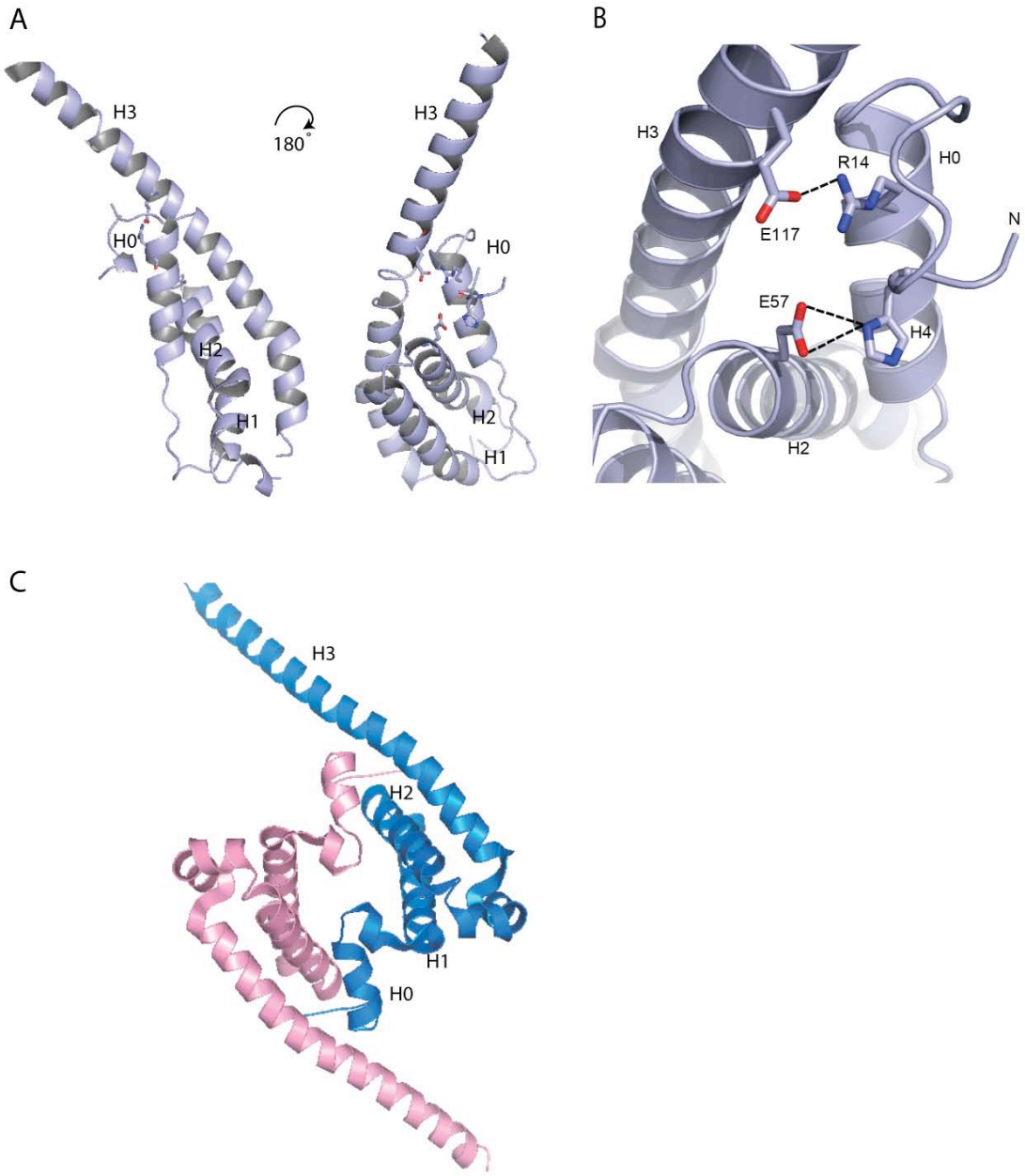

Figure 20. AMSH "closed" N-terminal domain monomer and UBPY "open" N-terminal dimerisation domain.

A. AMSH$^{1-146}$ in lilac, where the 'autoinhibitory' helix 0 is hinged to helices 2 and 3 of the AMSH MIT domain. A 180° rotation view is shown to reveal the intramolecular interactions more clearly.

B. The AMSH$^{1-146}$ helix 0 contacts helices 2 and 3 of the MIT domain via a His4 –Glu57 and Arg14 - Glu117 salt bridge.

C. UBPY dimer, one subunit in pink, one subunit in blue, where exchange of the N-terminal 'autoinhibitory' helix-0 permits dimerisation. PDB code 2A9U. Images prepared using PyMol (http://www.pymol.org/).

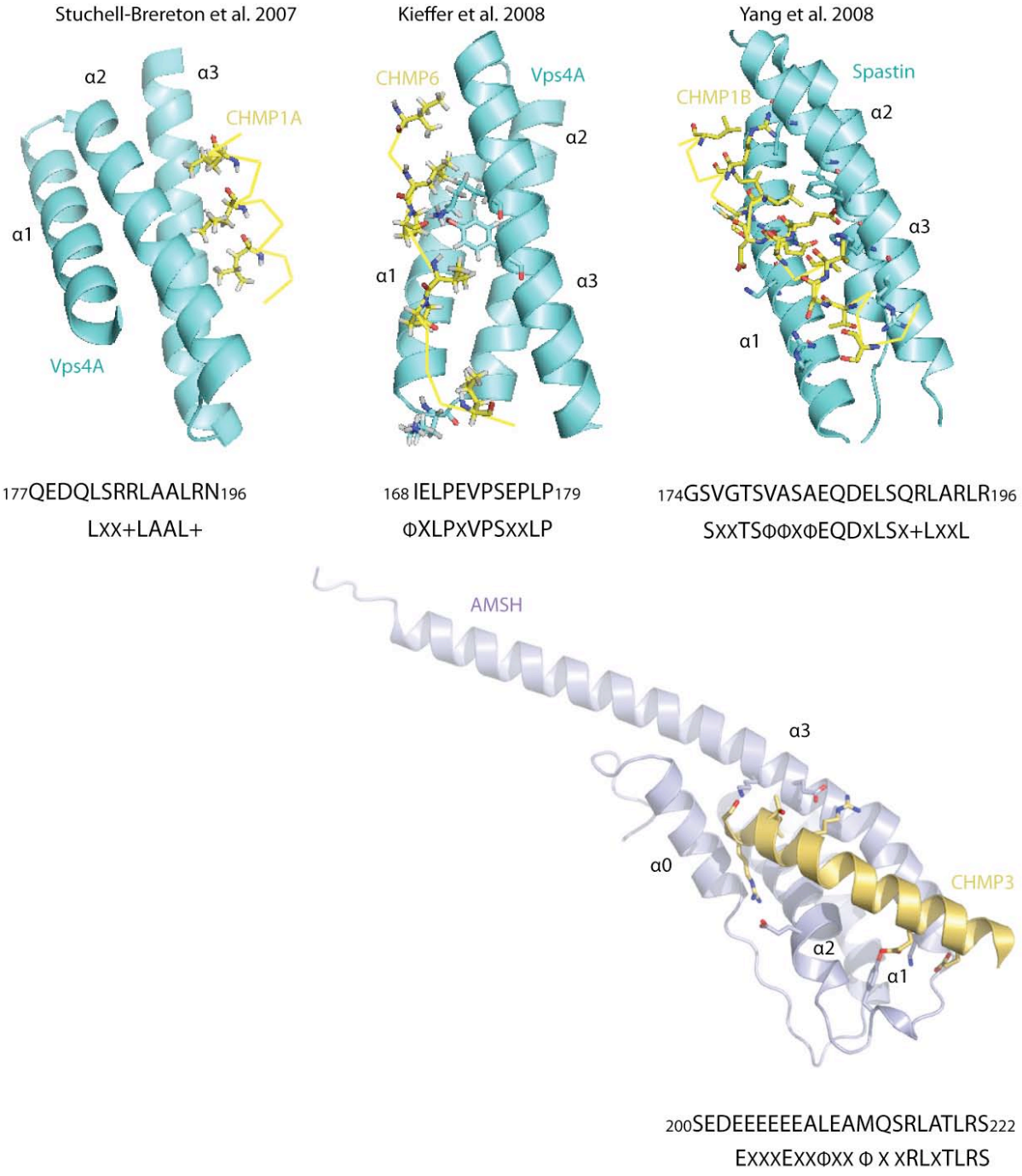

Figure 21. Ribbon diagrams of MIT-MIM structures solved to date, with consensus sequence of binding shown below. Images prepared using PyMol (http://www.pymol.org/).

Results 4 – Pursuit of Full-Length AMSH

4.1 AMSH is soluble when expressed in insect cells.

Reports in the literature that AMSH is phosphorylated led us to consider the importance of post-translational modification in solubility of AMSH, which would explain the insolubility seen in prokaryote expression systems such as *E-coli*, despite the observation that AMSH is not constitutively phosphorylated (F. Itoh et al. 2001). To explore if AMSH can be phosphorylated, and to see if this could improve the solubility of the protein, insect cells were pursued as a eukaryotic expression system.

AMSH was cloned into a pFastBacHta his-tagged vector, which was used to obtain a recombinant bacmid for insect cell expression. Transfection of SF21 cells was carried out for 2 bacmids, incubating each in three different bacmid DNA:lipid ratios, producing six P1 viral stocks in total. A large over-expression of soluble AMSH was seen in both SF21 and Hi5™ cell lines with all bacmid-derived P1 stocks, running at 51 kDa that would correspond to AMSH plus the his-tag and linker region. A Western blot using an anti-his antibody verified that the over-expressed band was indeed his-tagged AMSH. A high titre P3 viral stock was subsequently created, which an MOI (multiplicity of infection) test showed should be used at an MOI of 2 for maximum soluble AMSH production.

Expression of AMSH was high and soluble yields significant. Although his-AMSH elutes in the 10 mM imidazole wash of the nickel IMAC column it is quite pure after this first purification step, with just one major contaminant running at ~30 kDa on the SDS-PAGE (Figure 22A). The his-tag can be efficiently cleaved from his-AMSH with TEV protease, which also shifts the size of the contaminant down on a SDS-PAGE, suggesting this is in fact an N-terminal fragment of AMSH. Over time the apparition of a second contaminant band appears, running ~ 25 kDa. Neither of these species are removed by a second nickel-IMAC purification step, confirming they are degradation products rather than contaminants from non-specific binding in the first purification step. AMSH is soluble, running at 13.8 mL on a superdex-200 size exclusion column (Figure 22B). Interestingly, despite being half the size of AMSH, the degradation products elute alongside AMSH (Figure 22B).

Anionic exchange chromatography could not separate full-length AMSH from the degradation products. Neither did rapid purification at 4°C prevent this degradation occurring, suggesting the degradation fragments may have already been present, perhaps because the long expression time in the insect cells (48h) left AMSH susceptible to

proteolysis in a time-dependant manner. Alternatively, it may be due to the greater number of proteases carried over during purification from insect cells, coupled to a general susceptibility to proteolysis on the part of AMSH. No crystals were obtained with the full-length protein from insect cells and this was possibly due to the heterogeneity of full-length protein mixed with degraded fragments.

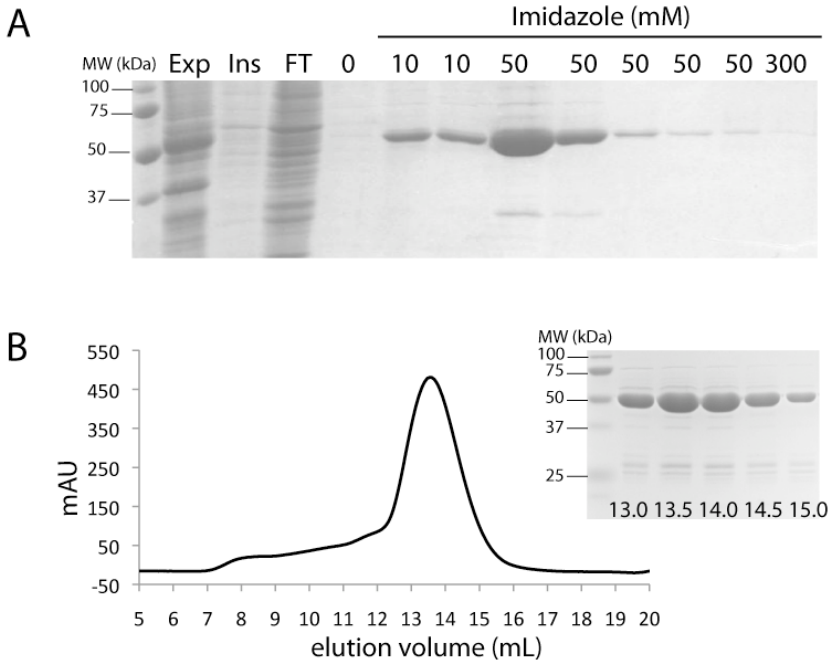

Figure 22. AMSH is well over-expressed and soluble when purified from insect cells.

A. AMSH can be purified in significant amounts from insect cell. Nickel-IMAC is used to fish out the his-tagged AMSH, which already elutes in the 10 mM imidazole wash.

B. Insect cell expressed AMSH is soluble, as verified by Superdex-200 size exclusion chromatography. Some AMSH degradation products are observed, which curiously co-elute with the full-length material.

4.2 Insect cell expressed AMSH binds CHMP3$^{9-222}$

Full-length AMSH material from insect cells binds CHMP3$^{9-222}$, as verified by a native gel band shift assay. Upon incubation of AMSH with CHMP3 a new band is seen, appearing above the running position of free AMSH (Figure 23A). CHMP3$^{9-222}$ also co-elutes with AMSH close to 13mL on superdex-200 SEC, a shift from the free CHMP3$^{9-222}$ peak that runs at 15mL (Figure 23B).

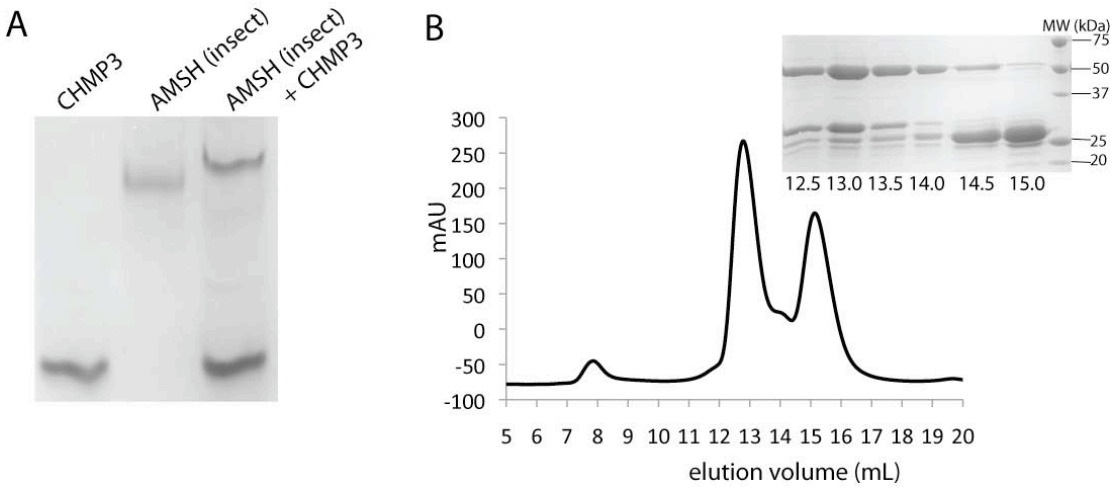

Figure 23. Insect-expressed AMSH binds to CHMP3.

A. Native gel band shift assay shows, upon incubation of AMSH and CHMP3, the formation of a new band corresponding to an AMSH CHMP3 complex, running above that of free AMSH.

B. The CHMP3 peak shifts on superdex-200 SEC, co-eluting with AMSH at 13 mL. The second defined peak corresponds to free CHMP3, the middle merged bump is either AMSH degradation products or free AMSH.

4.5 AMSH is soluble when expressed in *E-coli* with a his-tag.

As full-length AMSH was so soluble when expressed in insect cells it was considered whether the change in tag from large MBP to a smaller his tag may have been responsible. To pursue this AMSH was cloned into a pProExHta vector encoding for an N-terminal his tag. His-tagged-AMSH was both well expressed and soluble when expressed in *E-coli*, running in the soluble fraction of a superdex-200 SEC column. However, it was perplexing to see two peaks eluting on the Superdex-200, even though SDS-PAGE gel analysis depicted a pure AMSH sample with no contaminants, and more significantly, no degradation products as seen for the insect material (Figure 24). The heterogenous nature of the *E-coli* material discouraged crystallisation trials.

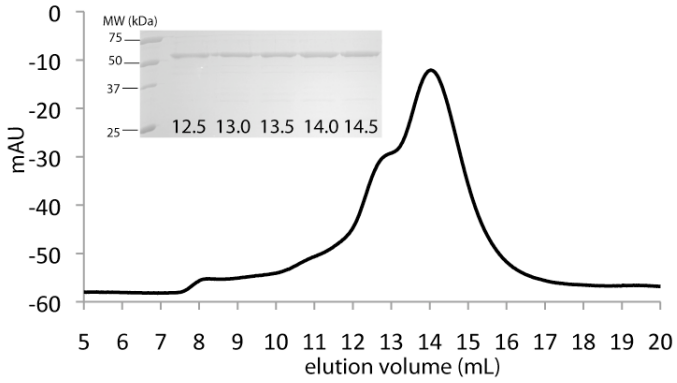

Figure 24. AMSH is soluble when expressed with an N-terminal his tag in *E-coli*, but despite sample purity, superdex-200 size exclusion chromatography shows the heterogeneity of the sample.

4.6 AMSH is soluble when expressed with no tag

As problems had now been encountered for both his-tagged and MBP-tagged AMSH, affinity tag purification strategies were abandoned, and AMSH was cloned into a pASK-IBA43plus, manipulating the restriction sites so as to leave AMSH untagged. Purification was achieved using a large anionic exchange column where, despite poor binding of AMSH requiring a lysis buffer with very low salt content, large quantities of pure AMSH were obtained. The eluted AMSH was also soluble as verified by superdex-200 SEC, and eluted in a single symmetrical peak, suggesting a homogeneity not seen when AMSH was expressed with a his-tag (Figure 25). However, the same degradation problem was encountered as for his-AMSH expressed in insect cells, which may be for a similar reason, that the long protein extraction protocol via a large anionic exchange column exposes the protein to proteolysis. It is interesting to note again that all the various degradation products elute together on anionic exchange chromatography and size exclusion chromatography, suggesting the individual components are sticking together (Figure 25).

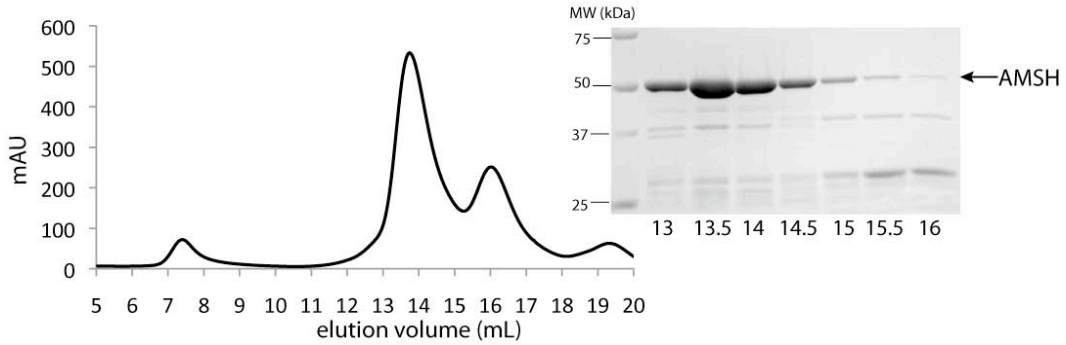

Figure 25. Untagged AMSH is soluble, but prone to degradation.

A symmetrical peak in Superdex-200 SEC confirms AMSH is soluble, but full-length AMSH co-elutes with degradation fragments.

4.7 Limited proteolysis of AMSH defines smaller soluble fragments

For homogenous full-length AMSH, obtained with a his-tag in insect cells and untagged in *E-coli* expression, degradation was a recurring problem, with the proteolysis fragments eluting in anionic exchange and size exclusion chromatography with the intact material. The natural proteolysis already confirms that these smaller fragments of AMSH are soluble, thus limited proteolysis was deemed a good strategy for identifying these smaller soluble fragments for individual cloning and characterisation.

Test proteolysis established a reproducible proteolysis pattern, with papain giving the clearest defined fragments. Interestingly, this pattern was different between insect and *E-coli* expressed AMSH, with the *E-coli* expressed protein more susceptible to proteolysis, consistently yielding smaller fragments (Figure 26A). This would imply the structure of AMSH is more compact when expressed eukaryotically, which might be due to phosphorylation of the protein.

Large-scale proteolysis with papain followed by Supedex-200 SEC showed proteolysed AMSH to be highly soluble. SDS-PAGE gel analysis revealed multiple proteolytic fragments present, yet the proteolysed material could be concentrated to as much as 30mg/mL – a concentration never before reached with any AMSH construct. It was felt if the proteolysis mixture could be cleaned up to just two or three species crystallisation trials could be considered.

Protease combinations were investigated to further proteolyse the multiple bands into just one or two major species. Initial papain digestion followed by thermolysin proteolysis was the most promising combination from the initial test proteolyses. Out of the three major bands produced in the initial single proteolysis experiment with papain, the papain/thermolysin combination completely proteolyses down the upper 25 kDa band to a lower band of 18 kDa, which after 120 mins is further proteolysed to a smaller 16 kDa fragment (Figure 26B).

Combined with the introduction of an anionic exchange step of proteolytic material after size exclusion chromatography, a scale-up limited dual proteolysis yields a sample that is pure and consists of only two fragments (Figure 26C, D). Crystallisation trials were repeated, however they were unsuccessful, and whilst the sample looked pure on the SDS-PAGE gel, and homogenous on the size exclusion column, the shoulder to the MonoQ peak reveals the presence of heterogeneity (Figure 26D). Further purification by MonoP column, a very high resolution chromatography column based on pI, was considered, but further purification steps would not have left enough protein for structural studies - already huge amounts of protein (≤200 mg) were being proteolysed to produce a low final yield of protein.

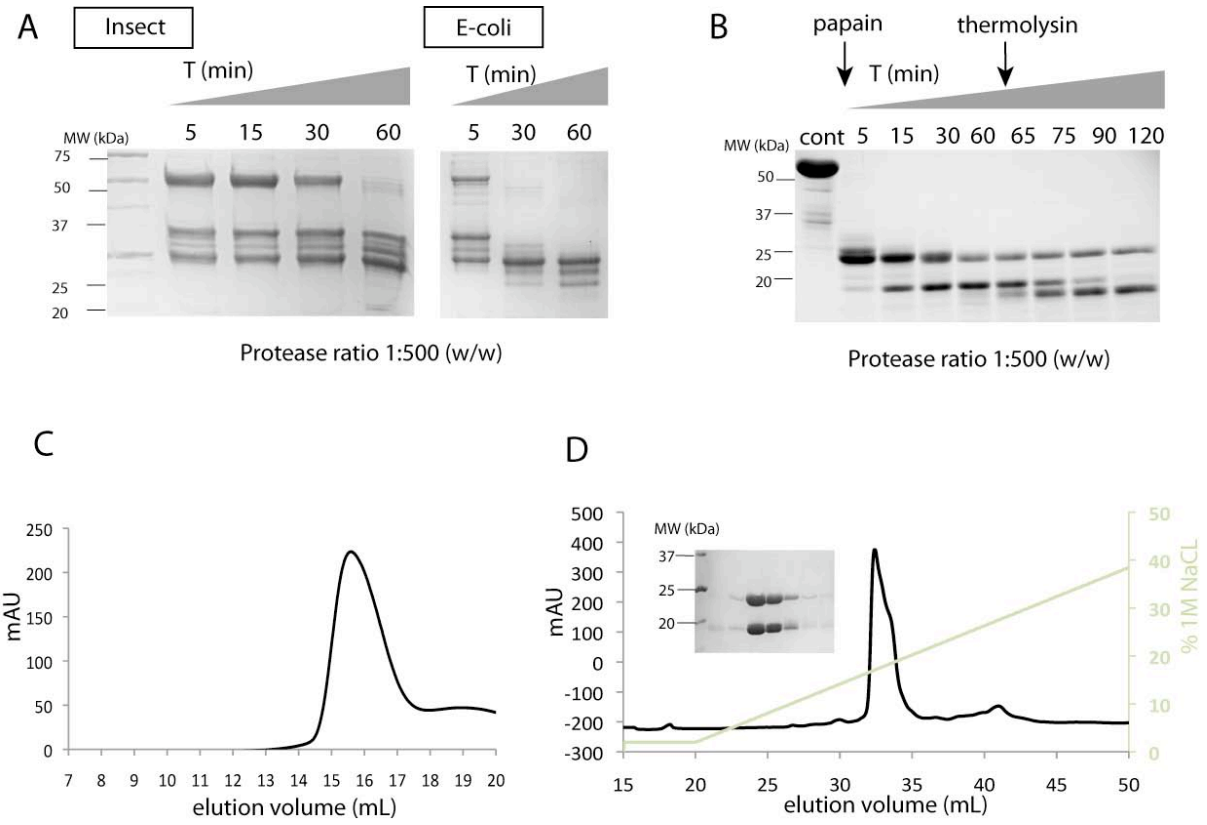

Figure 26. Papain/thermolysin combination proteolysis of AMSH produces two single soluble proteolytic fragments.

A. Papain proteolysis gave a reproducible pattern of defined fragments. *E-coli*-expressed AMSH was more susceptible to proteolysis than insect-expressed AMSH.

B. Extensive two hour proteolysis of AMSH with papain and thermolysin yields two defined proteolysis species, with the lower 18 kDa fragment proteolysing down further to a new fragment around 16 kDa.

C. Superdex-200 SEC of the large-scale proteolysis material shows a single monomeric peak.

D. Anionic exchange after Superdex-200 SEC of the large-scale proteolysis material shows that, despite the exceptional purity of the sample, there is a shoulder to the peak that demonstrates the heterogeneity of the sample.

4.8 Identification of AMSH proteolytic fragments

The second goal of proteolysis was to identify and individually clone the soluble fragments, which it was hypothesised would avoid the heterogeneity that proteolysis produced.

MALDI (matrix assisted laser desorption ionisation) mass spectrometry was used to analyse the natural degradation pattern of the insect cell expressed AMSH. The peak at 51154.76 corresponds to his-tagged AMSH (calculated mass 51098, thus an error within MALDI range) (Figure 27A). The major proteolytic species appearing around 27 kDa on SDS-PAGE was also found in the mass spectrum at 27743 g, and N-terminal sequencing analysis reveals this fragment to be the N-terminal of AMSH (Figure 27A, Figure 27C). If 27743 g is mapped onto the N-terminal of the AMSH sequence (including residues from the his-tag and linker region as the sample was uncleaved) this would correspond to residues 1-211 of AMSH. Peptide mapping of the fragment concurs with this, covering residues 1-200. There was some variation found for the mass spectrum of natural proteolytic fragments, but as there are many residue repeats in the N-terminal these were probably due to small variations in the protease cleavage site.

A peptide mapping analysis was also made of the degradation seen for insect expressed AMSH, and for the limited proteolysis of bacterially expressed AMSH (Figure 27B, left and middle gel), producing the following result: soluble C-terminal was found! And this despite attempts to clone the JAMM domain based on bioinformatic determination of the domain borders, which now could clearly be seen as too minimal (Appendix 1). The mapped JAMM domain spans residues 235-416. The shorter fragment for the N-terminal domain corresponds exactly to the AMSH$^{1-146}$ construct that was identified in the AMSH$^{1-206}$ CHMP3 complex proteolysis (Chapter III), with a longer one extending to residue 178 also found (Figure 27D). Finally, the minimal two bands produced from the dual proteolysis of bacterial his-tagged AMSH (Figure 27B, right gel) were peptide mapped, showing that the residues from the N- and C- termini are present.

The final proteolysis to just two species had already generated speculation that there may be one form corresponding to the N-terminal MIT domain and one corresponding to the enzymatic C-terminal JAMM domain. The sequencing results strengthen this theory, a theme to be elaborated on in Chapter V.

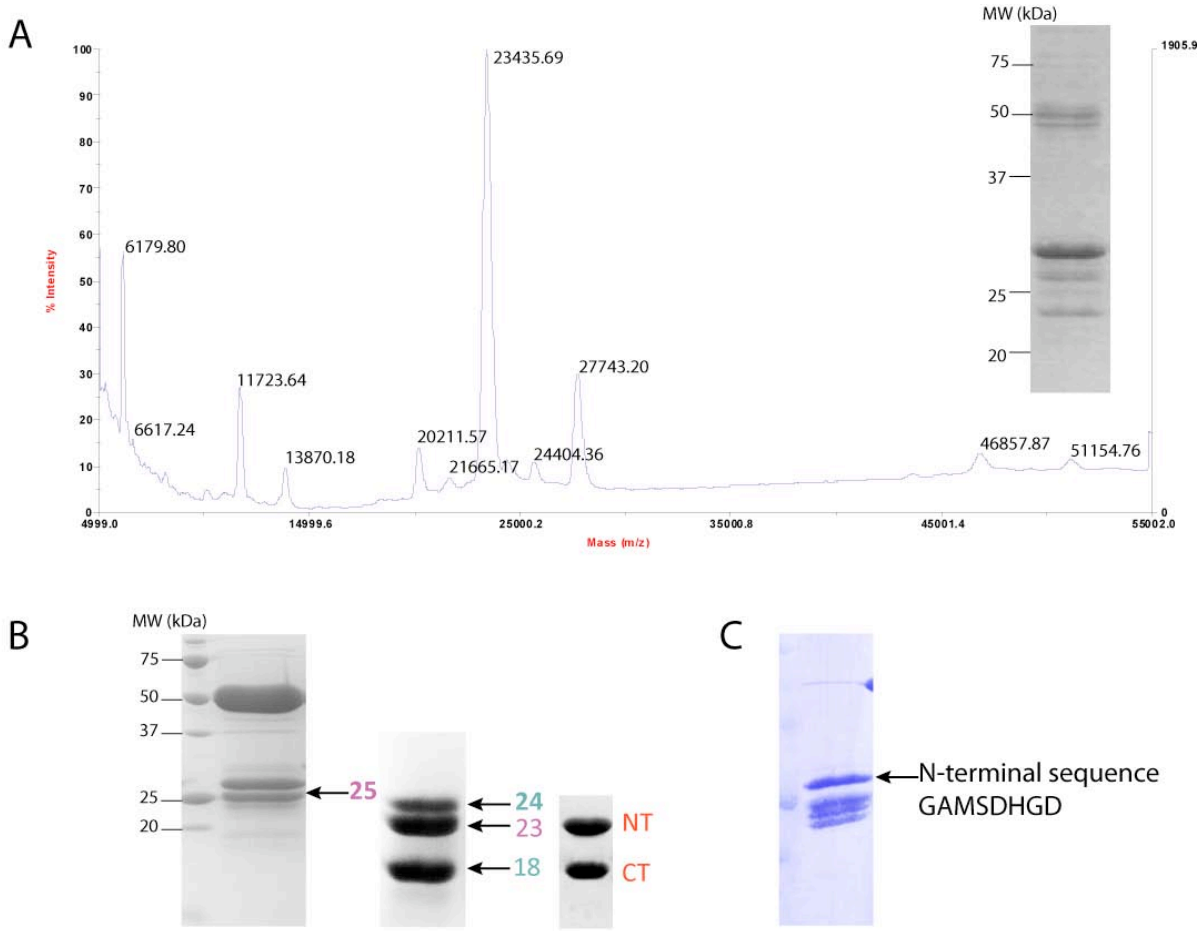

Figure 27. Sequence analysis of soluble AMSH proteolysis fragments reveals both N-terminal and C-terminal fragments are present.

A. MALDI-MS was used to analyse the natural proteolysis seen with his-AMSH expressed in insect cells. Two main fragments can be seen at mass 23436 g and 27743 g. Inset: An SDS-PAGE of the sample analysed.

B. SDS-PAGE of AMSH samples sent for peptide mapping. Left gel: Insect–expressed AMSH natural degradation. Middle gel: Limited proteolysis of his-tagged AMSH expressed in *E-coli*. Right gel: Dual proteolysis (papain, thermolysin) of his-tagged AMSH expressed in *E-coli*.

C. N-terminal sequencing of natural proteolysis of insect cell-expressed AMSH. The sequence shows the degradation product running ~30 kDa on SDS-PAGE corresponds to the N-terminal of AMSH.

D. Sequence coverage of the peptide mapping of various AMSH samples. The coloured sequences refer to residues identified from bands indicated in the respective colour in figure B. The N-terminal mapped sequences are highlighted in turquoise, the JAMM domain in pale mauve (*E-coli* middle gel) and dark mauve (insect, left gel), and the extreme N- and C-termini from the mapping of the dual proteolysis products (right gel, B) in red.

Results 5 – The JAMM domain structure and the AMSH Inter-domain Interaction

5.1 Peptide mapping constructs of the AMSH N-terminal domain.

A combination of degradation problems during purification, and subsequent limited proteolysis of full-length AMSH, identified in Chapter IV soluble AMSH fragments. Peptide mapping of these fragments revealed two to correspond to the AMSH N-terminal MIT domain, and a third to the C-terminally located enzymatic JAMM domain. Several constructs based on these mapping results were cloned into the his-tag encoding vector pProExHta.

The final peptide mapping of the dual proteolysis indicated the presence of the first 12 residues, which are important to maintaining the N-terminal soluble, as demonstrated by AMSH constructs spanning residues 12-146, 16-146, 12-178 and 16-178 that had been cloned following the first peptide mapping results (as up until the final mapping, the extreme N-terminal had only be seen for insect expressed AMSH or in the presence of CHMP3). Please note, whilst the structure of AMSH$^{1\text{-}146}$ in complex with CH3CT, which was previously described in Chapter III, demonstrates a clear structural importance of the first 12 residues, and thus why these constructs were not soluble, this structure was obtained in the very late stages of the thesis, after this work was completed. These N-terminally truncated constructs were either found directly in the insoluble fraction, or solubly in small chaperone-contaminated amounts.

A recloning of the N-terminal peptide mapping constructs to include the first 12 residues was made, producing his-tagged AMSH$^{1\text{-}146}$, AMSH$^{1\text{-}178}$ and AMSH$^{1\text{-}199}$. Whilst his-tagged AMSH$^{1\text{-}146}$ was partially soluble (and subsequently used to obtain the AMSH$^{1\text{-}146}$ CH3CT structure, see Chapter III), AMSH$^{1\text{-}178}$ was barely soluble, and AMSH$^{1\text{-}199}$ ran mainly in the void volume of a Superdex-200 SEC.

5.2 JAMM domain peptide mapping constructs.

Out of the JAMM domain constructs designed from the full-length proteolysis pattern, AMSH$^{235\text{-}416}$ and AMSH$^{235\text{-}424}$ (AMSH_CT) were very soluble, whilst the shorter construct AMSH$^{235\text{-}400}$ was poorly expressed (Figure 28A). At first it looked like the original peptide mapping result, missing the last few residues of the C-terminal, was correct, as AMSH_CT

seemed liable to proteolysis (Figure 28B). However, once the final peptide mapping results came in, showing that the last C-terminal residues are present in the minimal proteolysis complex, AMSH_CT was the construct pursued. Although purified with a 75kDa contaminant, the contaminant is clearly separated from the pure AMSH_CT material by Superdex-200 SEC (Figure 28B).

Whilst all small-scale solubility test purifications were made using Ni-NTA resin, scale-up preparations were purified using chelating sepharose resin. This change in protocol was met with huge precipitation of AMSH_CT. As the major difference between the two resins is the number of coordination sites for metal ions, and thus the strength of interaction with metal ions, it would seem that the greater metal ion leaching seen with chelating sepharose affects AMSH_CT solubility. As the JAMM domain is a zinc-binding enzymatic domain it is indeed reasonable that exposed zinc ions could be displaced by a large concentration excess of competing nickel metal ions, nickel ions being of similar size and charge as zinc ions.

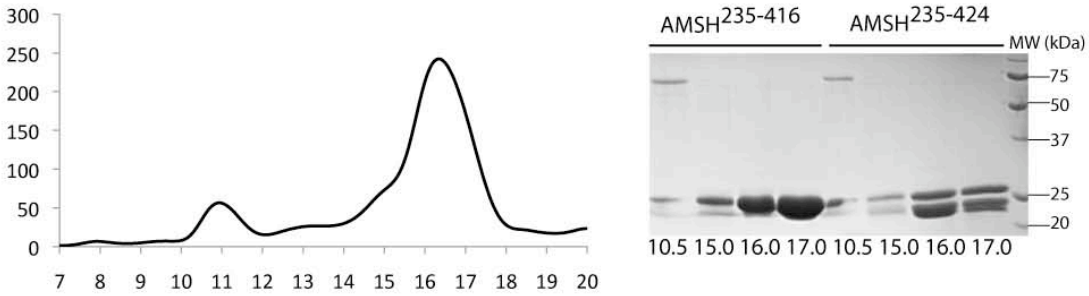

Figure 28. Soluble JAMM domain constructs based on peptide mapping of AMSH proteolysis.

A. AMSH$^{235-416}$ and AMSH$^{235-424}$ (AMSH_CT) are soluble, as verified by superdex-200 SEC. SDS-PAGE analysis of the fractions reveals AMSH_CT is susceptible to proteolysis over time.

5.3 AMSH_CT as an MBP-tagged construct is pure, soluble, homogenous and crystallises.

In light of the complications that developed with ion leaching during nickel purification of AMSH_CT, and the promise of this construct, AMSH_CT was recloned into pBADM-41 to have a hisMBP tag. Purification via amylose resin avoided the precipitation seen with the nickel-chelating sepharose. TEV cleavage of the tag was efficient and anionic exchange was used to bind the MBP, collecting AMSH_CT in the flowthrough, which elutes as a single peak when applied to a superdex-75 size exclusion column (Figure 29A).

AMSH_CT can be concentrated up to 30 mg/mL, and samples were submitted at concentrations of 8 mg/mL, 13mg/mL and 24 mg/mL to the EMBL crystallisation robot. The sample sent at 24 mg/mL gave many hits in a variety of precipitation agents; PEG 4K with ammonium sulphate, PEG 6K and 8K, alcohols like ethanol and MPD, across a pH range of 7.5 - 9.0 (Figure 29 B,C,D,E). Whilst single rhombic crystals appeared within a few days (Figure 29B), the "shark tooth" crystals took longer, continuing to grow in size over several weeks (Figure 29C). In some conditions it can be seen that the "shark tooth" crystals are more over-laid plates than 3-dimensional crystals, which would have implications for their diffraction potential (Figure 29E). The sample sent at 13 mg/mL also gave some hits, with the best giving beautiful rhombic crystals grown in drops with 20% ethanol as the precipitant (Figure 29D). Crystals grown in 5% PEG 6K, pH 9.0; 20% ethanol, pH 8.5; and 4% PEG 8K, pH 8.5 were mounted in 30% glycerol cryoprotectant, and diffracted x-rays at ID14-4 to 3.2 Å.

Manual screening gave the same crystal forms as the hits from the robot, forming nice single rhomboid crystals (Figure 30A). In certain conditions these rhomboid crystals take on a more plate-like appearance, with a tendency to cluster (Figure 30B). No better diffraction than that seen with the robot crystals was obtained, with the best resolution of 3.5 Å obtained with crystals grown in 4% PEG 8K, pH 8.0, 30% glycerol cryoprotectant.

Before this structural project could be pursued further the structure of a human JAMM domain from a very similar protein, AMSH-like protein (AMSH-LP) was released from the PDB, with simultaneous publication of an article in the journal Nature (Y. Sato et al. 2008). Although AMSH and AMSH-LP differ substantially in their N-terminal sequences and capacity to bind STAM, most critically their JAMM domains are highly conserved, and all residues implicated in the enzymatic function of the JAMM domain are retained between the two proteins.

We tried to solve our native dataset using molecular replacement but this strategy failed due to the poor quality of the data. Problems were encountered reproducing soluble protein and thus crystals for zinc anomalous phasing.

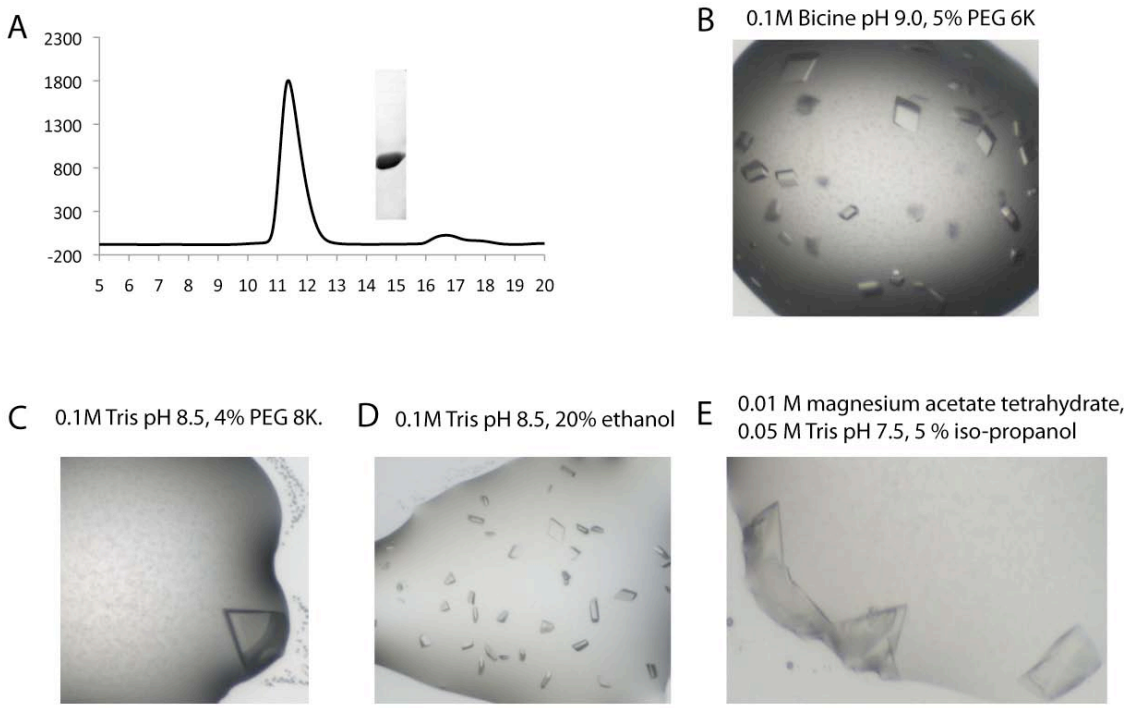

Figure 29. AMSH_CT is homogenous and crystallises in a wide range of precipitant and pH conditions.

A. AMSH_CT gives a symmetrical peak on Superdex-75 SEC, showing its homogeneity. Inset: SDS-PAGE of the pure sample sent for crystallisation trials.

B. AMSH_CT concentrated to 24 mg/mL gives single rhombic crystals in 5% PEG 6K, pH 9.0.

C. AMSH_CT at 24 mg/mL gives 3-dimensional "shark tooth" shaped crystals in 4% PEG 8K, pH 8.5.

D. AMSH_CT at 16 mg/mL gives crystals, with beautiful 3-D rhomboid crystals growing in 20% EtOH, pH 8.5.

E. AMSH_CT at 24 mg/mL in some conditions gives "shark tooth" crystals that are more overlaid plates than 3-dimensional crystals, as seen here in 0.01M magnesium acetate tetrahydrate, 5% iso-propanol, pH 7.5.

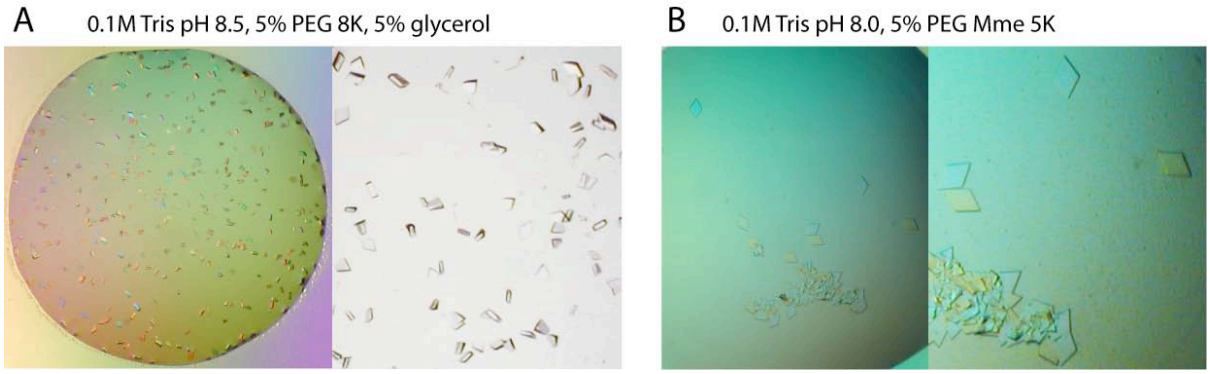

Figure 30. Crystals of AMSH_CT obtained by robot screening can be reproduced by hand.

A. Left panel: The same rhombic crystals obtained by robot screening can be obtained in manual drops, here with 5% PEG 8K, 5% glycerol, pH 8.5. Right panel: zoom in of crystals.

B. Left panel: Manual drops of AMSH_CT give rhombic shaped crystals, with a tendency to cluster in thin-plate aggregates. Drop conditons: 5% PEG Mme 5K, pH 8.0. Right panel: zoom in of crystals.

5.5 Interaction between the AMSH N-terminal and JAMM domain.

The proteolysis of full-length material showed a striking stoichiometry between quantities of N-terminal domain and C-terminal JAMM domain fragments. In particular, the final dual proteolysis with papain and thermolysin produced in equal quantity, as analysed by peptide mapping, one species corresponding to the AMSH N-terminal domain, and one corresponding to the JAMM domain. The way these domains co-elute on superdex-200 SEC and anionic exchange, despite the fact AMSH_CT is usually found in the flowthrough of anionic exchange, suggests these two fragments may be bound to each other in the full-length molecule.

MBP-AMSH_CT pulls out a small amount of his-tagged AMSH$^{1-146}$ by amylose resin purification. After purification via anionic exchange and amylose affinity chromatography to remove free MBP, a pure sample of AMSH$^{1-146}$ with AMSH_CT can be obtained. AMSH$^{1-146}$ and AMSH_CT co-elute on a superdex-75 column, and the shift in elution profile for AMSH_CT from 11.5 mL to 10.2 mL affirms complex formation (Figure 31A). The observation that the complex elutes at the same volume as the AMSH$^{1-146}$.CH3CT complex suggests AMSH_CT binding to AMSH$^{1-146}$ does not increase the hydrodynamic radius of the N-terminal domain, indicating a binding area within the hydronamic radius of the extended 70 Å long third helix of the AMSH MIT domain. The purified AMSH$^{1-146}$ AMSH_CT complex can be cross-linked, forming a new band migrating at 40 kDa on SDS-PAGE that would correspond to the size of AMSH$^{1-146}$ (17kDa) and AMSH_CT (23kDa) together (Figure 31B).

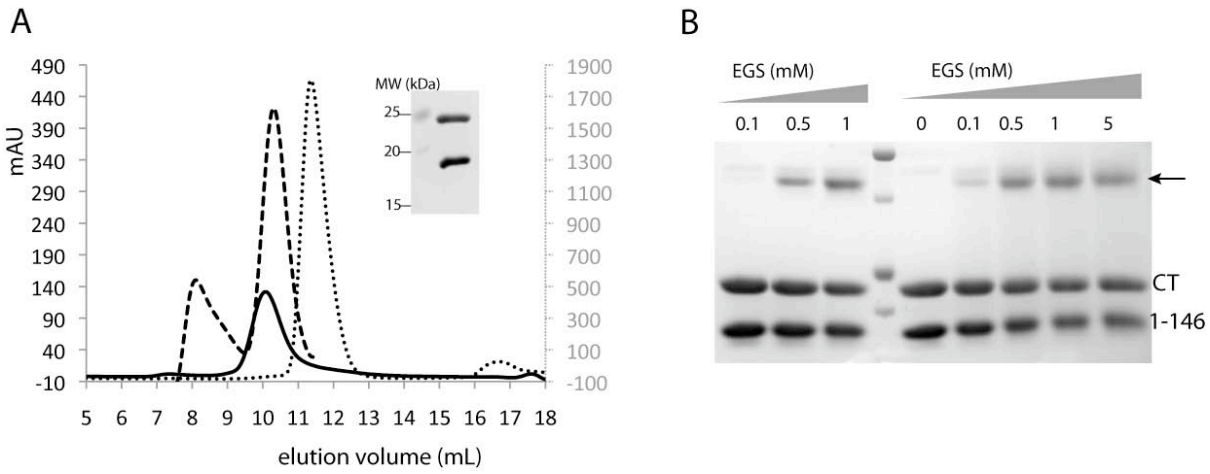

Figure 31. AMSH MIT construct AMSH$^{1-146}$ forms a complex with AMSH_CT.

A. AMSH_CT and AMSH$^{1-146}$ co-elute together in a single symmetrical peak on a superdex-75 SEC column (solid line). A shift in elution profile is seen for AMSH_CT from 11.5 mL to 10.2 mL (dotted line). The elution of the complex at the same volume as the AMSH$^{1-146}$ CH3CT complex (broken line) indicates AMSH_CT binds within the hydrodynamic radius of the AMSH N-terminal domain.

B. Cross-linking fractions from the AMSH_CT and AMSH$^{1-146}$ SEC peak produces a new band, running at 40 kDa on an SDS-PAGE, exactly the size expected for the complex.

5.6 The ubiquitin hydrolase activity of AMSH.

The ubiquitin hydrolase activity assay of AMSH was initially exploited as a means to quality control the functionality of insect cell expressed AMSH, and later bacterial-expressed JAMM constructs. Both show ubiquitin hydrolase activity, hydrolysing tetraubiquitin chains to diubiquitin (Figure 32). Later we wanted to investigate how the activity of the JAMM domain alone compared with its activity in the context of the full-length protein. It is surprising to note that full-length AMSH has a higher activity than the JAMM domain (AMSH_CT) alone, and activity of AMSH_CT is enhanced in the presence of the AMSH N-terminal construct AMSH$^{1-146}$ (Figure 32). Instead of negatively regulating the JAMM domain's activity it would seem the AMSH N-terminal domain is stimulating its deubiquitinating activity. An anti-ubiquitin band corresponding to AMSH_CT is seen for AMSH_CT alone, but not when AMSH$^{1-146}$ is added, suggesting some ubiquitin remains bound to the JAMM domain when the AMSH N-terminal domain is not present. The AMSH full-length material used for comparison in these assays was untagged AMSH expressed in *E-coli*.

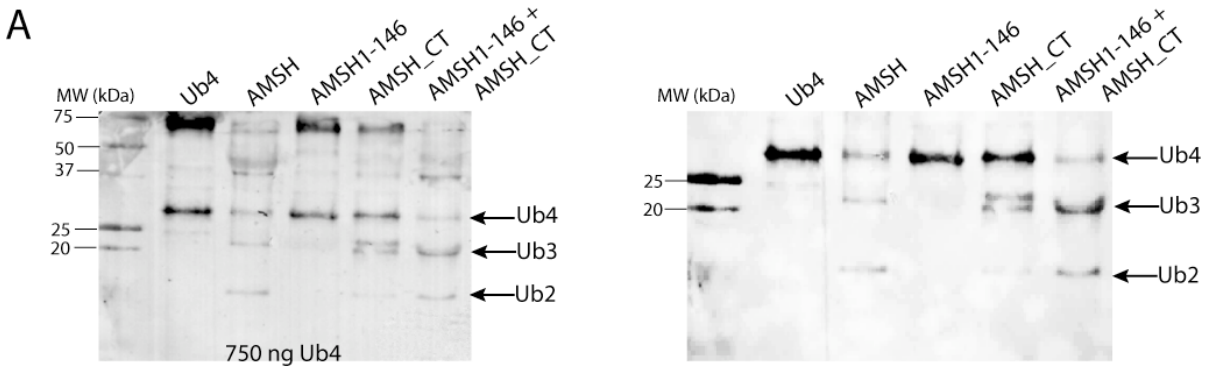

Figure 32. AMSH can hydrolyse K-63 linked ubiquitin chains.

Left panel: AMSH full-length material hydrolyses K-63 linked tetraubiquitin chains to di-ubiquitin. The JAMM domain, expressed here as AMSH_CT, hydrolyses K-63 Ub_4 to diubiquitin, albeit with a lower efficiency than the full-length material. The activity seen with the full-length material can be restored to the JAMM domain upon addition of the AMSH N-terminal. The AMSH N-terminal itself has no deubiquitinating activity. A band corresponding to AMSH_CT is seen for AMSH_CT alone, but not when $AMSH^{1-146}$ is added. Right panel: Same as for A. Cut down of blot to remove higher ubiquitin chains found in the initial tetraubiquitin chains mixture.

Appendix 1. Schematic presentation of AMSH constructs.

AMSH constructs cloned during the thesis work are presented schematically. Start and end residues are labelled to the left and right of the construct diagram.

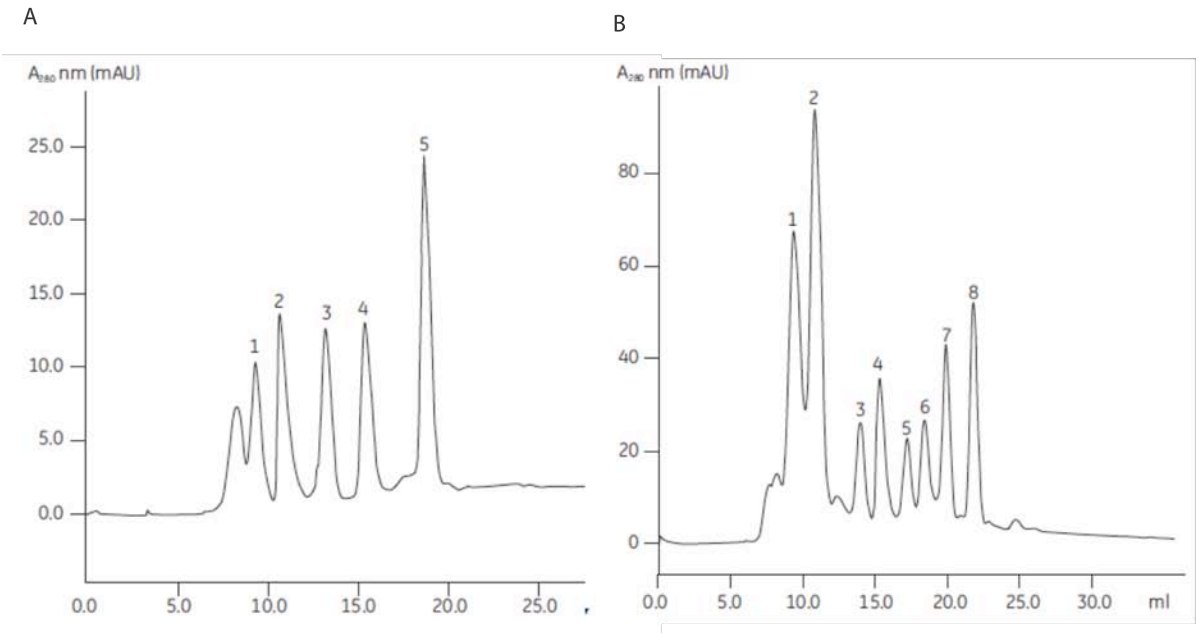

Appendix 2. Typical chromatograms from function tests of Superdex-75 and Superdex-200 10/300 GL columns (GE Healthcare).

A. Superdex-75 10/300 GL column chromatogram. 1. BSA (MW 67 000), 2. Ovalbumin (MW 43 000), 3. Ribonuclease A (MW 13 700), 4. Aprotinin (MW 6 512), 5. Vitamin B12 (MW 1 355).
B. Superdex-200 10/300 GL column chromatogram. 1. Thyroglobulin (MW 669 000), 2. Ferritin (MW 440 000), 3. BSA (MW 67 000), 4. ß-lactoglobulin (MW 35 000), 5. Ribonuclease A (MW 13 700), 6. Cytochrome C (MW 13 600), 7. Aprotinin (MW 6 512), 8. Vitamin B12 (MW 1 355).

(Taken from GE Healthcare Instruction Manual 71-5017-96 AF)

Discussion

D.1 AMSH CHMP3 interaction

CHMP proteins of the ESCRT-III complex are proposed to function in cell membrane remodelling and scission events; at the endosomal membrane for membrane invagination leading to MVB formation, in cytokinesis for membrane scission of daughter cells, and as usurped proteins by enveloped viruses for budding of progeny viral particles. Once activated through removal of a C-terminal autoinhibitory domain, some CHMPs have been shown to form heteropolymer tubules upon incubation with their respective CHMP binding partner; CHMP2 with CHMP3, and CHMP1 with hIST1 (Lata, Schoehn et al. 2008)(Bajorek, Schubert et al. 2009). CHMP tubule formation, combined with the observed action of Vps4 to disassemble CHMP polymers and an external presentation of the CHMP membrane binding surface, elucidates how CHMP polymers could deform the membrane to form a vesicle, before subtraction of CHMP units by Vps4 disassembly draws together the limiting membranes to either close the vesicle neck, or in the case of cytokinesis, fuse the limiting membranes of the daughter cells (Lata, Schoehn et al. 2008). There is increasing evidence that CHMP6 (Vps20), CHMP4 (Snf7) and CHMP3 (Vps24) of ESCRT-III are the minimal components for membrane scission events (Teis et al. 2008)(Saksena et al. 2009)(Wollert et al. 2009), with accessory proteins likely to regulate this process morphologically and temporally *in vivo*. Although CHMP4 (Snf7) and CHMP3 (Vps24) spontaneously polymerise when over-expressed (Ghazi-Tabatabai et al. 2008)(Hanson et al. 2008), polymerisation has never been observed for human CHMP3, and it is still unclear how CHMP3 is activated *in vivo* for CHMP2 binding and polymer formation. Removal of CHMP3's autoinhibitory C-terminal domain converts CHMP3 into a dominant-negative inhibitor of HIV-1 budding, an effect also seen when full-length CHMP3 is co-expressed with AMSH, suggesting binding of AMSH activates CHMP3 by relieving the autoinhibition mechanism (Zamborlini et al. 2006).

An important prerequisite to receptor incorporation into intralumenal vesicles is the removal of the ubiquitin tag used as the initial signal for receptor down-regulation, and the interaction of CHMP proteins with deubiquitinating enzymes (DUBs) such as UBPY (Row et al. 2007) and AMSH (Agromayor & Martin-Serrano 2006)(Tsang et al. 2006)(Agromayor et al. 2009) implies the ESCRT-III complex is involved in the recruitment of DUB enzymes to perform this function. The interaction of AMSH and UBPY through the autoinhibitory C-terminal portion of CHMP proteins has led to the proposition of these DUBs as potential activators of CHMP proteins for polymerisation, constraining the progression to vesicle

formation to a dependency on recruitment of DUBs for effective prior removal of ubiquitin moieties. The deubiquitinating activity of AMSH affects endosomal receptor degradation and viral budding in a CHMP3 dependant manner, with both CHMP3 binding and enzymatic activity required for efficient endosomal sorting (Agromayor & Martin-Serrano 2006)(Kyuuma et al. 2007). A chimeric protein consisting of the C-terminal domain of CHMP2 (Vps2) fused to the N-terminal domain of CHMP3 (Vps24) could not rescue sorting defects in cells lacking either CHMP2 (Vps2) or CHMP3 (Vps24), highlighting a required function for the C-terminal of CHMP3 (Vps24) in sorting (Ghazi-Tabatabai et al. 2008). It is proposed the requirement for the C-terminal of CHMP3 is linked to its role in recruiting DUBs such as AMSH, and that this recruitment of AMSH and deubiquitinating activity of AMSH is required for sorting.

AMSH was reported to bind to CHMP1A, CHMP1B, CHMP2A and CHMP3 of the endosomal sorting pathway (Agromayor & Martin-Serrano 2006)(Tsang et al. 2006)(Agromayor et al. 2009). The portion of AMSH involved in this interaction was a predicted helical MIT domain between residues 17-113 of the N-terminal, as identified from sequence alignment with Vps4B (Tsang et al. 2006). We verified CHMP3 binding to AMSH, and identified a minimal AMSH CHMP3 complex through limited proteolysis of full-length AMSH in complex with CHMP3, and by a further limited proteolysis of CHMP3 in complex with an N-terminal construct of AMSH spanning residues 1-206 that had been designed based on bioinformatic primary sequence analysis for helical content. AMSH residues 1-146 were found to be sufficient for CHMP3 binding.

The affinity of the interaction between the AMSH N-terminal domain and CHMP3 was measured by ITC using the longer AMSH N-terminal construct $AMSH^{1-206}$ fused to hisMBP, isolated in the monomeric form. Displaying a nanomolar affinity of K_D 31.9 nM, the interaction of $AMSH^{1-206}$ and CHMP3 is orders of magnitude higher than any previously measured MIT-MIM interaction.

CHMP3 was isolated in two distinct forms, eluting as separate defined peaks on size exclusion chromatography, dependant on absence (0 mM) or high (500 mM) salt content in the running buffer (Lata, Roessle et al. 2008). SAXS analysis of each species, combined to fitting of the previously determined crystal structure of the CHMP3 N-terminal residues 1-183 (Muzioł et al. 2006), showed the low salt species corresponds to a closed autoinhibited form, whilst the second isolated in high salt is a more open structure, where the high ionic

strength of the buffer is hypothesised to disrupt the electrostatic affinity of the CHMP3 N-terminal for the C-terminal, artificially activating the CHMP3 molecule. ITC studies to assay if AMSH would bind both forms of CHMP3 gave nanomolar affinity of $AMSH^{1-206}$ for both CHMP3 conformers, with dissociation constants as follows: K_D 5.6 nM in 0 mM NaCl and K_D 392 nM in 500 mM NaCl. AMSH binds both the autoinhibited and the activated form of CHMP3 with high affinity, supporting the hypothesis AMSH could be responsible for CHMP3 activation and indicating that activation of CHMP3 by AMSH would not result in release of CHMP3 from AMSH. Removal of the C-terminal of CHMP3 targets CHMP3 to membranes *in vivo*, suggesting a cytosolic activation where the membrane-binding surface would only become available in the activated form (Muzioł et al. 2006). AMSH binding to both the inactivated and activated form of CHMP3 indicates this interaction occurs in the cytosol, which in turn provides a candidate recruitment mechanism for AMSH to the endosomal membrane via CHMP3 interaction. This concurs with the observation that CHMP3 binding is not required for AMSH's *in vitro* deubiquitinating activity, but *in vivo* expression of an AMSH mutant lacking CHMP3-binding ability ($AMSH^{83-424}$) resulted in accumulation of ubiquitinated cargo on aberrant endosomes (Kyuuma et al. 2007); although CHMP3 has no direct effect on the deubiquitinating activity of AMSH (McCullough et al. 2004), it would appear CHMP3 is required for localisation of AMSH to the site of its deubiquitinating activity (Kyuuma et al. 2007).

The first MIT-MIM interactions to be characterised, namely those of Vps4A with CHMP1A, Vps4A with CHMP1B and Vps4B with CHMP2B, displayed affinities around K_D 30 μM, relying on a few key hydrophobic residues, most notably two highly conserved C-terminal Leu residues, forming a fairly superficial binding pocket range (Scott et al. 2005)(Stuchell-Brereton et al. 2007)(Obita et al. 2007). Later, the structure of CHMP1B with spastin showed a higher affinity could be reached if a more substantial burying binding pocket was formed, still relying on mainly hydrophobic interactions yet attaining a slightly higher affinity than Vps4 for CHMP1B of 12 μM (Yang et al. 2008). Mutational studies and sequence analysis of previous MIT-MIM structure sequences led to a consensus sequence of LXX+LAAL+ being determined for MIT domain binding of CHMP proteins. We designed a CHMP3 peptide of the last 28 amino acids of the CHMP3 C-terminal ($CH3CT^{28}$), encompassing the equivalent CHMP3 sequence to that of the MIM consensus sequence, MXX+LAAL+ (where the first leucine of the consensus sequence is replaced by a methionine in CHMP3), which gave an affinity of K_D 24 μM for $AMSH^{1-206}$, an affinity value comparable with those of previously published MIT-MIM affinities but a lower affinity than for the titration of full-length CHMP3 with $AMSH^{1-206}$. The discrepancy between binding values for

full-length CHMP3 and the CH3CT[28] peptide led us to question if a longer region of CHMP3 is involved in binding AMSH. A longer CHMP3 C-terminal construct covering residues 183-222 (CH3CT) bound with the same nanomolar affinity as the full-length CHMP3 molecule, with a binding of K_D 63 nm. A larger binding surface area could explain the high affinity seen for the AMSH MIT- CHMP3 MIM interaction.

A crystallographic structure of AMSH$^{1-146}$ in complex with CH3CT (CHMP3$^{183-222}$) was obtained to an atomic resolution of 1.7Å. AMSH$^{1-146}$ folds into a four helical bundle, where three of these correspond to a MIT domain arrangement reminiscent of previously published MIT domains. However, this structure reveals several unique features of the AMSH MIT domain and its mode of interaction with CHMP3. The additional fourth helix located at the extreme N-terminal of AMSH (helix 0), is tethered to the second and third helices of the MIT domain via a His4-Glu57 and Arg14-Glu117 salt bridge. Residues 200-222 of CH3CT bind in parallel to AMSH, in a groove between helices 2 and 3 of the MIT domain three-helix bundle. A number of hydrogen bonds and salt bridges are made between CHMP3 and AMSH; salt bridges of Glu203 to Lys88, Arg216 to Glu104, Arg221 to Glu72, a hydrogen bond of Glu207 to Tyr80, and additionally AMSH Lys107 coordinates three hydrogen bonds to the CHMP3 peptide carbonyls of Thr219, Leu220 and Ser222A. This polar interaction contrasts the previously hydrophobic nature of previously described MIT-CHMP structures, deviating from the previously proposed MIM1 consensus sequence and highlighting the importance of individual key residues for each CHMP protein (Figure 33).

Whilst residues 1-100 were reported to be required for CHMP3 binding (Tsang et al.2006), the construct AMSH$^{1-102}$ no longer binds CHMP3 (Zamborlini et al. 2006). A loss of deubiquitinating activity of AMSH affects endosomal receptor degradation and viral budding in a CHMP3 dependant manner (Zamborlini et al. 2006)(Agromayor & Martin-Serrano 2006)(Kyuuma et al. 2007). When co-expressed with CHMP3, AMSH$^{1-102}$ no longer inhibited viral budding, in contrast to the sharp reduction in viral release seen upon co-expression of AMSH$^{1-127}$, indicating residues 102-127 are required for CHMP3 binding (Zamborlini et al. 2006). This result can be explained by our structure, which reveals how AMSH makes key hydrogen bonds with CHMP3 via Glu104, and Lys107, with Phe100 contributing a complementary hydrophobicity to Met213 and Leu220 of CHMP3. In addition, loss of residues 103-127 may destabilise the conformation of AMSH by losing a vital salt bridge between Arg14 and Glu117 keeping helix-0 hinged to helix 3 of the MIT domain.

It was surprising to only see density for the last 20 residues of the CHMP3 C-terminal in the structure, as these residues were also present in the original CHMP3CT[28] peptide designed for the ITC experiments which demonstrated only micromolar affinity for AMSH, contrasting sharply with the nanomolar affinity gained by using full-length CHMP3. The structure does not illuminate why the additional 12 residues present in the CH3CT construct (residues 183-194) increase AMSH affinity to the nanomolar range, suggesting our structure represents only a part of the total CHMP3 binding interface.

The affinity of CHMP6 for Vps4 increases from K_D 33±7μM to K_D 5.8$^{\pm}$0.8 μM when the C-terminal domain is deleted down to a 165−181 fragment, removing the MIM consensus sequence (Kieffer et al. 2008). This showed residues located further towards the N-terminal of the CHMP C-terminal domain could interact with MIT domains, and was termed a MIM2 site. The structure of the CHMP6 MIM2 (CHMP6$^{166-181}$) was determined in complex with the MIT domain of Vps4A, binding between helices 1 and 3 as in the spastin CHMP1B structure and demonstrating how the same mode of binding can be employed from a different sequence specificity (Kieffer et al. 2008). hIST1 was recently shown by NMR chemical shift footprinting and biosensor binding studies to contain two MIM sites that can simultaneously bind to the Vps4A MIT, one conforming to the proposed MIM1 consensus sequence of LXX+LAAL+ and a second MIM2 consensus sequence of LPEØP based on the Vps4A CHMP6 structure (Bajorek et al. 2009). Sequence alignment studies using proposed MIM1 and MIM2 consensus sequences suggest CHMP3 could contain a second MIM sequence (Figure 33). However, the lack of solid consensus sequences due to selectivity for CHMP proteins through subtle sequence recognition by MIT domain-containing binding partners [a good example of which being spastin, which binds CHMP1B but not its close homologue CHMP1A(Yang et al. 2008)], makes it difficult to bioinformatically predict the presence of MIM domains in CHMP proteins without supporting biochemical data. It can be that our crystal structure reflects only one of two CHMP3 MIM binding sites, the first MIM1 site visible in our structure located between helices 2 and 3, leaving the possibility of a second MIM2 binding site between helices 1 and 3.

In the spastin MIT CHMP1B structure the residues in the CHMP1B C-terminal fragment that would correspond to the missing residues 183-194 of the CH3CT construct we crystallised, are found in the electron density folding back onto the helix interacting with the spastin MIT domain. Only minimal contacts are found between these extra residues and the MIT domain, implying that for this interaction these residues do not significantly contribute to binding, which is in accord with the micromolar affinity of this interaction. CHMP1B was

demonstrated to only bind Vps4A through a single MIM1 site (Kieffer et al. 2008), and it may be that only select CHMP proteins contain a MIM2 binding site. The location of a second MIM domain in some CHMP C-terminal domains may be critical in conferring very high affinities to a few MIT-CHMP interactions, affecting the dynamics of CHMP transfer between MIT-domain containing proteins.

An additional consideration is the possibility of different CHMPs simultaneously binding to the AMSH MIT domain. CHMP3 binds in the helices 2/3 position, but there are a range of CHMP binding partners of AMSH that may bind in the helices 1/3 position. hIST1 binds to AMSH (Agromayor et al. 2009), and sequence analysis of hIST1 shows a particular conservation of charged residues involved in the CHMP3 interaction with AMSH (Figure 33, lower panel). Interestingly, the last 17 C-terminal residues of hIST1 were shown sufficient for binding MIT domain-containing proteins, such as VPS4 and UBPY, but AMSH bound poorly, suggesting either a requirement for the same extended MIM1 sequence as for the AMSH CHMP3 interaction, or perhaps the involvement of the hIST MIM2 sequence. AMSH binds CHMP1A, the binding partner of hIST1, as well as CHMP3 and CHMP3's binding partner CHMP2A. It can be speculated whether simultaneous binding of complementary CHMP binding partner proteins through two MIM interaction sites of AMSH could bring about activation and proximity of CHMPs for polymerisation, with high affinity for one protein in the heterodimer pair creating a point of control. This poses the question whether polymerisation can occur whilst CHMP proteins are bound to AMSH. It would be interesting to determine if a) AMSH can simultaneously bind CHMP3 and CHMP2A, or if they compete for AMSH binding, b) if simultaneous binding triggers polymerisation, or c) if addition of CHMP2A to the AMSH CHMP3 complex produces polymers. The results of these experiments would also elucidate if AMSH indeed relieves the autoinhibition of CHMP proteins to activate them for polymerisation. A further experiment would be to see if AMSH binding to CHMP2A can activate CHMP2A to polymerise, as CHMP2A spontaneously forms rings when artificially activated through deletion of its C-terminal autoinhibitory domain (Lata, Schoehn et al. 2008). It may be that release from AMSH is required for polymerisation to occur, creating a regulatory mechanism. We show that the AMSH CHMP3 complex can be purified *in vitro* in a monomeric state, eluting around 12.8 mL on a superdex-200 size exclusion chromatography column, thus if AMSH activates CHMP3 it does not permit polymerisation as a complex, confirming previous studies where CHMP3 requires its activated binding partner CHMP2A for polymerisation to occur, with neither CHMP3ΔC alone nor CHMP3ΔC with CHMP2A polymerising (Lata, Schoehn et al. 2008).

The disassembly of C-terminally truncated CHMP2A / full-length CHMP3 polymers by Vps4 confirmed that CHMP3 can bind Vps4 (Lata, Schoehn et al. 2008), a finding consistent with the presence of the MIM1 consensus sequence required for Vps4 binding in the C-terminus of CHMP3, with the exception of the replacement of a leucine for a methionine at amino acid 213 (Figure 33). It is unlikely Vps4 could compete with AMSH for CHMP3 binding given the high affinity we present here. Studies in yeast propose CHMP2 as the recruiter of Vps4 (Ghazi-Tabatabai et al. 2008)(Teis et al. 2008)(Saksena et al. 2009), and it may be that the observed *in vitro* Vps4 binding of CHMP3 results from a lack of competition from the C-terminally truncated CHMP2A used in the Lata et al. experiment. Vps4B can compete with AMSH for CHMP1B binding, yet the affinity of the Vps4A CHMP1B interaction is only K_D 20 ±13 μM (Agromayor & Martin-Serrano 2006)(Scott et al. 2005), indicating that the affinity of AMSH for CHMP proteins other than CHMP3 may be lower than nanomolar. Thus *in vivo*, AMSH could bind to CHMP3, with Vps4 competing effectively to bind to CHMP2. The high affinity seen between AMSH and CHMP3 is thus far unique, is retained upon activation of CHMP3, and hints at a particular regulatory step in the release of CHMP3 from AMSH.

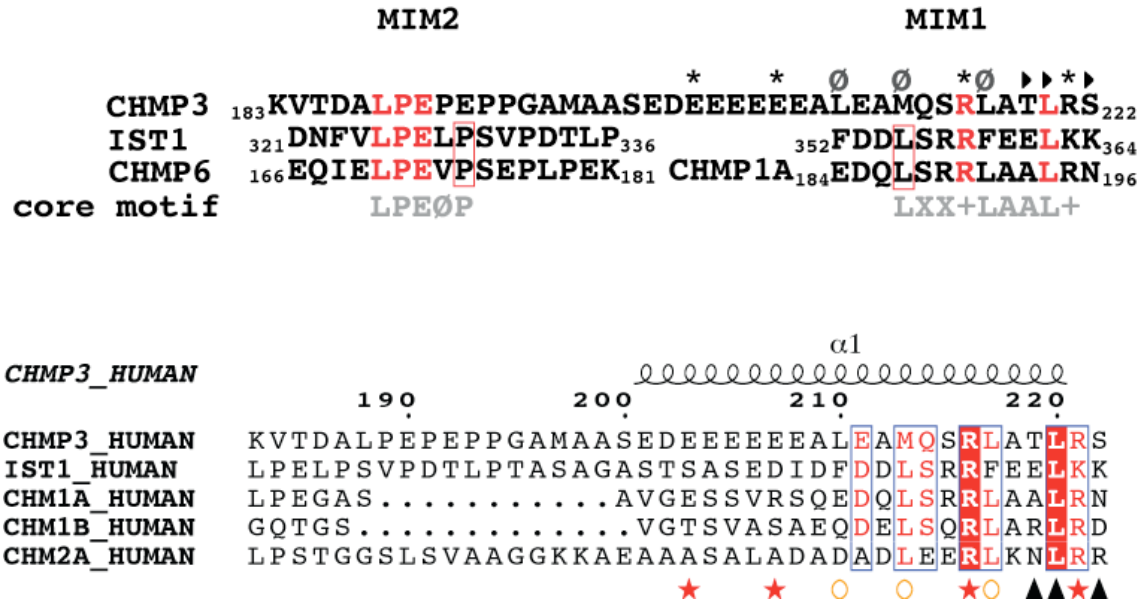

Figure 33. Sequence comparison of CHMP3 with other CHMP proteins.

Upper panel: Sequence alignment of CHMP3$^{183-222}$ with consensus MIM1 and MIM2 binding sequences. Consensus MIM1 and MIM2 binding sequences from CHMP1A and CHMP6 respectively were aligned manually with CHMP3$^{183-222}$. As for IST1, a putative MIM2 sequence can be found further towards the N-terminal end of the CHMP3 C-terminal. Analysis of the MIM1 sequence conservation reveals conservation of two of the three key leucine residues mediating the typical micromolar affinity MIT-MIM1 interaction. The third leucine being replaced by a methionine would not disrupt the required hydrophobicity required in this position. *Adapted from (Bajorek, Morita et al. 2009).*

Lower panel: Sequence alignment of CHMP3$^{183-222}$ with CHMP binding partners of AMSH, comprising CHMP1A, CHMP1B, CHMP2A and hIST1. Interacting residues in the AMSH$^{1-146}$ CHMP3$^{183-222}$ structure are highlighted below. Red stars contrbute hydrogen bonds and salt bridges, orange circles contribute hydrophobic interactions, black triangles highlight backbone interactions.

D.2 AMSH intramolecular domain interaction and deubiquitinating activity

AMSH displays a preference for K63-linked ubiquitin chains over K48-linked ubiquitin chains (McCullough et al. 2006). Deubiquitinating assays using K63 linked tetraubiquitin chains demonstrated our recombinant AMSH (untagged AMSH, expressed in *E-coli*) could hydrolyse K63-linked ubiquitin chains *in vitro*. We also isolated a soluble construct of the AMSH JAMM domain that hydrolysed K63-linked ubiquitin chains *in vitro* and could be crystallised.

Concurrent with our work on the AMSH JAMM domain came the publication of the AMSH-LP JAMM domain, which revealed the structural basis for the K-63 linkage specificity of AMSH for ubiquitin chains (Y. Sato et al. 2008). The high sequence conservation between the JAMM domains of these two proteins indicates their structures are likely to be highly similar. The authors describe the crystal structure of AMSH-LP JAMM domain alone and in complex with a Lys63-linked di-ubiquitin at 1.2 Å and 1.6 Å resolution, respectively. Two insertions appertaining specifically to the AMSH protein family, Ins-1 (residues 314-339) and Ins-2 (residues 393-415) are key additions involved in coordination of the ubiquitin moieties, and their absence from the previously characterised *Archaeoglobulus fulgidus* archaeal JAMM domain accounts for the lack of ubiquitin hydrolysis activity from this protein (Ambroggio et al. 2004). K63-linked ubiquitin adopts an extended conformation in the AMSH-LP^{E292A}K63-Ub_2 complex, in accordance with NMR studies showing K-63 ubiquitin linkage gives an extended chain lacking stable intra-chain ubiquitin-ubiquitin interactions and in contrast to the compact globular form K-48 linked ubiquitins (Datta et al. 2009). In addition, two hydrogen bonds between the JAMM core and Gln62 and Glu64 of the proximal ubiquitin are indicated to confer specificity for K-63 linked chains.

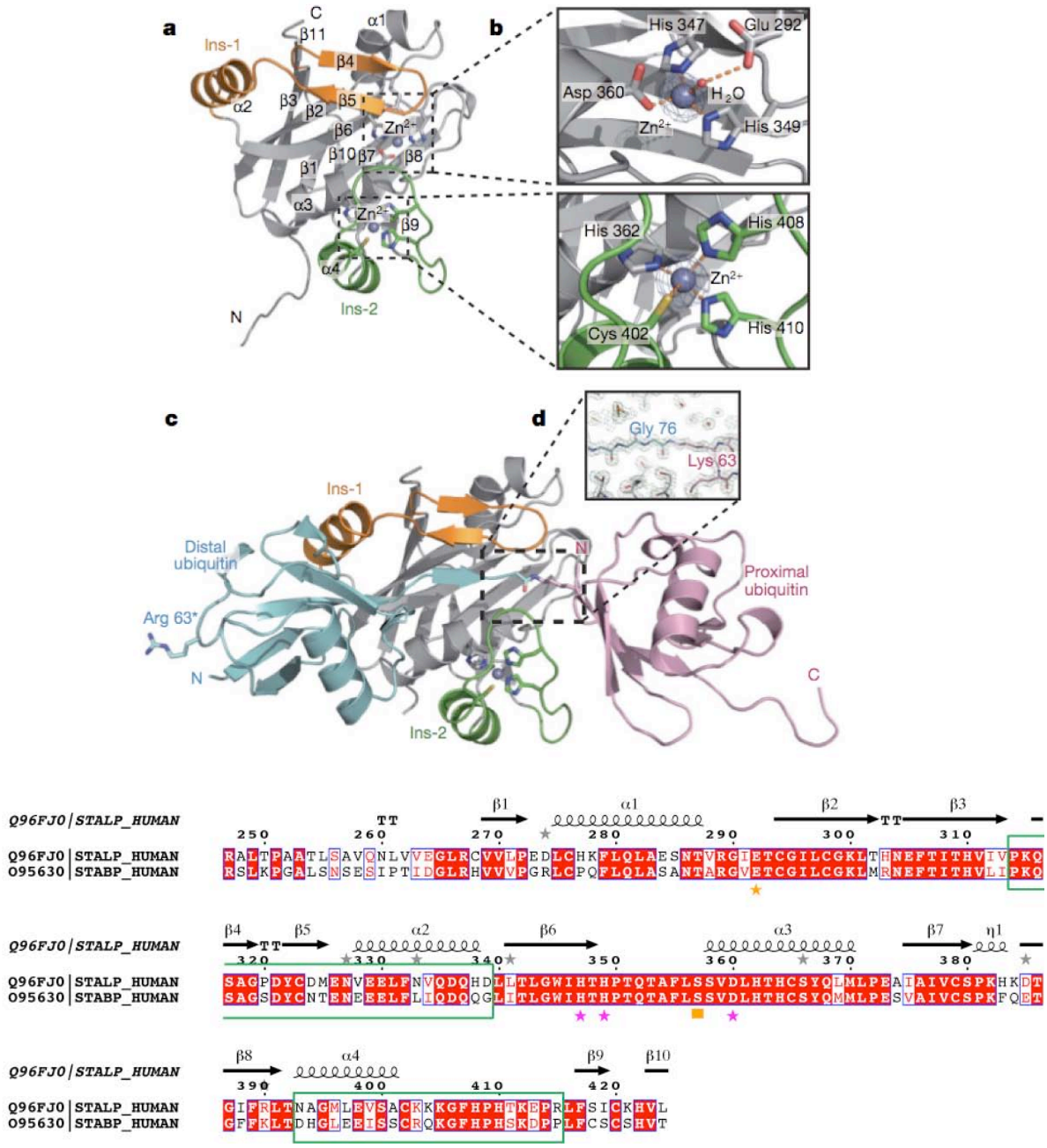

Figure 34. AMSH-LP and AMSH have highly conserved JAMM domains, with all key enzymatic residues retained.

a. The AMSH-LP JAMM domain. α-helices and β-strands are numbered α1-α4 and β1-β11, respectively. b. Zn^{2+}-coordinating sites. c. The AMSH-LP^{E292A}K63-Ub_2 complex. Arg63 in the disal ubiquitin (Lys 63 in wild-type) is shown by a stick model. d. The isopeptide linkage: Gly76 (C-terminal carboxyl) of the distal ubiquitin and K63 of the proximal ubiquitin. *Adapted from Sato et al. 2008*. Bottom panel. Sequence alignment of AMSH-LP and AMSH JAMM domains. The structure motifs of AMSH-LP JAMM domain are indicated above the sequence. Purple stars indicate zinc-coordinating residues His347, His349 and Asp 360, an orange box highlights the intermediate-stabilising Ser 357, an orange star highlights Glu280 that hydrogen bonds to a catalytic water molecule coordinating to the zinc ion. Ins-1 (residues 314-339) and Ins-2 (residues 393-415) are outlined in green boxes. Image prepared with the ESPRIPT server http://espript.ibcp.fr.

This work presents evidence that the N-terminal of AMSH comprising the MIT domain, and the C-terminal of AMSH comprising the JAMM domain, interact intramolecularly. Extensive dual proteolysis of AMSH with papain and thermolysin for 2 hours yields stoichiometric quantities of two fragments, one corresponding to the N-terminal domain and one corresponding to the C-terminal JAMM domain, which remain together on anionic exchange chromatography and superdex-200 SEC. The N-terminal domain construct $AMSH^{1-146}$ can be co-purified with the JAMM domain construct AMSH_CT, and the resulting material can be cross-linked to a molecular weight corresponding to the size of an $AMSH^{1-146}$ AMSH_CT complex. Furthermore, $AMSH^{1-146}$ and AMSH_CT co-elute in size exclusion chromatography, with $AMSH^{1-146}$ drawing AMSH_CT from its elution point at 11.5 mL into the $AMSH^{1-146}$ elution peak at to 10.2 mL, supporting evidence for a complex and also hinting that AMSH_CT binds to $AMSH^{1-146}$ in a way that does not increase the overall hydrodynamic radius of $AMSH^{1-146}$, which would place the JAMM domain packing against the extended 70 Å long third helix of the AMSH MIT domain.

During the deubiquitinating assays we observed that the JAMM domain construct AMSH_CT had a lower activity than full-length AMSH, with AMSH_CT activity reconstituted to the level of full-length AMSH upon addition of the AMSH N-terminal domain construct $AMSH^{1-146}$. This result indicates that interaction with the N-terminal domain of AMSH stimulates the deubiquitinating activity of the JAMM domain. The activity of AMSH in our deubiquitinating assay is low, and a possible reason for this could be a lack of stable interaction between the N-terminal and JAMM domains. AMSH's binding partner STAM has been observed to stimulate AMSH deubiquitinating activity, thus in line with our results STAM may serve to stabilise the interaction of the AMSH N-domain to the JAMM domain to increase enzymatic activity.

Post translational modifications such as phosphorylation are commonly employed in the regulation of protein activity, often modulating protein-protein interactions. Itoh et al. reported phosphorylation at five serine positions in AMSH, Ser2, Ser48, Ser235, Ser237 and Ser239 (F. Itoh et al. 2001). Three of the phosphorylation sites lie clustered within the STAM binding site, and could be hypothesised to play a role in AMSH interaction with STAM. Co-expression of certain receptors such as the constitutively active BMP (bone morphogenic protein) type I receptor, [also known as activin receptor-like kinase (ALK)6], promotes AMSH phosphorylation (F. Itoh et al. 2001), demonstrating a possible mechanism of up-regulation of AMSH activity in response to receptor activity, where phosphorylation could act as a mediator of STAM binding and/or the intramolecular interaction of the AMSH MIT and

JAMM domains, both of which have been shown to stimulate AMSH enzymatic activity. Consequently, the instability of the N-terminal-JAMM domain interaction in our *in vitro* studies can be a result of missing post-translational modifications such as phosphorylation that are only made in response to a need for increased AMSH activity. A phosphorylation stimulus can be mimicked using glutamic acid mutation of phosphorylation sites, and it would be interesting to see if the interaction between the AMSH N-terminal domain and JAMM domain is strengthened when a phosphorylation stimulus is created, and the subsequent effect on the deubiquitinating activity of the JAMM domain. Addition of STAM, or mock phosphorylation through Ser→Glu mutation, may help stabilise the N- terminal - JAMM domain interaction enough to crystallise full-length AMSH.

AMSH affects endosomal receptor degradation and viral budding in a CHMP3 dependant manner, with both CHMP3 binding and enzymatic activity required for efficient endosomal sorting and viral budding; AMSH can convert full-length CHMP3 into a dominant-negative inhibitor of HIV-1 budding, but a stronger inhibition is seen upon incubation of CHMP3 with a catalytically inactive $AMSH^{D348A}$ mutant, an effect abolished by point mutations in the CHMP3 binding site of AMSH (Zamborlini et al. 2006). An AMSH N-terminal construct spanning residues 1–127, excluding the JAMM domain and STAM binding motif, also inhibited HIV-1 particle production but again only when co-expressed with CHMP3 (Zamborlini et al. 2006). Expression of $AMSH^{D348A}$ inhibits retroviral budding in a dominant-negative manner and induces the accumulation of ubiquitinated HIV and MLV gag, yet AMSH is non-essential for viral budding as was shown by knockdown studies, indicating that a disruption in the deubiquitinating capacity of AMSH affects virus budding in an indirect fashion, where it is speculated the removal of a deubiquitinating step blocks release of binding partners directly required for viral budding, such as the ESCRT-III proteins; AMSH was observed to bind more strongly to CHMP1A and CHMP2A when catalytically inactive (Agromayor & Martin-Serrano 2006). These results show disruption of AMSH's enzymatic activity affects virus budding only in relation to AMSH binding of CHMP, and suggest CHMP3 becomes locked in complex with AMSH in the absence of enzymatic activity, with the deubiquitinating activity of the AMSH JAMM domain required for CHMP3 release. Our observation of an interaction between the AMSH JAMM domain and CHMP binding N-terminal domain could provide the mechanism for a deubiquitinating-dependant CHMP3 release mechanism. Our finding that this intramolecular interaction in AMSH stimulates the enzymatic activity of the JAMM domain could provide a link between efficient enzymatic activity and simultaneous release of CHMP proteins, especially in the context of STAM enhancement of AMSH enzymatic activity and CHMP3 stimulation of the interaction

between AMSH and STAM (McCullough et al. 2006). A requirement for a conformational change would explain how the affinity of the AMSH CHMP3 interaction could finally be modified to allow CHMP3 release.

In this work I propose a model where AMSH binding to the C-terminal domain of CHMP3 disrupts the autoinhibitory binding of the CHMP3 N-terminal domain to the CHMP3 C-terminal domain, opening up the structure into its active conformation. The accompanying exposure of the membrane-targeting interface then recruits both active CHMP3 and AMSH to the endosomal membrane. A high affinity interaction between AMSH and CHMP3 retains activated CHMP3 bound to AMSH, creating a point of control between activation of CHMP3 and its polymerisation with its heterodimer partner CHMP2A. Binding to CHMP3 promotes interaction with STAM, stabilising an interaction of the AMSH N-terminal domain to the enzymatic JAMM domain, resulting in an efficient deubiquitinating activity of AMSH for removal of ubiquitin moieties from receptors before their incorporation into MVBs. The interaction of the JAMM domain with the AMSH N-terminal domain causes a simultaneous release of CHMP3 for polymerisation, linking release of CHMP3 for polymerisation and a role in membrane remodelling events to a completed deubiquitination of receptors by AMSH. Increased phosphorylation in response to a stimulated activity of receptors, may also serve to stabilise STAM binding and inter-domain interaction, linking up-regulation of AMSH deubiquitinating activity with receptor activity. AMSH binding of process-specific CHMP proteins, such as hIST1 that is critical for cytokinesis but not HIV budding (Agromayor et al. 2009), demonstrates how subsets of complementary CHMP proteins could confer roles in different cellular processes, be that endosomal sorting, cytokinesis, or as yet unidentified pathways.

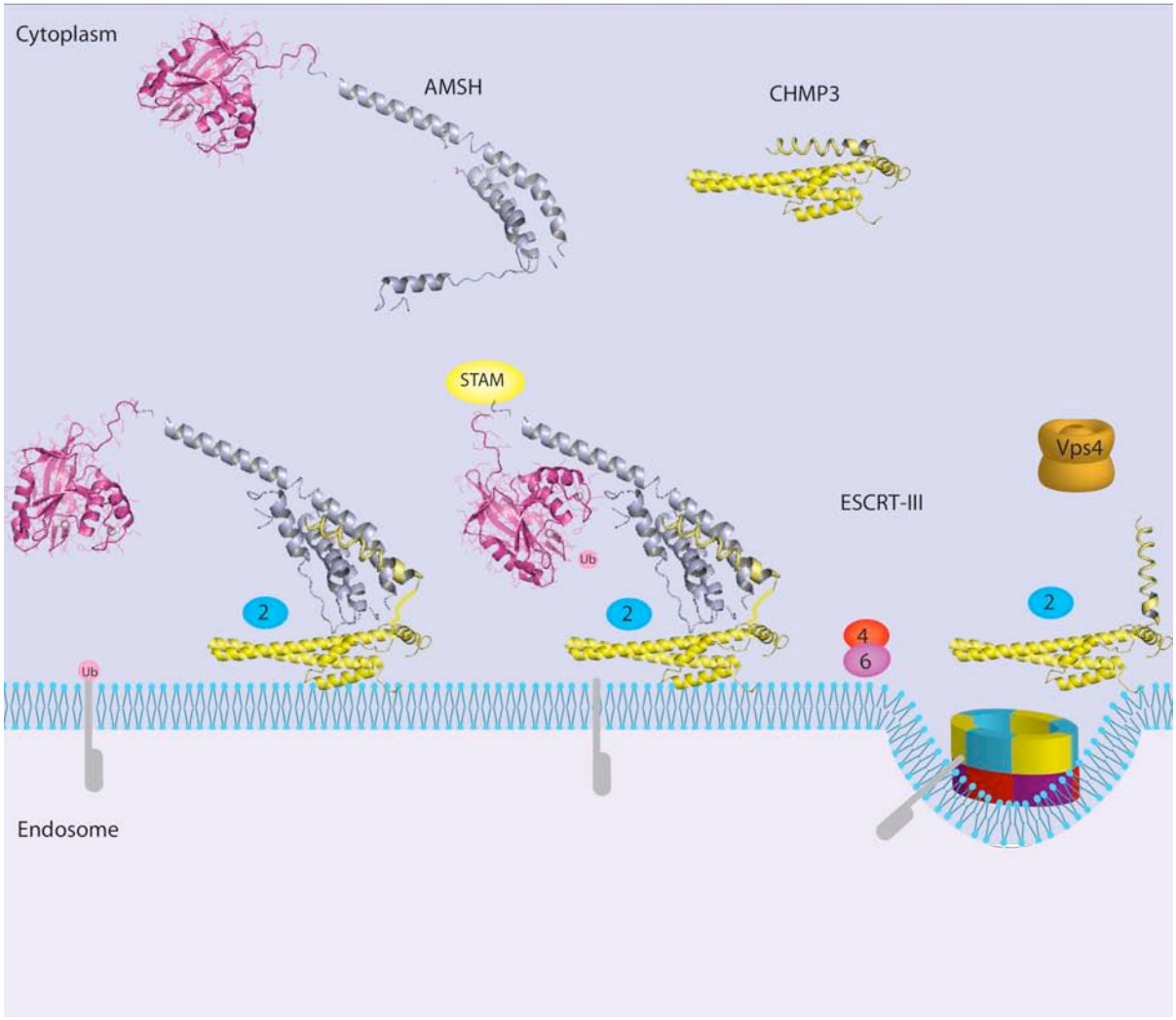

Figure 35. Final model linking efficient AMSH deubiquitination of receptors to AMSH binding and release of CHMP3 for polymerisation, providing a potential point of regulation in the endosomal sorting pathway.

AMSH binding to the C-terminal domain of CHMP3 in the cytosol disrupts the autoinhibitory binding of the CHMP3 N-terminal domain to the CHMP3 C-terminal domain, opening up the structure into its active conformation and exposing the membrane-targeting interface which recruits both active CHMP3 and AMSH to the endosomal membrane. A high affinity interaction between AMSH and CHMP3 retains activated CHMP3 bound to AMSH and promotes interaction with STAM, stabilising an interaction of the AMSH N-terminal domain to the enzymatic JAMM domain, resulting in an efficient deubiquitinating activity of AMSH for removal of ubiquitin moieties from receptors before their incorporation into MVBs. The interaction of the JAMM domain with the AMSH N-terminal domain causes a simultaneous release of CHMP3 for polymerisation linking release of CHMP3 for polymerisation and a role in membrane remodelling events to a completed deubiquitination of receptors by AMSH.

Conclusions

AMSH was confirmed to bind to CHMP3. The affinity of the interaction between an AMSH N-terminal construct AMSH$^{1-206}$ and full-length CHMP3 was probed using ITC, revealing a nanomolar affinity (K_D 31.9 nM) that is orders of magnitude higher than previously characterised MIT-CHMP interactions. AMSH also bound with nanomolar affinity to both salt-induced 'open' and 'closed' forms of CHMP3, contributing to evidence for AMSH activation of CHMP3 by relieving autoinhibition. ITC studies using a CHMP3 C-terminal peptide containing residues 194-222 displayed micromolar affinity for AMSH, whilst a longer CHMP3 C-terminal construct comprising residues 183-222 increased affinity into the nanomolar range, comparable to the affinity of full-length CHMP3 and revealing a much larger binding site than previously described CHMP binding sites.

Crystals were obtained for an AMSH$^{1-146}$ construct in complex with the last 40 residues of the CHMP3 C-terminal. An x-ray crystallographic structure of the complex was obtained to 1.7Å. Surprisingly only residues 200-222 of CHMP3 were found in the electron density, leaving the requirement of residues 183-194 for maximum affinity unexplained and hinting at the presence of a second CHMP binding site non-visible in our structure. The N-terminal of AMSH folds into a four-helix bundle, where three of the helices are reminiscent of previously determined TPR-like MIT domains. CHMP3 residues 200-222 bind in parallel fashion between helices 2 and 3 of the MIT domain, forming several salt bridges and hydrogen bonds contrasting the previously predominantly hydrophobic MIT-CHMP interactions. The fourth extreme N-terminal helix of the AMSH N-terminal domain (helix-0) is tethered to the second and third helices of the MIT domain via His4-Glu57 and Arg14-Glu117 salt bridges. The similarity of our structure with that of the N-terminal domain of UBPY suggests we have crystallised a closed form of this domain, where in UBPY the structure presents an open form allowing dimerisation through exchange of this helix.

We isolated and crystallised a soluble JAMM domain comprising residues 235-424 of AMSH. A concurrent publishing of the JAMM domain structure from the highly conserved AMSH homologue AMSH-LP reveals how two AMSH-family specific sequence insertions provide for binding of two ubiquitin moieties. The overall topology of the structure explains the preference for the more elongated arrangement of K-63 linked ubiquitin chains over K-48 globular ubiquitin chains.

We provide evidence of interaction between the AMSH CHMP binding N-terminal domain and enzymatic JAMM domain, and show that this interaction stimulates the ubiquitin hydrolase activity of the JAMM domain.

Our findings highlight a high affinity interaction between AMSH and CHMP3, with a nanomolar affinity of K_D 31.9 nM. The structure obtained of $AMSH^{1-146}$ with the C-terminal domain of CHMP3 goes partly towards explaining this high affinity, identifying several salt bridges and hydrogen-bonds unseen in previously determined, predominantly hydrophobic, MIT-CHMP interaction structures. However, only 20 of the 40 amino acids identified in our ITC studies required for maximal binding are visualised in the structure. It is thus proposed that a second binding site for the CHMP3 C-terminal is not visible in our structure. The nanomolar affinity of AMSH for both open and closed CHMP3 forms supports the hypothesis that AMSH is implicated in activation of CHMP3. We can at least conclude that activation of CHMP3 does not cause its release from AMSH, and the high affinity of the interaction diminishes the possibility that competition from binding partners such as Vps4 would bring about CHMP3 release.

The interaction of the N-terminal domain of AMSH with the enzymatic C-terminal JAMM domain, and the observation that this interaction stimulates the ubiquitin hydrolase activity of the JAMM domain, suggests how binding partners such as STAM could enhance the deubiquitinating activity of AMSH, with STAM binding in this instance proposed to stabilise the otherwise transient intramolecular interaction between the N-terminal and JAMM domains. Increased phosphorylation of AMSH in response to receptor activity could also play a role in up-regulating AMSH activity, either by increasing STAM binding or by stabilising the N-terminal-JAMM domain interaction. The interaction between the JAMM domain and the CHMP binding N-terminal domain elucidates how a conformational change brought about by the deubiquitinating activity of the JAMM domain could modulate AMSH's affinity for CHMP3 to release CHMP3 for polymerisation. This could provide a regulatory link between prior removal of ubiquitin moieties and CHMP3 polymerisation and membrane remodelling events.

Conclusions

Nous avons confirmé qu'AMSH se lie à CHMP3. L'affinité de l'interaction entre la construction N-terminale d'AMSH et la forme entière de CHMP3 fut étudiée par isothermal titration calorimetry. Cette affinité fut évaluée à l'échelle du nanomolaire par ITC (K_D 31.9 nM), et correspond à un ordre de grandeur plus fort que les interactions MIT-CHMP déjà caractérisées. AMSH se lie aussi avec une affinité de l'ordre du nanomolaire aux deux formes, ouverte et fermée, de CHMP3. Ainsi, AMSH activerait CHMP3 en levant son autoinhibition. Les études utilisant un peptide du domaine C-terminal de CHMP3 contenant les résidus 194-222 ont montré une affinité de l'ordre du nanomolaire comparable à l'affinité noté pour la forme entière de CHMP3. Cette observation suggère la présence d'un site de liaison plus grand que les sites de liaison CHMP3 décris précédemment.

La structure cristallographique du complexe $AMSH^{1-146}$ avec les 40 derniers résidus de la partie C-terminal de CHMP3 fut résolue à 1.7Å, par diffraction aux rayons X. Étonnamment, seuls les derniers résidus 200 à 222 de CHMP3 furent présents dans la densité électronique, alors que les résidus 183 à 194 sont également requis pour obtenir une affinité maximale. L'absence de ces résidus supposerait la présence d'un deuxième site de liaison entre CHMP3 et AMSH dont l'interface ne serait pas visible dans notre structure. Le domaine N-terminal d'AMSH se structure en un fagot de 4 hélices, où trois de ces hélices répliquent les structures des MIT domaines déjà déterminés. Les acides aminés de CHMP3 se lient en mode parallèle entre les hélices 2 et 3 du domaine MIT, formant des ponts salins et des liaisons hydrogènes. Ce mode de liaison diffère des interactions hydrophobes notées pour les autres complexes MIT-CHMP déjà publiées. La quatrième hélice située à l'extrémité N-terminale d'AMSH (hélice-0) est enchaînée aux hélices 2 et 3 du domaine MIT par des ponts salins His4-Glu57 et Arg14-Glu117. La similarité de notre structure avec celle du domaine N-terminale d'UBPY suggèrerait que nous avons cristallisé une forme fermée de ce domaine, alors que la structure d'UBPY présente une forme ouverte permettant la dimérisation par échange de cette hélice.

Nous avons isolé et cristallisé un domaine soluble JAMM comprenant les résidus 235-424 d'AMSH. Une publication concomitant de la structure du domaine JAMM d'AMSH-LP, un homologue proche d'AMSH, révéla comment deux insertions spécifiques de la famille des protéines AMSH permettent la liaison avec deux molécules d'ubiquitine. La topologie de la structure explique la préférence pour la forme étiré des chaînes liaisons K-63 plutôt que la forme globulaire des chaînes de liaison K-48.

On montre que le domaine N-terminal et le domaine JAMM d'AMSH interagissent entre eux, et que cette interaction stimule l'activité déubiquitinase du domaine JAMM. Nos résultats soulignent également une affinité à l'échelle du nanomolaire entre AMSH et CHMP3, avec un K_D de 31.9 nM. La structure d'AMSH$^{1-146}$ en complexe avec le domaine C-terminale de CHMP3 a contribué à la compréhension de cette haute affinité via l'identification de plusieurs ponts salins et de liaisons hydrogènes. Ce type d'interactions n'avait pas été identifié dans les autres structures MIT-CHMP, celle-ci présentant des liaisons de nature hydrophobe. Néanmoins, seulement 20 des 40 résidus, identifiés comme requis pour une affinité maximale via les études d'ITC, sont visualisés dans notre structure. Nous soupçonnons la présence d'un deuxième site de liaison du domaine C-terminal de CHMP3 qui ne serait pas visible dans notre structure. L'affinité d'AMSH pour les formes fermée et ouverte de CHMP3 supporte l'hypothèse qu'AMSH est impliquée dans l'activation de CHMP3. Nous pouvons en conclure que l'activation de CHMP3 n'entrainerait pas à un relâchement d'AMSH, et que la haute affinité de cette interaction diminuerait la possibilité que d'autres partenaires de liaison comme Vps4 puissent déclencher le relâchement de CHMP3.

L'interaction du domaine N-terminal d'AMSH avec le domaine enzymatique JAMM, associée à la stimulation de l'activité hydrolase ubiquitine du domaine JAMM par celle-ci, suggère comment la liaison avec les protéines tel que STAM augmenterait l'activité deubiquitinase d'AMSH. Dans ce cas, la liaison avec STAM stabiliserait l'interaction intramoléculaire entre le domaine N-terminal et le domaine JAMM. Une augmentation de la phosphorylation d'AMSH en fonction de l'activité des récepteurs contribuerait à accroitre l'activité AMSH, soit en favorisant la liaison avec STAM, soit en stabilisant l'interaction intramoléculaire entre le domaine N-terminal et le domaine JAMM. Cette interaction révèle comment un changement conformationnel provoqué par l'activité deubiquitinase du domaine JAMM modulerait l'affinité entre AMSH et CHMP3. Cette modulation déclencherait un relâchement de CHMP3 puis sa polymérisation, ce qui fournirait une liaison réglementaire entre l'élimination en premier d'ubiquitine par AMSH suivie par la polymerisation de CHMP3 aboutissant au remodelage de la membrane.

References

Agromayor, Monica, Jez G Carlton, John P Phelan, Daniel R Matthews, Leo M Carlin, Simon Ameer-Beg, Katherine Bowers, and Juan Martin-Serrano. 2009. Essential Role of hIST1 in Cytokinesis. *Molecular Biology of the Cell* (January 7). doi:10.1091/mbc.E08-05-0474. http://www.ncbi.nlm.nih.gov/pubmed/19129480.

Agromayor, Monica, and Juan Martin-Serrano. 2006. Interaction of AMSH with ESCRT-III and deubiquitination of endosomal cargo. *The Journal of Biological Chemistry* 281, no. 32 (August 11): 23083-91. doi:M513803200.

Ambroggio, Xavier I, Douglas C Rees, and Raymond J Deshaies. 2004. JAMM: a metalloprotease-like zinc site in the proteasome and signalosome. *PLoS Biology* 2, no. 1 (January): E2. doi:10.1371/journal.pbio.0020002.

Amerik, Alexander Y., Jonathan Nowak, Sowmya Swaminathan, and Mark Hochstrasser. 2000. The Doa4 Deubiquitinating Enzyme Is Functionally Linked to the Vacuolar Protein-sorting and Endocytic Pathways. *Mol. Biol. Cell* 11, no. 10 (October 1): 3365-3380.

Avvakumov, George V, John R Walker, Sheng Xue, Patrick J Finerty, Farrell Mackenzie, Elena M Newman, and Sirano Dhe-Paganon. 2006. Amino-terminal dimerization, NRDP1-rhodanese interaction, and inhibited catalytic domain conformation of the ubiquitin-specific protease 8 (USP8). *The Journal of Biological Chemistry* 281, no. 49 (December 8): 38061-70. doi:M606704200.

Babst, M, B Wendland, E J Estepa, and S D Emr. 1998. The Vps4p AAA ATPase regulates membrane association of a Vps protein complex required for normal endosome function. *The EMBO Journal* 17, no. 11 (June 1): 2982-93. doi:10.1093/emboj/17.11.2982.

Babst, Markus, David J Katzmann, Eden J Estepa-Sabal, Timo Meerloo, and Scott D Emr. 2002. Escrt-III: an endosome-associated heterooligomeric protein complex required for mvb sorting. *Developmental Cell* 3, no. 2 (August): 271-282.

Bache, Kristi G, Camilla Raiborg, Anja Mehlum, and Harald Stenmark. 2003. STAM and Hrs are subunits of a multivalent ubiquitin-binding complex on early endosomes. *The Journal of Biological Chemistry* 278, no. 14 (April 4): 12513-21. doi:10.1074/jbc.M210843200.

Bajorek, Monika, Eiji Morita, Jack J Skalicky, Scott G Morham, Markus Babst, and Wesley I Sundquist. 2009. Biochemical analyses of human IST1 and its function in cytokinesis. *Molecular Biology of the Cell* 20, no. 5 (March): 1360-73. doi:10.1091/mbc.E08-05-0475.

Bajorek, Monika, Heidi L Schubert, John McCullough, Charles Langelier, Debra M Eckert, William-May B Stubblefield, Nathan T Uter, David G Myszka, Christopher P Hill, and Wesley I Sundquist. 2009. Structural basis for ESCRT-III protein autoinhibition. *Nature Structural & Molecular Biology* 16, no. 7 (July): 754-762. doi:10.1038/nsmb.1621.

Bowers, Katherine, Jillian Lottridge, Stephen B Helliwell, Lisa M Goldthwaite, J Paul Luzio, and Tom H Stevens. 2004. Protein-protein interactions of ESCRT complexes in the yeast Saccharomyces cerevisiae. *Traffic (Copenhagen, Denmark)* 5, no. 3 (March): 194-210. doi:10.1111/j.1600-0854.2004.00169.x.

Carlton, Jez G., and Juan Martin-Serrano. 2007. Parallels Between Cytokinesis and Retroviral Budding: A Role for the ESCRT Machinery. *Science* 316, no. 5833 (June 29): 1908-1912. doi:10.1126/science.1143422.

CCP4. 1994. The CCP4 Suite: Programs for Protein Crystallography, no. 50: 760-763.

Datta, Ajit B, Greg L Hura, and Cynthia Wolberger. 2009. The Structure and Conformation of Lys63-Linked Tetraubiquitin. *Journal of Molecular Biology* (August 4). doi:10.1016/j.jmb.2009.07.090. http://www.ncbi.nlm.nih.gov/pubmed/19664638.

Delano, W. 2009. http://www.pymol.org.

Doublié, S. 1997. Preparation of selenomethionyl proteins for phase determination. *Methods in Enzymology* 276: 523-30.

Doyotte, Aurelie, Aleksandr Mironov, Edward McKenzie, and Philip Woodman. 2008. The Bro1-related protein HD-PTP/PTPN23 is required for endosomal cargo sorting and multivesicular body morphogenesis. *Proceedings of the National Academy of Sciences of the United States of America* 105, no. 17 (April 29): 6308-6313. doi:10.1073/pnas.0707601105.

Dukes, Joseph D, Judith D Richardson, Ruth Simmons, and Paul Whitley. 2008. A dominant-negative ESCRT-III protein perturbs cytokinesis and trafficking to lysosomes. *The Biochemical Journal* 411, no. 2 (April 15): 233-9. doi:10.1042/BJ20071296.

Emsley, Paul, and Kevin Cowtan. 2004. Coot: model-building tools for molecular graphics. *Acta Crystallographica. Section D, Biological Crystallography* 60, no. Pt 12 Pt 1 (December): 2126-2132. doi:10.1107/S0907444904019158.

Evans, Philip. 2006. Scaling and assessment of data quality. *Acta Crystallographica. Section D, Biological Crystallography* 62, no. Pt 1 (January): 72-82. doi:10.1107/S0907444905036693.

Fisher, Robert D, Bin Wang, Steven L Alam, Daniel S Higginson, Howard Robinson, Wesley I Sundquist, and Christopher P Hill. 2003. Structure and ubiquitin binding of the ubiquitin-interacting motif. *The Journal of Biological Chemistry* 278, no. 31 (August 1): 28976-84. doi:10.1074/jbc.M302596200.

Garrus, J E, U K von Schwedler, O W Pornillos, S G Morham, K H Zavitz, H E Wang, D A Wettstein, et al. 2001. Tsg101 and the vacuolar protein sorting pathway are essential for HIV-1 budding. *Cell* 107, no. 1 (October 5): 55-65.

Gaullier, J M, A Simonsen, A D'Arrigo, B Bremnes, H Stenmark, and R Aasland. 1998. FYVE fingers bind PtdIns(3)P. *Nature* 394, no. 6692 (July 30): 432-3. doi:10.1038/28767.

Ghazi-Tabatabai, Sara, Suraj Saksena, Judith M Short, Ajaybabu V Pobbati, Dmitry B Veprintsev, R Anthony Crowther, Scott D Emr, Edward H Egelman, and Roger L Williams. 2008. Structure and disassembly of filaments formed by the ESCRT-III subunit Vps24. *Structure (London, England: 1993)* 16, no. 9 (September 10): 1345-1356. doi:10.1016/j.str.2008.06.010.

Göttlinger, H G, T Dorfman, J G Sodroski, and W A Haseltine. 1991. Effect of mutations affecting the p6 gag protein on human immunodeficiency virus particle release. *Proceedings of the National Academy of Sciences of the United States of America* 88, no. 8 (April 15): 3195-9.

Haglund, Kaisa, Sara Sigismund, Simona Polo, Iwona Szymkiewicz, Pier Paolo Di Fiore, and Ivan Dikic. 2003. Multiple monoubiquitination of RTKs is sufficient for their endocytosis and degradation. *Nature Cell Biology* 5, no. 5 (May): 461-466. doi:10.1038/ncb983.

Hanson, Phyllis I, Robyn Roth, Yuan Lin, and John E Heuser. 2008. Plasma membrane deformation by circular arrays of ESCRT-III protein filaments. *The Journal of Cell Biology* 180, no. 2 (January 28): 389-402. doi:10.1083/jcb.200707031.

Hao, Quan. 2004. ABS: a program to determine absolute configuration and evaluate anomalous scatterer substructure. *Journal of Applied Crystallography* 37, no. 3 (5): 498-499. doi:10.1107/S0021889804008696.

Hirano, Satoshi, Masato Kawasaki, Hideaki Ura, Ryuichi Kato, Camilla Raiborg, Harald Stenmark, and Soichi Wakatsuki. 2006. Double-sided ubiquitin binding of Hrs-UIM in endosomal protein sorting. *Nature Structural & Molecular Biology* 13, no. 3 (March): 272-7. doi:10.1038/nsmb1051.

Hong, Yoon-Hun, Hee-Chul Ahn, Jongsoo Lim, Hong-Man Kim, Hye-Young Ji, Seunga Lee, Ji-Hun Kim, Eun Young Park, Hyun Kyu Song, and Bong-Jin Lee. 2009. Identification of a novel ubiquitin binding site of STAM1 VHS domain by NMR spectroscopy. *FEBS Letters* 583, no. 2 (January 22): 287-92. doi:10.1016/j.febslet.2008.12.034.

Horii, Mio, Hideki Shibata, Ryota Kobayashi, Keiichi Katoh, Chiharu Yorikawa, Jiro Yasuda, and Masatoshi Maki. 2006. CHMP7, a novel ESCRT-III-related protein, associates with CHMP4b and functions in the endosomal sorting pathway. *The Biochemical Journal* 400, no. 1 (November 15): 23-32. doi:10.1042/BJ20060897.

Huang, Fangtian, Donald Kirkpatrick, Xuejun Jiang, Steven Gygi, and Alexander Sorkin. 2006. Differential regulation of EGF receptor internalization and degradation by multiubiquitination within the kinase domain. *Molecular Cell* 21, no. 6 (March 17): 737-748. doi:10.1016/j.molcel.2006.02.018.

Ichioka, Fumitaka, Ryota Kobayashi, Keiichi Katoh, Hideki Shibata, and Masatoshi Maki. 2008. Brox, a novel farnesylated Bro1 domain-containing protein that associates with charged multivesicular body protein 4 (CHMP4). *The FEBS Journal* 275, no. 4 (February): 682-692. doi:10.1111/j.1742-4658.2007.06230.x.

Ichioka, Fumitaka, Emi Takaya, Hironori Suzuki, Sachiko Kajigaya, Vladimir L Buchman, Hideki Shibata, and Masatoshi Maki. 2007. HD-PTP and Alix share some membrane-traffic related proteins that interact with their Bro1 domains or proline-rich regions. *Archives of Biochemistry and Biophysics* 457, no. 2 (January 15): 142-149. doi:10.1016/j.abb.2006.11.008.

Im, Young Jun, and James H Hurley. 2008. Integrated structural model and membrane targeting mechanism of the human ESCRT-II complex. *Developmental Cell* 14, no. 6 (June): 902-913. doi:10.1016/j.devcel.2008.04.004.

Im, Young Jun, Thomas Wollert, Evzen Boura, and James H Hurley. 2009. Structure and function of the ESCRT-II-III interface in multivesicular body biogenesis. *Developmental Cell* 17, no. 2 (August): 234-243. doi:10.1016/j.devcel.2009.07.008.

Itoh, F, H Asao, K Sugamura, C H Heldin, P ten Dijke, and S Itoh. 2001. Promoting bone morphogenetic protein signaling through negative regulation of inhibitory Smads. *The EMBO Journal* 20, no. 15 (August 1): 4132-42. doi:PMC149146.

Jones, D T. 1999. Protein secondary structure prediction based on position-specific scoring matrices. *Journal of Molecular Biology* 292, no. 2 (September 17): 195-202. doi:10.1006/jmbi.1999.3091.

Kato, M, K Miyazawa, and N Kitamura. 2000. A deubiquitinating enzyme UBPY interacts with the Src homology 3 domain of Hrs-binding protein via a novel binding motif PX(V/I)(D/N)RXXKP. *The Journal of Biological Chemistry* 275, no. 48 (December 1): 37481-7. doi:10.1074/jbc.M007251200.

Katzmann, D J, M Babst, and S D Emr. 2001. Ubiquitin-dependent sorting into the multivesicular body pathway requires the function of a conserved endosomal protein sorting complex, ESCRT-I. *Cell* 106, no. 2 (July 27): 145-155.

Katzmann, David J, Greg Odorizzi, and Scott D Emr. 2002. Receptor downregulation and multivesicular-body sorting. *Nature Reviews. Molecular Cell Biology* 3, no. 12 (December): 893-905. doi:10.1038/nrm973.

Katzmann, David J, Christopher J Stefan, Markus Babst, and Scott D Emr. 2003. Vps27 recruits ESCRT machinery to endosomes during MVB sorting. *The Journal of Cell Biology* 162, no. 3 (August 4): 413-423. doi:10.1083/jcb.200302136.

Kieffer, Collin, Jack J Skalicky, Eiji Morita, Ivana De Domenico, Diane M Ward, Jerry Kaplan, and Wesley I Sundquist. 2008. Two distinct modes of ESCRT-III recognition are required for VPS4 functions in lysosomal protein targeting and HIV-1 budding. *Developmental Cell* 15, no. 1 (July): 62-73. doi:10.1016/j.devcel.2008.05.014.

Kikuchi, Kazu, Naoto Ishii, Hironobu Asao, and Kazuo Sugamura. 2003. Identification of AMSH-LP containing a Jab1/MPN domain metalloenzyme motif. *Biochemical and Biophysical Research Communications* 306, no. 3 (July 4): 637-43. doi:12810066.

Kostelansky, Michael S, Cayetana Schluter, Yuen Yi C Tam, Sangho Lee, Rodolfo Ghirlando, Bridgette Beach, Elizabeth Conibear, and James H Hurley. 2007. Molecular architecture and functional model of the complete yeast ESCRT-I heterotetramer. *Cell* 129, no. 3 (May 4): 485-498. doi:10.1016/j.cell.2007.03.016.

Kostelansky, Michael S, Ji Sun, Sangho Lee, Jaewon Kim, Rodolfo Ghirlando, Aitor Hierro, Scott D Emr, and James H Hurley. 2006. Structural and functional organization of the ESCRT-I trafficking complex. *Cell* 125, no. 1 (April 7): 113-126. doi:10.1016/j.cell.2006.01.049.

Kyuuma, Masanao, Kazu Kikuchi, Katsuhiko Kojima, Yuriko Sugawara, Mariko Sato, Nariyasu Mano, Junichi Goto, et al. 2007. AMSH, an ESCRT-III associated enzyme, deubiquitinates cargo on MVB/late endosomes. *Cell Structure and Function* 31, no. 2: 159-72. doi:JST.JSTAGE/csf/06023.

Lata, Suman, Manfred Roessle, Julianna Solomons, Marc Jamin, Heinrich G Gottlinger, Dmitri I Svergun, and Winfried Weissenhorn. 2008. Structural basis for autoinhibition of ESCRT-III CHMP3. *Journal of Molecular Biology* 378, no. 4 (May 9): 818-27. doi:S0022-2836(08)00350-1.

Lata, Suman, Guy Schoehn, Ankur Jain, Ricardo Pires, Jacob Piehler, Heinrich G Gottlinger, and Winfried Weissenhorn. 2008. Helical structures of ESCRT-III are disassembled by VPS4. *Science (New York, N.Y.)* 321, no. 5894 (September 5): 1354-7. doi:10.1126/science.1161070.

Leslie, A.G.W. 1992. Recent changes to the MOSFLM package for processing film and image plate data. *Joint CCP4 + ESF-EAMCB Newsletter on Protein Crystallography.* No. 26.

Martin-Serrano, J, T Zang, and P D Bieniasz. 2001. HIV-1 and Ebola virus encode small peptide motifs that recruit Tsg101 to sites of particle assembly to facilitate egress. *Nature Medicine* 7, no. 12 (December): 1313-9. doi:10.1038/nm1201-1313.

Martin-Serrano, Juan. 2007. The role of ubiquitin in retroviral egress. *Traffic (Copenhagen, Denmark)* 8, no. 10 (October): 1297-303. doi:10.1111/j.1600-0854.2007.00609.x.

Martin-Serrano, Juan, Trinity Zang, and Paul D Bieniasz. 2003. Role of ESCRT-I in retroviral budding. *Journal of Virology* 77, no. 8 (April): 4794-4804.

McCullough, John, Michael J Clague, and Sylvie Urbé. 2004. AMSH is an endosome-associated ubiquitin isopeptidase. *The Journal of Cell Biology* 166, no. 4 (August 16): 487-92. doi:PMC2172215.

McCullough, John, Robert D Fisher, Frank G Whitby, Wesley I Sundquist, and Christopher P Hill. 2008. ALIX-CHMP4 interactions in the human ESCRT pathway. *Proceedings of the National Academy of Sciences of the United States of America* 105, no. 22 (June 3): 7687-7691. doi:10.1073/pnas.0801567105.

McCullough, John, Paula E Row, Oscar Lorenzo, Mary Doherty, Robert Beynon, Michael J Clague, and Sylvie Urbé. 2006. Activation of the endosome-associated ubiquitin isopeptidase AMSH by STAM, a component of the multivesicular body-sorting machinery. *Current Biology: CB* 16, no. 2 (January 24): 160-5. doi:S0960-9822(05)01524-1.

McGuffin, L J, K Bryson, and D T Jones. 2000. The PSIPRED protein structure prediction server. *Bioinformatics (Oxford, England)* 16, no. 4 (April): 404-405.

Mizuno, Emi, Takanobu Iura, Akiko Mukai, Tamotsu Yoshimori, Naomi Kitamura, and Masayuki Komada. 2005. Regulation of epidermal growth factor receptor down-regulation by UBPY-mediated deubiquitination at endosomes. *Molecular Biology of the Cell* 16, no. 11 (November): 5163-5174. doi:10.1091/mbc.E05-06-0560.

Mizuno, Emi, Kensuke Kawahata, Masaki Kato, Naomi Kitamura, and Masayuki Komada. 2003. STAM proteins bind ubiquitinated proteins on the early endosome via the VHS domain and ubiquitin-interacting motif. *Molecular Biology of the Cell* 14, no. 9 (September): 3675-89. doi:10.1091/mbc.E02-12-0823.

Mizuno, Emi, Kaoru Kobayashi, Akitsugu Yamamoto, Naomi Kitamura, and Masayuki Komada. 2006. A deubiquitinating enzyme UBPY regulates the level of protein ubiquitination on endosomes. *Traffic (Copenhagen, Denmark)* 7, no. 8 (August): 1017-31. doi:TRA452.

Morita, Eiji, Virginie Sandrin, Steven L Alam, Debra M Eckert, Steven P Gygi, and Wesley I Sundquist. 2007. Identification of human MVB12 proteins as ESCRT-I subunits that function in HIV budding. *Cell Host & Microbe* 2, no. 1 (July 12): 41-53. doi:10.1016/j.chom.2007.06.003.

Morita, Eiji, Virginie Sandrin, Hyo-Young Chung, Scott G Morham, Steven P Gygi, Christopher K Rodesch, and Wesley I Sundquist. 2007. Human ESCRT and ALIX proteins interact with proteins of the midbody and function in cytokinesis. *The EMBO Journal* 26, no. 19 (October 3): 4215-27. doi:10.1038/sj.emboj.7601850.

Mukai, Akiko, Emi Mizuno, Kaoru Kobayashi, Masaki Matsumoto, Keiichi I Nakayama, Naomi Kitamura, and Masayuki Komada. 2008. Dynamic regulation of ubiquitylation and deubiquitylation at the central spindle during cytokinesis. *Journal of Cell Science* 121, no. Pt 8 (April 15): 1325-33. doi:10.1242/jcs.027417.

Murshudov, G N, A A Vagin, and E J Dodson. 1997. Refinement of macromolecular structures by the maximum-likelihood method. *Acta Crystallographica. Section D, Biological Crystallography* 53, no. Pt 3 (May 1): 240-255. doi:10.1107/S0907444996012255.

Muzioł, Tadeusz, Estela Pineda-Molina, Raimond B Ravelli, Alessia Zamborlini, Yoshiko Usami, Heinrich Göttlinger, and Winfried Weissenhorn. 2006. Structural basis for budding by the ESCRT-III factor CHMP3. *Developmental Cell* 10, no. 6 (June): 821-30. doi:10.1016/j.devcel.2006.03.013.

Nakamura, Michihiko, Nobuyuki Tanaka, Naomi Kitamura, and Masayuki Komada. 2006. Clathrin anchors deubiquitinating enzymes, AMSH and AMSH-like protein, on early endosomes. *Genes to Cells: Devoted to Molecular & Cellular Mechanisms* 11, no. 6 (June): 593-606. doi:GTC963.

Obita, Takayuki, Suraj Saksena, Sara Ghazi-Tabatabai, David J Gill, Olga Perisic, Scott D Emr, and Roger L Williams. 2007. Structural basis for selective recognition of ESCRT-III by the AAA ATPase Vps4. *Nature* 449, no. 7163 (October 11): 735-9. doi:10.1038/nature06171.

Oestreich, Andrea J, Brian A Davies, Johanna A Payne, and David J Katzmann. 2007. Mvb12 is a novel member of ESCRT-I involved in cargo selection by the multivesicular body pathway. *Molecular Biology of the Cell* 18, no. 2 (February): 646-657. doi:10.1091/mbc.E06-07-0601.

Ott, D E, L V Coren, T D Copeland, B P Kane, D G Johnson, R C Sowder, Y Yoshinaka, S Oroszlan, L O Arthur, and L E Henderson. 1998. Ubiquitin is covalently attached to the p6Gag proteins of human immunodeficiency virus type 1 and simian immunodeficiency virus and to the p12Gag protein of Moloney murine leukemia virus. *Journal of Virology* 72, no. 4 (April): 2962-2968.

Panjikar, Santosh, Venkataraman Parthasarathy, Victor S Lamzin, Manfred S Weiss, and Paul A Tucker. 2005. Auto-Rickshaw: an automated crystal structure determination platform as an efficient tool for the validation of an X-ray diffraction experiment. *Acta Crystallographica. Section D, Biological Crystallography* 61, no. Pt 4 (April): 449-457. doi:10.1107/S0907444905001307.

Perrakis, A, R Morris, and V S Lamzin. 1999. Automated protein model building combined with iterative structure refinement. *Nature Structural Biology* 6, no. 5 (May): 458-463. doi:10.1038/8263.

Pires, Ricardo, Bettina Hartlieb, Luca Signor, Guy Schoehn, Suman Lata, Manfred Roessle, Christine Moriscot, et al. 2009. A crescent-shaped ALIX dimer targets ESCRT-III CHMP4 filaments. *Structure (London, England: 1993)* 17, no. 6 (June 10): 843-856. doi:10.1016/j.str.2009.04.007.

Pohl, Christian, and Stefan Jentsch. 2008. Final Stages of Cytokinesis and Midbody Ring Formation Are Controlled by BRUCE. *Cell* 132, no. 5 (March): 832-845. doi:10.1016/j.cell.2008.01.012.

Pullan, Lee, Srinivas Mullapudi, Zhong Huang, Philip R Baldwin, Christopher Chin, Wei Sun, Susan Tsujimoto, et al. 2006. The endosome-associated protein Hrs is hexameric and controls cargo sorting as a "master molecule". *Structure (London, England: 1993)* 14, no. 4 (April): 661-71. doi:10.1016/j.str.2006.01.012.

Row, Paula E, Han Liu, Sebastian Hayes, Rebecca Welchman, Panagoula Charalabous, Kay Hofmann, Michael J Clague, Christopher M Sanderson, and Sylvie Urbé. 2007. The MIT domain of UBPY constitutes a CHMP binding and endosomal localization signal required for efficient epidermal growth factor receptor degradation. *The Journal of Biological Chemistry* 282, no. 42 (October 19): 30929-37. doi:M704009200.

Row, Paula E, Ian A Prior, John McCullough, Michael J Clague, and Sylvie Urbé. 2006. The ubiquitin isopeptidase UBPY regulates endosomal ubiquitin dynamics and is essential for receptor down-regulation. *The Journal of Biological Chemistry* 281, no. 18 (May 5): 12618-24. doi:M512615200.

Saksena, Suraj, Judit Wahlman, David Teis, Arthur E Johnson, and Scott D Emr. 2009. Functional reconstitution of ESCRT-III assembly and disassembly. *Cell* 136, no. 1 (January 9): 97-109. doi:10.1016/j.cell.2008.11.013.

Sato, Yusuke, Azusa Yoshikawa, Atsushi Yamagata, Hisatoshi Mimura, Masami Yamashita, Kayoko Ookata, Osamu Nureki, Kazuhiro Iwai, Masayuki Komada, and Shuya Fukai. 2008. Structural basis for specific cleavage of Lys 63-linked polyubiquitin chains. *Nature* 455, no. 7211 (September 18): 358-62. doi:nature07254.

Schneider, Thomas R, and George M Sheldrick. 2002. Substructure solution with SHELXD. *Acta Crystallographica. Section D, Biological Crystallography* 58, no. Pt 10 Pt 2 (October): 1772-1779.

Scott, Anna, Jason Gaspar, Melissa D Stuchell-Brereton, Steven L Alam, Jack J Skalicky, and Wesley I Sundquist. 2005. Structure and ESCRT-III protein interactions of the MIT domain of human VPS4A. *Proceedings of the National Academy of Sciences of the United States of America* 102, no. 39 (September 27): 13813-8. doi:10.1073/pnas.0502165102.

Sheldrick, George M. 2002. Macromolecular phasing with SHELXE 217: 644-650.

Shields, S Brookhart, Andrea J Oestreich, Stanley Winistorfer, Doris Nguyen, Johanna A Payne, David J Katzmann, and Robert Piper. 2009. ESCRT ubiquitin-binding domains function cooperatively during MVB cargo sorting. *The Journal of Cell Biology* 185, no. 2 (April 20): 213-224. doi:10.1083/jcb.200811130.

Shih, Susan C, David J Katzmann, Joshua D Schnell, Myra Sutanto, Scott D Emr, and Linda Hicke. 2002. Epsins and Vps27p/Hrs contain ubiquitin-binding domains that function in receptor endocytosis. *Nature Cell Biology* 4, no. 5 (May): 389-393. doi:10.1038/ncb790.

Stauffer, D R, T L Howard, T Nyun, and S M Hollenberg. 2001. CHMP1 is a novel nuclear matrix protein affecting chromatin structure and cell-cycle progression. *Journal of Cell Science* 114, no. Pt 13 (July): 2383-2393.

Strack, B, A Calistri, M A Accola, G Palu, and H G Gottlinger. 2000. A role for ubiquitin ligase recruitment in retrovirus release. *Proceedings of the National Academy of Sciences of the United States of America* 97, no. 24 (November 21): 13063-8. doi:PMC27178.

Strack, Bettina, Arianna Calistri, Stewart Craig, Elena Popova, and Heinrich G Göttlinger. 2003. AIP1/ALIX is a binding partner for HIV-1 p6 and EIAV p9 functioning in virus budding. *Cell* 114, no. 6 (September 19): 689-699.

Stuchell-Brereton, Melissa D, Jack J Skalicky, Collin Kieffer, Mary Anne Karren, Sanaz Ghaffarian, and Wesley I Sundquist. 2007. ESCRT-III recognition by VPS4 ATPases. *Nature* 449, no. 7163 (October 11): 740-4. doi:10.1038/nature06172.

Tanaka, N, K Kaneko, H Asao, H Kasai, Y Endo, T Fujita, T Takeshita, and K Sugamura. 1999. Possible involvement of a novel STAM-associated molecule "AMSH" in intracellular signal transduction mediated by cytokines. *The Journal of Biological Chemistry* 274, no. 27 (July 2): 19129-35. doi:10383417.

Teis, David, Suraj Saksena, and Scott D Emr. 2008. Ordered assembly of the ESCRT-III complex on endosomes is required to sequester cargo during MVB formation. *Developmental Cell* 15, no. 4 (October): 578-589. doi:10.1016/j.devcel.2008.08.013.

Teo, Hsiangling, Olga Perisic, Beatriz González, and Roger L Williams. 2004. ESCRT-II, an endosome-associated complex required for protein sorting: crystal structure and interactions with ESCRT-III and membranes. *Developmental Cell* 7, no. 4 (October): 559-569. doi:10.1016/j.devcel.2004.09.003.

Tran, Huong J T T, Mark D Allen, Jan Löwe, and Mark Bycroft. 2003. Structure of the Jab1/MPN domain and its implications for proteasome function. *Biochemistry* 42, no. 39 (October 7): 11460-11465. doi:10.1021/bi035033g.

Tsang, Hilda T.H., James W. Connell, Stephanie E. Brown, Amanda Thompson, Evan Reid, and Christopher M. Sanderson. 2006. A systematic analysis of human CHMP protein interactions: Additional MIT domain-containing proteins bind to multiple components of the human ESCRT III complex. *Genomics* 88, no. 3 (September): 333-346. doi:10.1016/j.ygeno.2006.04.003.

Vagin, A.A., and Teplyakov, A. 1997. MOLREP: an automated program for molecular replacement. 30: 1022-1025.

Varadan, Ranjani, Michael Assfalg, Aydin Haririnia, Shahri Raasi, Cecile Pickart, and David Fushman. 2004. Solution conformation of Lys63-linked di-ubiquitin chain provides clues to functional diversity of polyubiquitin signaling. *The Journal of Biological Chemistry* 279, no. 8 (February 20): 7055-7063. doi:10.1074/jbc.M309184200.

Wollert, Thomas, Christian Wunder, Jennifer Lippincott-Schwartz, and James H Hurley. 2009. Membrane scission by the ESCRT-III complex. *Nature* 458, no. 7235 (March 12): 172-177. doi:10.1038/nature07836.

Yang, Dong, Neggy Rismanchi, Benoît Renvoisé, Jennifer Lippincott-Schwartz, Craig Blackstone, and James H Hurley. 2008. Structural basis for midbody targeting of spastin by the ESCRT-III protein CHMP1B. *Nature Structural & Molecular Biology* 15, no. 12 (December): 1278-86. doi:10.1038/nsmb.1512.

Yorikawa, Chiharu, Hideki Shibata, Satoshi Waguri, Kazumi Hatta, Mio Horii, Keiichi Katoh, Toshihide Kobayashi, Yasuo Uchiyama, and Masatoshi Maki. 2005. Human CHMP6, a myristoylated ESCRT-III protein, interacts directly with an ESCRT-II component EAP20 and regulates endosomal cargo sorting. *The Biochemical Journal* 387, no. Pt 1 (April 1): 17-26. doi:10.1042/BJ20041227.

Yu, Zhiheng, Malgorzata D. Gonciarz, Wesley I. Sundquist, Christopher P. Hill, and Grant J. Jensen. 2008. Cryo-EM Structure of Dodecameric Vps4p and Its 2:1 Complex with Vta1p. *Journal of Molecular Biology* 377, no. 2 (March 21): 364-377. doi:10.1016/j.jmb.2008.01.009.

Zamborlini, Alessia, Yoshiko Usami, Sheli R Radoshitzky, Elena Popova, Giorgio Palu, and Heinrich Göttlinger. 2006. Release of autoinhibition converts ESCRT-III components into potent inhibitors of HIV-1 budding. *Proceedings of the National Academy of Sciences of the United States of America* 103, no. 50 (December 12): 19140-5. doi:PMC1748189.